People's Democratic Republic of Algeria
Ministry of Higher Education and Scientific Research

University of 8 Mai 1945 Guelma

جامعة 8 ماي 1945 قالمة
UNIVERSITE 8 MAI 1945 GUELMA

Faculty of Science and Technology
Department of Process Engineering
Laboratory of Industrial Analysis and Materials Engineering (LAIGM)

Thesis

Submitted in Candidacy for the Degree of *Doctorate in Third Cycle*

Field: Science and Technology   Stream: Process Engineering
Speciality: Chemical engineering

Presented by:
Sabrina Houam

Title

Theoretical and experimental study of the electrochemical

detection of chemical compounds in aqueous medium

(*Etude théorique et expérimentale de la détection électrochimique*

des composés chimiques en milieu aqueux)

Defended on: Before the jury composed of:

Mr BORDJIBA Tarik	Prof.	Univ. of 8 Mai 1945 Guelma	President
Mr AFFOUNE Abed Mohamed	Prof.	Univ. of 8 Mai 1945 Guelma	Supervisor
Mr CHELAGHMIA Mohamed Lyamine	Prof.	Univ. of 8 Mai 1945 Guelma	Co-supervisor
Mr HAMLAOUI Yousef	Prof.	Univ. of M.C.M. Souk Ahras	Examiner
Ms NIGRI Soraya	Prof.	Univ. of 8 Mai 1945 Guelma	Examiner
Mrs VAUTRIN-UL Christine	Prof.	Univ. of Orléans, France	Examiner

Academic year: 2023-2024

ACKNOWLEDGMENTS

Abstract

In this study, the simulation and calculation of linear sweep voltammetry (LSV) profiles for quasi-reversible soluble-soluble systems using the semi-analytical approach are investigated. A thorough qualitative and quantitative analysis of the shape and position of linear sweep voltammograms is conducted by varying the adimensional rate constant (Λ) and charge transfer coefficient (α). Specifically, by varying both the Λ and α on the voltammetric peak characteristics, a series of kinetic diagrams are constructed. Subsequently, sigmoidal Boltzmann functions and linear equations are presented based on the interpolation functions of these kinetic curves. The derived equations serve as user-friendly tools for calculating the electrochemical standard rate constant for quasi-reversible charge transfer. Theoretical results are validated through the examination of the electro-oxidation of ferrocyanide, as well as the electrochemical determinations of dopamine (DA), uric acid (UA), and ascorbic acid (AA) on screen-printed graphite electrodes.

Keywords: Simulation, Linear sweep voltammetry, Quasi-reversible, Standard rate constant, Detection, Ferrocyanide, Dopamine, Uric acid, Ascorbic acid, Screen-printed graphite electrodes.

Résumé

Dans cette étude, la simulation et le calcul des profils de voltampérométrie à balayage linéaire (LSV) pour les systèmes solubles-solubles quasi-réversibles sont étudiés en utilisant une approche semi-analytique. Une analyse qualitative et quantitative approfondie de la forme et de la position des voltampérogrammes à balayage linéaire est effectuée en faisant varier le coefficient de transfert de charge (α) et la constante de vitesse cinétique sans dimension (Λ). Particulièrement, en faisant varier à la fois le Λ et le α sur les caractéristiques des pics voltampérométriques tels que le courant de pic, la largeur de la demi-pic et le potentiel de pic, une série de courbes cinétiques est construite. Ensuite, des fonctions de Boltzmann sigmoïdales et des équations linéaires sont présentées sur la base des fonctions d'interpolation de ces courbes cinétiques. Les équations dérivées servent d'outils facile à utiliser pour calculer la constante de vitesse cinétique hétérogène pour le transfert de charge quasi-réversible. La validation expérimentale et théorique est réalisée sur l'oxidation du ferrocyanure, ainsi que sur la détection électrochimique de la dopamine (DA), de l'acide urique (UA) et de l'acide ascorbique (AA) sur des électrodes sérigraphiées.

Mots-clés : Simulation, Voltampérométrie à balayage linéaire, Quasi-réversible, Constante de vitesse standard, Détection, Ferrocyanide, Dopamine, Acide urique, Acide ascorbique, Electrode en graphite sérigraphiées.

الملخص

في هذه الدراسة، يتم استكشاف محاكاة وحساب بيانات الفولتمتيرية الخطية للأنظمة نصف القابلة للانعكاس القابلة للذوبان باستخدام نهج نصف تحليلي. يتم إجراء تحليل كمي ونوعي شامل لشكل وموضع البيانات الفولتمتيرية الخطية عن طريق تغيير معامل نقل الشحنة (α) وثابت معدل السرعة بلا أبعاد (Λ). على وجه التحديد، من خلال تغيير كل من معامل نقل الشحنة وثابت معدل السرعة بلا أبعاد على الخصائص الذروية للبيانات الفولتمتيرية مثل تيار الذروة، ونصف عرض الذروة، وتوتر الذروة، يتم بناء سلسلة من المنحنيات الحركية. بعد ذلك، يتم تقديم دوال بولتزمان السيني والمعادلات الخطية استنادًا إلى النماذج التكميلية لهذه المنحنيات الحركية. تعتبر المعادلات المشتقة أدوات سهلة الاستخدام لحساب الثابت السرعي البعدي لنقل الشحنة نصف قابلة للانعكاس. يتم إجراء التحقق من التجربة-النظرية على أكسدة الفيروسيانيد، بالإضافة إلى الكشف الكهروكيميائي للدوبامين، وحمض البوليك، وحمض الأسكوربيك على الأقطاب المطبوعة على الشاشة.

الكلمات الرئيسية: محاكاة، الطريقة الفولتميتيرية الخطية، نصف قابلة للانعكاس، ثابت السرعة القياسي، الكشف، الفيروسيانيد، الدوبامين، حمض البوليك، حمض الأسكوربيك، على الأقطاب المطبوعة على الشاشة.

TABLE OF CONTENTS

CHAPTER I

Background and literature review on electrochemistry and voltammetry

CHAPTER II

Introduction to sensors and literature review of electrochemical detection of dopamine, uric acid and ascorbic acid

CHAPTER III

Simulation and experimental method

CHAPTER IV

Simulation and analysis of linear sweep voltammetry for soluble-soluble quasi-reversible systems

CHAPTER V

Experimental and modelling study of electrochemical sensor for Dopamine Uric acid and ascorbic Acid detection

NOMENCLATURE

I	Current, A
n	Number of electrons
F	Faraday's constant, C mole^{-1}
A	Surface area of electrode, cm^2
D_{Ox}	Diffusion coefficient of oxidized species (Ox), cm^2 s^{-1}
D_{Red}	Diffusion coefficient of reduced species (Red), cm^2 s^{-1}
k^0	Standard rate/speed constant, cm s^{-1}
α	Anodic charge transfer coefficient
β	Cathodic charge transfer coefficient
R	Universal gas constant, J K^{-1} mol^{-1}
T	Absolute temperature, K
E	Electrode potential, V
E_f^0	Equilibrium potential, V
E^0	Standard potential, V
E_i	Initial potential, V
ΔE_{pp}	Peak-to-peak potential separation, V
v	Scan rate/speed, V s^{-1}
T	Time, s
Λ	Dimensionless/Adimensional kinetic rate/ speed parameter
σ	Dimensionless/Adimensional scan rate/speed
Φ	Dimensionless/Adimensional applied potential
χ	Dimensionless/Adimensional current
δ	Small time interval

LIST OF ABBREVIATIONS

LSV	Linear sweep voltammetry
CV	Cyclic voltammetry
PDEs	Partial differential equations
DPV	Differential pulse voltammetry
SWV	Square wave voltammetry
SPGE	Screen-printed graphite electrode
GCE	Glassy carbon electrode
CPE	Carbon paste electrode
WE	Working electrode
RE	Reference electrode
DA	Dopamine
UA	Uric acid
AA	Ascorbic acid
LOD	Limit of detection

LIST OF TABELS

LIST OF FIGURES

Introduction

Introduction

This thesis focuses on the study of electrochemical systems via potential sweep voltammetry technique. The reactions of electron transfer are involved in electrochemical systems, and depending on the nature of the participating redox species, two important kinds of electrochemical systems are considered: soluble-insoluble and soluble-soluble systems. This work focuses on the latter, which has been extensively studied in a various application involving electrochemical sensing [1].

In electrochemical systems investigation, voltammetry stands out as one of the main sophisticated electro-analytical techniques. It is based on applying of the scanning potential onto the systems, and measuring the corresponding current. The recorded data can be represented graphically on coordinate axes, where current is plotted versus potential, resulting in a plot known as a voltammogram [2]. Among several types of voltammetry, linear scanning voltammetry and cyclic voltammetry are extensively utilized for characterizing electrochemical systems owing to their advantages in obtaining easily electrochemical information on kinetic and thermodynamic data for the systems under study [3-7].

In voltammetric analysis, the position and shape of the peak are helpful tools for evaluating electrochemical systems. However, obtaining insights into kinetic and thermodynamic properties of electrochemical process is not always feasible, due to the less interpretation of voltammteric data. With this regard, simulation computer becomes an attractive alternative and successful approach for analyzing electrochemical processes, and getting a qualitative and quantitative interpretation of the experimental voltammetric data. [1, 8-10].

In this context, several theoretical studies of LSV and CV have been reported with different reversibility degrees (reversible, quasi-reversible or totally irreversible) and for a given type of solubility of redox couples (soluble-soluble or soluble-insoluble).

Moreover, and in terms of quantifying the kinetics and the reversibility of electron transfer, the estimation of the standard rate constant k^0 stands as crucial. Various diagnostic criteria as well as working curves have been established from LSV and CV data under different types of reversibility, which make it possible for the experimenter to determine the rate constant.

In this direction, for soluble-insoluble system, Atek et al. [11] presented an in-depth analysis via linear scanning voltammetry under quasi-reversible condition, in which kinetic diagrams have been established adding to that a series of useful equations were represented which enables an easy estimation of k^0. For quasi-reversible soluble-soluble system, Matsuda and Ayab [12] have reported a well-known paper for estimating k^0. In their study, different kinetic diagrams have been introduced. While these diagrams provide a rough estimation of the k^0, but they remain insufficient for quantitative analysis.

Nevertheless, to our knowledge, there are no practical equations in literature that allow to determine directly the k^0, for soluble redox couples using LSV method.

The main objectives of this thesis are:
- Calculation of theoretical LS voltammograms for soluble-soluble quasi-reversible systems via semi-analytical simulation.
- Development of practical equations from linear sweep data to use in direct calculation of standard rate constant of soluble-soluble systems whatever the degree of the reversibility.

Essential to our objectives is the validation of theoretical results, demonstrating the utility and the precision of our developed equations with experimental studies. First, an electrochemical oxidation of ferrocyanide was tested on screen-printed graphite electrodes. Next, an electrochemical detection application for three biomolecules (dopamine, uric acid, and ascorbic acid) was conducted.

Within this thesis, background information on basic theories in electrochemistry, as well as the principles of electrochemical techniques are presented in the first chapter. The second chapter provides an overview to the electrochemical sensor, focusing on the application of screen-printed electrodes for electrochemical detection of biomolecules via voltammetry techniques. The third chapter describes the basics of simulation and experimental procedures used in the subsequently chapters. In the fourth chapter, a theoretical study of LSV for soluble redox reactions with Butler-Volmer kinetics using a semi-analytical simulation was presented. In particular, new equations for calculation the rate constant k^0 using peaks characteristics of linear sweep voltammetry data are developed. Testing and validation of the developed equations are also introduced. The fifth chapter comprises two parts, in the first part an investigation of the cyclic voltammetry for an electrochemical detection of three interesting biomolecules including, dopamine, uric acid and ascorbic acid was presented and discussed. The second part

focuses on the use of the developed equations introduced in chapter 4 to determine of the standard rate constant for the electro-oxidation of dopamine, uric acid and ascorbic acid. Finally, a simulation of linear sweep voltammetry responses of these three biomolecules was established and discussed.

References

[1] A.J. Bard, L.R. Faulkner, Electrochemical Methods — Fundamentals and Applications, *Wiley*, New York, 1980.

[2] N. Elgrishi, K.J. Rountree, B.D. McCarthy, E.S. Rountree, T.T. Eisenhart, J.L. Dempsey, *Journal of Chemistry Education*, 95 (2018) 197–206.

[3] T. Gueshi, K. Tokuda, H. Matsuda, *Journal of Electroanalytical Chemistry*, 101 (1979) 29–38.

[4] J. Gonzalez-Velasco, *Electroanalysis*, 6 (1994) 711–724.

[5] F. Lantelme, E. Cherrat, *Journal of Electroanalytical Chemistry*, 244 (1988) 61–68.

[6] C.A. Basha, M.V. Sangaranarayanan, *Journal of Electroanalytical Chemistry*, 261 (1989) 431–436.

[7] T. Suzuki, I. Mori, H. Nagamoto, M.M. Ito, H. Inoue, *Journal of Electroanalytical Chemistry*, 324 (1992) 397–404.

[8] R.G. Compton, E. Laborda, K.R. Ward, Understanding Voltammetry: Simulation of Electrode Processes, *Imperial College Press*, London, 2014.

[9] G. Codina, G. Sanchez, A. Aldaz, *Electrochimica Acta*. 36 (1991) 1129–1133.

[10] Keith B. Oldham, Jan C. Myland, *Electrochimica Acta*, 56 (2011) 10612–10625.

[11] I. Atek, *Journal of Electroanalytical Chemistry*, 818 (2018) 35–43.

[12] H. Matsuda, Y. Ayabe, *Zeicschrift Elektrochemie*, 59 (1955) 494–503.

CHAPTER I

Background and literature review on electrochemistry and voltammetry

I.1. Introduction

This chapter outlines some basic concepts and insights into electrochemical fundamentals. Electrode process, mass transport, steps of electrode process, Faradaic and non-Faradaic processes, kinetics of the electrode and the electrochemical cell configuration are presented. Following this, voltammetric techniques used in this thesis are described. Then, the literature review about voltammetry simulation for electrochemical systems is introduced.

I.2. Electrochemical fundamentals

I.2.1. Electrode process

Electrochemical system is the study of charge transfer across the interface between an electrode and an electrolyte [1]. An electrode is a material considered as an electronic conductor in which charged particles (electrons) can move due the influence of an electric field. Common electrode materials comprise solid metals (e.g., Pt, Au), liquid metals (Hg, amalgams), carbon (graphite), and semiconductors (such as indium-tin oxide, Si). An electrolyte is a material considered to be an ionic conductor in which the mobile species are ions. Ionic conductors include molten salts, dissociated salts in solution, and some ionic solids [2].

Typically, an electrochemical system comprises two electrodes connected to an external electronic circuit and separated by an electrolyte. Ions cross from one electrode to the next through the electrolyte, and electrons flowing through the electrodes complete the circuit [2].

I.2.2. Electrical Double Layer (EDL)

When the electrode acquires charged particles on its surface, comes into contact with an electrolyte containing ions. An attractive interaction occurs between the charged surface and the ions in the electrolyte under an electric field gradient, leading to formulation of an electrical double layer between the electrode and electrolyte [3]. Multiple models have been proposed to elucidate the structure of the EDL.

The initial model was suggested by Helmholtz, who described the electrical double layer structure as a basic parallel plate capacitor. According to this model, the ions within electrolyte are necessary to equilibrium the charge on the electrode with an opposing layer of oppositely charged and solvated ions. The separation between the electrode surface and solvated ions is commonly referred to as the "Outer Helmholtz Plane" (OHP). In this distance, a linear potential drop occurs [4].

The Helmholtz model was further improved through the contributions of Gouy and Chapman by considering the distribution of ions. They introduced the concept of a diffuse layer, wherein ions exhibit random thermal motion and interact with the electrode surface. Subsequently, Stern proposed a new model of the double-layer structure based on the Helmholtz and Gouy-Chapman models. The Stern model integrated the inner compact layer referred to as the Helmholtz layer and a diffuse layer as presented in the model of Gouy and Chapman [4]. Figure I.1 shows the distribution of potential in Helmholtz, Gouy-Chapman and Stern models of EDL.
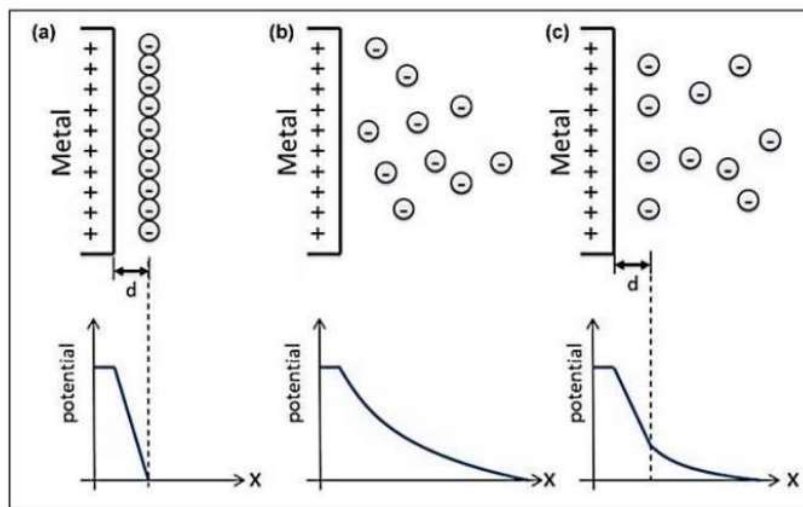
Figure I.1. Schematic illustration of the potential distribution in the electrical double layer based on different models: (a) Helmholtz, (b) Gouy-Chapman and (c) Stern [5].

In the Grahame model (Fig. I.2), which proposed a further refinement of the Stern model, the compact plane is subdivided into two distinct planes: the inner Helmholtz plane (IHP) and the outer Helmholtz plane (OHP). The inner Helmholtz plane (IHP) consists of specifically adsorbed anions and solvent molecules on the surface of the electrode. In contrast, the outer Helmholtz plane (OHP) comprises of solvated ions and nonspecifically adsorbed ions [6].
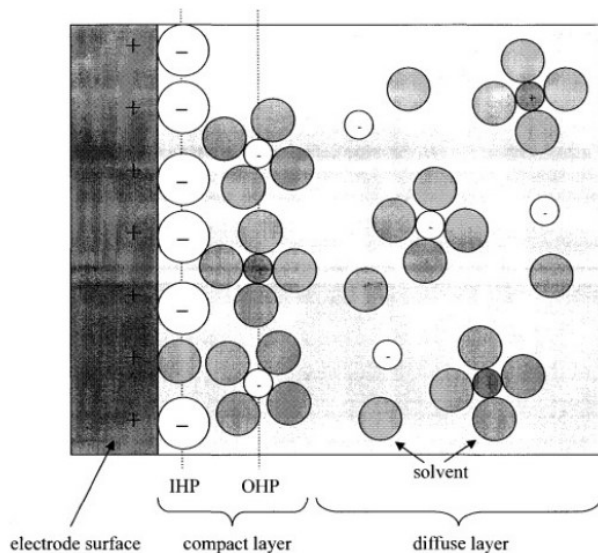
Figure I.2. Illustration of the Grahame model of the electrical double layer [6].

I.2.3. Steps of electrode process

At the electrode/electrolyte interface, an electrochemical reaction takes place, in which different steps of processes and phenomena that characterize the mechanism of an electrochemical electrode reaction. A simplified representation of the electrode reaction mechanism is presented in Fig. I.3. The first step is mass transport i.e. the displacement of the electroactive species from the bulk solution towards the electrode surface. The second one is the electrons transfer at the electrode surface. Additionally, chemical reactions and other surface reactions such as adsorption or desorption preceding or following the electron transfer can also occur [7].
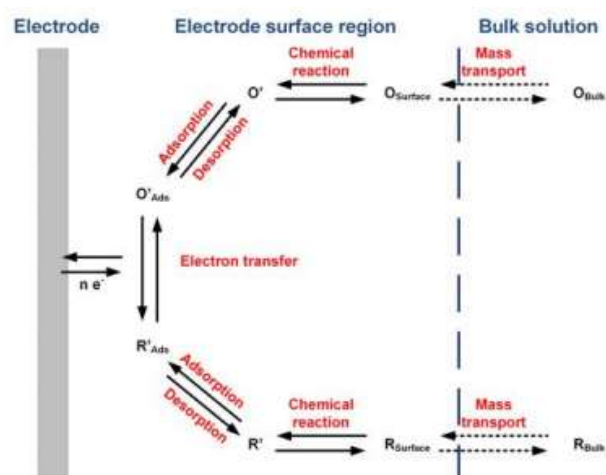
Figure I.3. Schematic mechanism of essential steps for electrode reactions [8].

I.2.4. Mass transport

The mass transfer of electro-active species from the bulk solution to the electrode-solution interface is considered as an interesting phenomenon influencing the performance of an electrochemical reaction. Mass transport and electrons transfer determine the rate of electrochemical reaction at the electrode surface. The three main modes of mass transport that have an influence on a reaction are: diffusion, migration, and convection [9, 10].

I.2.4.1. Diffusion

Diffusion is the spontaneous movement or transport of electroactive species driven by a concentration gradient between the electrode surface and solution. The diffusion process can be quantified by Fick's first and second laws, which describe the dependence between the rate of diffusion and the changes in concentration gradient [11, 12].

Fick's Laws

Fick's laws describe the change in the diffusive flux of an electroactive species and its concentration as functions of time and position. In the case of one dimension (linear diffusion), Fick's first law quantifies the diffusional flux of the electroactive species that is proportional to concentration gradient with the diffusion coefficient D and it is given by the following equation:

$$J = -D\frac{\partial C}{\partial X} \tag{1}$$

Where J is the diffusional flux of the electroactive species, $\frac{\partial C}{\partial X}$ is the concentration gradient of the electroactive species at diffusion distance X, D is the diffusion coefficient of the electroactive species. Fick's second law describes the change in concentration of the electroactive species over time and position in a single spatial dimension by the equation as follows:

$$\frac{\partial C}{\partial t} = D\frac{\partial^2 C}{\partial X^2} \tag{2}$$

I.2.4.2. Migration

Migration represents the movement of charged species due to the influence of an electric field. And it is given by equation [13]:

$$J = \frac{zF}{RT} DC\Delta\phi \tag{3}$$

J is the migration flux, z is the charge of the species, $\Delta\phi$ is the electrical filed gradient.

Thus, an electrical field arises owing to the potential drop across the electrode-solution interface, which can be generated due to the migration of charged species. Hence, the migration of charged species can be neglected during the electrochemical experiment, by addition of a large quantity/concentration of supporting electrolyte. This adding of supporting electrolytes decreases the potential drop at the electrode-solution interface [14].

I.2.4.3. Convection

Convection is the movement of species in solution due to different internal and external forces. It can be generally classified as "natural" or "forced". Natural convection can arise usually from the gradient of density in the bulk solution due to a change at the electrode surface, or thermal differences. The electrochemical experiments are often restricted for short time periods, in which the effect of naturel convection is minimized. Forced convection takes place in which an external force is applied to the solution such as stirring solution, which can be achieved by using a rotating disc electrode [9, 15].

I.2.5. Faradaic and non-Faradaic processes

There are two types of processes that can take place at the electrode-solution interface known as Faradaic and non-Faradaic. In a Faradaic process, charges are transferred across the electrode-solution interface which leads in an oxidation or reduction to occur. This processes is described by the law of Faraday:

$$N = \frac{Q}{zF} \tag{4}$$

Where N is the amount in moles of reactants, Q is the charge that is transferred across the electrode-solution interface and z is the number of electrons passed per ion and F is the Faraday constant. On the other hand, a non-faradaic processes occur due to adsorption and desorption processes at the electrode-solution interface as well as changes in the potential of the electrode or the composition of the solution [10].

I.2.6. The Nernst equation

Let us consider the generalized electrode reaction of a one-electron transfer:

Chapter I

$$Ox + e^- \rightleftarrows Red \tag{5}$$

Where Ox is the oxidized species in a bulk solution, which gains an electron from the electrode to form Red, the reduced species.

In an electrochemical reaction, the electrical potential of the electrode is related to the changes of the electroactives species in the solution, which introduced the electrochemical potential of the electroactives species j (Ox, Red), and it can be expressed by the following equation [8]:

$$\bar{\mu}_j = \mu_j + Z_j F\phi \tag{6}$$

Where Z_j is the charge of species j and ϕ is the electrical potential in solution, μ_j is the chemical potential rewritten as,

$$\mu_j = \frac{\partial G_j}{\partial N_j} \tag{7}$$

Which is the gradient between its Gibbs energy (G_j) and molar quantity (N_j). Thus, the chemical potential of species in solution would be:

$$\bar{\mu}_j = \mu_j{}^0 + RT \ln \frac{a_j}{C^0} \tag{8}$$

$$a_j = \gamma_j C_j \tag{9}$$

$\mu_j{}^0$ is the standard chemical potential, a_j is the activity of species j, and γ_j corresponds to the activity coefficient. C^0 is the standard concentration, which equals to one Molar (1 mol L^{-1}). When the reaction system reaches the state of equilibrium, the Gibbs energy change is zero which leads to the balancing of the electrochemical potentials:

$$\bar{\mu}_{Ox} + \bar{\mu}_e = \bar{\mu}_{Red} \tag{10}$$

Hence, according to the electrochemical potential equation eq. (6), given as:

$$(\mu_{Ox} + Z_{Ox}F\phi_s) + (\mu_e - Z_e F\phi_e) = (\mu_{Red} + Z_{Red}F\phi_s) \tag{11}$$

Then,

$$\left(\mu_{Ox}{}^0 + RT \ln \frac{a_{Ox}}{C^0} + Z_{Ox}F\phi_s \right) + (\mu_e{}^0 - F\phi_e) = \left(\mu_{Red}{}^0 + RT \ln \frac{a_{Red}}{C^0} + Z_{Red}F\phi_s \right) \tag{12}$$

Where ϕ_s and ϕ_e are the electric potential at the solution and the electrode, respectively. Thus, the interfacial potential difference is [16]:

$$\phi_e - \phi_s = \frac{1}{F}\left(\mu_{Ox}{}^0 + \mu_e{}^0 - \mu_{Red}{}^0\right) + \frac{RT}{F}\ln\left(\frac{a_{Ox}}{a_{Red}}\right) \tag{13}$$

By replacing $\Delta\mu^0 = \mu_{Ox}{}^0 + \mu_e{}^0 - \mu_{Red}{}^0$ in eq. (13), it can be written as:

$$\phi_e - \phi_s = \frac{1}{F}\Delta\mu^0 + \frac{RT}{F}\ln\left(\frac{a_{Ox}}{a_{Red}}\right) \tag{14}$$

As a result, the recorded potential difference between the working electrode (WE) and the reference electrode (RE) is. [16]:

$$E = (\phi_e - \phi_s) - (\phi_e^r - \phi_s^r) \tag{15}$$

Which is:

$$E = \frac{1}{F}\Delta\mu^0 + \frac{RT}{F}\ln\left(\frac{a_{Ox}}{a_{Red}}\right) - (\phi_e^r - \phi_s^r) \tag{16}$$

Using the activity definition of species Ox and Red, the following is given:

$$E = \frac{1}{F}\Delta\mu^0 + \frac{RT}{F}\ln\left(\frac{\gamma_{Ox}C_{Ox}}{\gamma_{Red}C_{Red}}\right) - (\phi_e^r - \phi_s^r) \tag{17}$$

Thus:

$$E = \frac{1}{F}\Delta\mu^0 + \frac{RT}{F}\ln\left(\frac{\gamma_{Ox}}{\gamma_{Red}}\right) - (\phi_e^r - \phi_s^r) + \frac{RT}{F}\ln\left(\frac{C_{Ox}}{C_{Red}}\right) \tag{18}$$

The standard electrode potential E^0 is expressed as follows:

$$E^0 = \frac{1}{F}\Delta\mu^0 - (\phi_e^r - \phi_s^r) \tag{19}$$

The formal potential E_f^0 is:

$$E_f^0 = E^0 + \frac{RT}{F}\ln\left(\frac{\gamma_{Ox}}{\gamma_{Red}}\right) \tag{20}$$

Hence, the equation (18) becomes:

$$E = E_f^0 + \frac{RT}{F}\ln\left(\frac{C_{Ox}}{C_{Red}}\right) \tag{21}$$

This equation is the well-known form of the Nernst equation.

I.2.7. The Butler-Volmer relationship

In electrode kinetics, the Butler-Volmer equation is a fundamental equation that describes the relationship between the rate of electron transfer reactions at the electrode-solution interface and the potential (voltage) applied to the electrode. It plays a crucial role in understanding and modeling electrochemical processes [17].

According the following simple electrochemical equilibrium reaction simple:

$$Ox + ne^- \underset{k_{Ox}}{\overset{k_{Red}}{\rightleftarrows}} Red \tag{22}$$
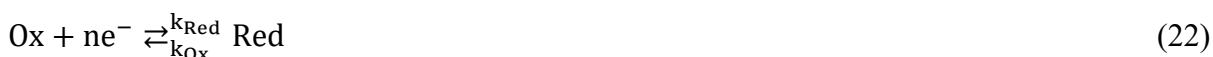
k_{Red} and k_{Ox} are the reduction and oxidation heterogeneous rate constants respectively.

At the electrode-solution interface, the electron transfers due to electron flux (J) between the electrode and the species in solution leads to the generation of a faradic current through the electrode [13, 18], which can be given by equation:

$$I = nFA_e J \tag{23}$$

Where A_e is the electrode area, J is the heterogeneous reaction flux at the electrode-solution interface. *I* is the faradic current recorded, which is a combination of the cathodic current I_c (the negative contribution from the reduction of Ox) and the anodic current I_a (the positive contribution from the oxidation of Red) expressed as [13]:

$$I = I_a + I_c \tag{24}$$

The net heterogeneous reaction flux *J* is:

$$J = k_{Red}[Ox]_{x=0} - k_{Ox}[Red]_{x=0} \tag{25}$$

Where $[Ox]_{x=0}$ and $[Red]_{x=0}$ are the surface concentrations of the electroactive species at surface electrode. The heterogeneous rate constant for a redox reaction at an electrode-solution interface is influenced by various conditions, including temperature, potential, transition state, and pressure [9, 10].

The transition state theory states that an electrochemical reaction proceed by passing through a well-defined transition state or activated complex [19]. Figure I.4 shows the standard Gibbs energy profiles for an electrochemical reaction. The change in the standard Gibbs energy is related to the electrode potential, and it can be expressed by the following expression [18]:

$$\Delta G = -nF\Delta E = -nF(E - E_f^0) \tag{26}$$

The standard Gibbs energy can be described for the forward (anodic) reaction by the following equation [13, 18]:

$$\Delta G_{Red}^{\neq} = \Delta G_{0,Red}^{\neq} - \alpha F(E - E_f^0) \tag{27}$$

For reverse (cathodic) reaction is:

$$\Delta G_{Ox}^{\neq} = \Delta G_{0,Ox}^{\neq} - \beta F(E - E_f^0) \tag{28}$$

Where $\Delta G_{Red}^{\neq}$ and $\Delta G_{Ox}^{\neq}$ are the standard Gibbs energies of activation for the respective oxidation and reduction reactions. α and β are the anodic and cathodic transfer coefficients, respectively.

According to the Arrhenius equation, which describes the temperature dependence of rate constants for oxidation and reduction reactions k_{Red} and k_{Ox}. It is given as follows:

$$k_{Red} = A_{Red}\, exp\left(\frac{-\Delta G^{\neq}_{Red}}{RT}\right) \tag{29}$$

$$k_{Ox} = A_{Ox}\, exp\left(\frac{-\Delta G^{\neq}_{Ox}}{RT}\right) \tag{30}$$

A_{Red} and A_{Ox} are the pre-exponential factors for the oxidation and reduction reactions respectively.

Using relations of $(\Delta G_{Red}^{\neq})$ and $(\Delta G_{Red}^{\neq})$ in eqs. (29, 30) yields:

$$k_{Red} = A_{Red}\, exp\left(\frac{-\alpha F(E - E_f^0)}{RT}\right) \tag{31}$$

$$k_{Ox} = A_{Ox}\, exp\left(\frac{\beta F(E - E_f^0)}{RT}\right) \tag{32}$$

When the system is at equilibrium, the concentration of active species are equal:

$$J = k_{Red}[Ox]_{x=0} - k_{Ox}[Red]_{x=0} = 0 \tag{33}$$

Thus,

$$k_{Red}[Ox]_{x=0} = k_{Ox}[Red]_{x=0} \tag{34}$$

$$k^0 = k_{Red} = k_{Ox} = A_{Red} \exp\left(\frac{-\alpha F(E - E_f^0)}{RT}\right) = A_{Ox} \exp\left(\frac{\beta F(E - E_f^0)}{RT}\right) \qquad (35)$$

Where, k^0 is the standard rate constant, and the rate constants k_{Red} and k_{Ox} can be written in term of k^0 as:

$$k_{Red} = k^0 \exp\left(\frac{-\alpha F(E - E_f^0)}{RT}\right) \qquad (36)$$

$$k_{Ox} = k^0 exp\left(\frac{\beta F(E - E_f^0)}{RT}\right) \qquad (37)$$

Substituting Equations eq. (36) and eq. (37) into Eq. (33) yields:

$$J = k^0 [Ox]_{x=0} \exp\left(\frac{-\alpha F(E - E_f^0)}{RT}\right) - k^0 [Red]_{x=0} \exp\left(\frac{\beta F(E - E_f^0)}{RT}\right) \qquad (38)$$

By replacing Eq. (38) in Eq. (23), the equation becomes as follows :

$$I = nFA_e k^0 \left[[Ox]_{x=0}\exp\left(\frac{-\alpha F(E - E_f^0)}{RT}\right) - [Red]_{x=0}\exp\left(\frac{\beta F(E - E_f^0)}{RT}\right)\right] \qquad (39)$$

It represents the potential-current relationship, which corresponds to the well-known Butler-Volmer equation [17].
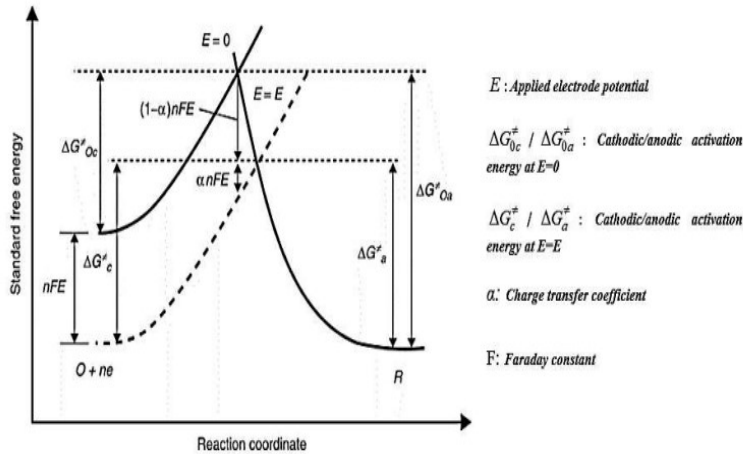
Figure I.4. Standard Gibbs energy profiles for electron transfer reaction [20].

1.2.8. The Tafel equation

According to the Butler-Volmer equation, the electrode current depends on the overpotential ($\eta = E - E_f^0$) and the transfer coefficients (α and β). Furthermore, when the

overpotential is higher and positive, the oxidation term is predominant and the reduction term becomes negligible [14]. The Butler-Volmer equation can be written as:

$$I_{Red} = nFA_e k^0 \left[[Ox]_{x=0} \exp\left(\frac{-\alpha F(E - E_f^0)}{RT}\right) \right] \tag{40}$$

Similarly, when the overpotential is higher and negative, the reduction term dominants and the oxidation term is neglected yields:

$$I_{Ox} = nFA_e k^0 \left[[Red]_{x=0} \exp\left(\frac{\beta F(E - E_f^0)}{RT}\right) \right] \tag{41}$$

By considering that the concentration of species are constant. It follows that the above equations are given by:

$$\ln(I_{Red}) = \frac{-\alpha F(E - E_f^0)}{RT} + C_1 \tag{42}$$

$$\ln(I_{Ox}) = \frac{\beta F(E - E_f^0)}{RT} + C_2 \tag{43}$$

These equations (42, 43) are called the Tafel equations [21].

I.3. Electrochemical Cell

An electrochemical cell is the basic of experimental setup in the electrochemistry measurements, which consists of an electrolyte and 3 electrodes [10]: the working electrode (WE), the reference electrode (RE) and the counter electrode (CE) as the scheme shown in **Fig. I.5**. The electrolyte in electrochemical cell containing electro-inactive species, which are not interfered with electrochemical reaction of interest. Higher concentration of electrolyte increases the conductivity of the solution and prevents the migration effect [10, 22].

In electrochemical experiments, the three electrodes are controlled by a potentiostat, which used to impose a fixed potential E between the working electrode and the reference electrode, and followed by measuring the current between working electrode and counter electrode. The working electrode is where the redox reaction of interest occurs. The reference electrode plays important role in electrochemical equilibrium, it serves to provide a stable potential throughout the measurement at the working electrode. The commonly used reference electrodes are the standard hydrogen electrode (SHE), the saturated calomel electrode (SCE) and the silver/silver chloride electrode (Ag/AgCl). The counter electrode, also called as the auxiliary electrode, has the purpose of completing the electrical circuit in the electrochemical

system. It is made of conductive but inert material. Common materials for counter electrodes include platinum, carbon electrodes [10, 23-24].
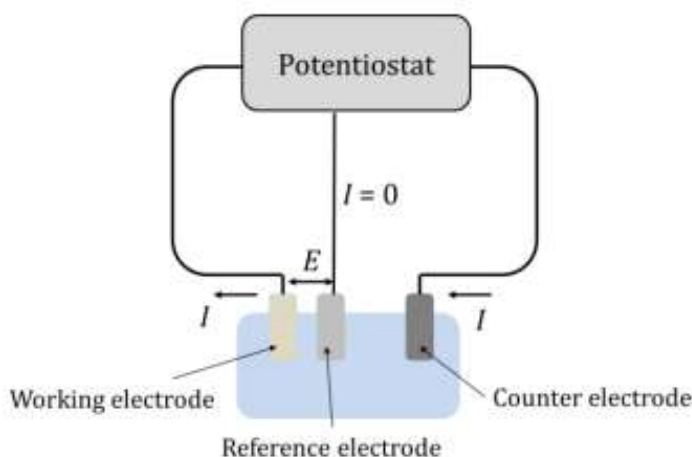
Figure I.5. Schematic representation of typical electrochemical cell controlled by a potentiostat [3].

I.4. Voltammetry techniques

The linear sweep voltammetry (LSV) and cyclic voltammetry (CV) methods are the most powerful and extensively employed electroanalytical methods for studying electrochemical processes, understanding reaction mechanisms and quantifying the kinetics [9, 25-27]. Their principle is measuring the current at the (WE) as function of an applied potential [9, 15]. In this section, both linear sweep voltammetry (LSV) and cyclic voltammetry (CV) were introduced, and utilized throughout this thesis.

I.4.1. Linear Sweep Voltammetry

LSV is performed by scanning the potential in one direction linearly from a starting potential E_i to a second potential E_f as function of time, at a scan rate (v).The potential waveform is given as (Fig. I.6 (a)) [26, 27]:

$$E = E_i \mp vt \tag{44}$$

The interval potential between E_i and E_f is chosen to cover the oxidation or reduction process of interest. The resulting current is recorded through the working electrode as function of the applied potential and a plot of current versus potential is known as a voltammogram. A typical linear sweep voltammogram is illustrated in Fig. I.6 (b).
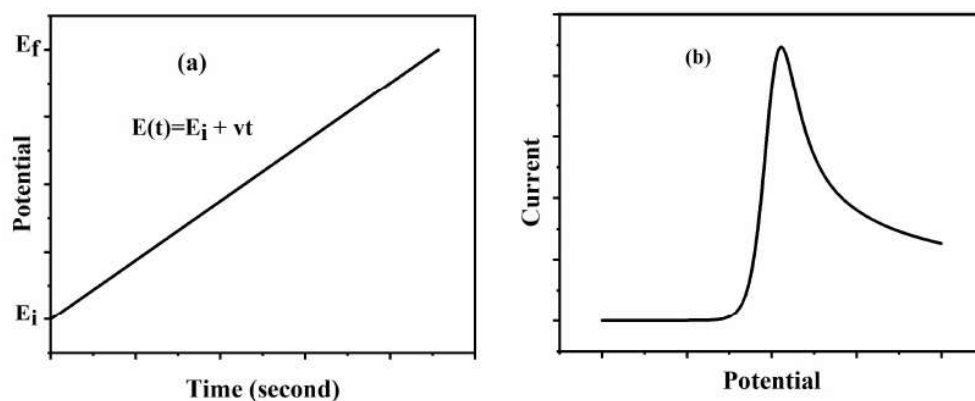
Figure I.6. (a) The potential waveform in linear sweep voltammetry. (b) Linear sweep voltammogram.

I.4.2. Cyclic Voltammetry

CV is similar to LSV, but it involves both forward and reverse direction scans in a cyclic manner. In CV, the potential is applied linearly on the (WE) from an initial potential, E_i to a second potential, E_λ, and then, at time t_λ swept back in the reversed direction to E_i.

The triangular potential waveform is illustrated in Fig. I.7 (a) and is given by the following equations [28, 29]:

$$E = E_i \pm vt, t \in [0, \lambda] \tag{45}$$

$$E = E_\lambda - vt = E_i \pm 2v\lambda - vt, t > \lambda \tag{46}$$

Where the positive or negative (±) signs indicate oxidation or reduction sweeps. The current is measured against the potential in both scan direction, resulting in a cyclic voltammogram (Fig. I.7 (b)).
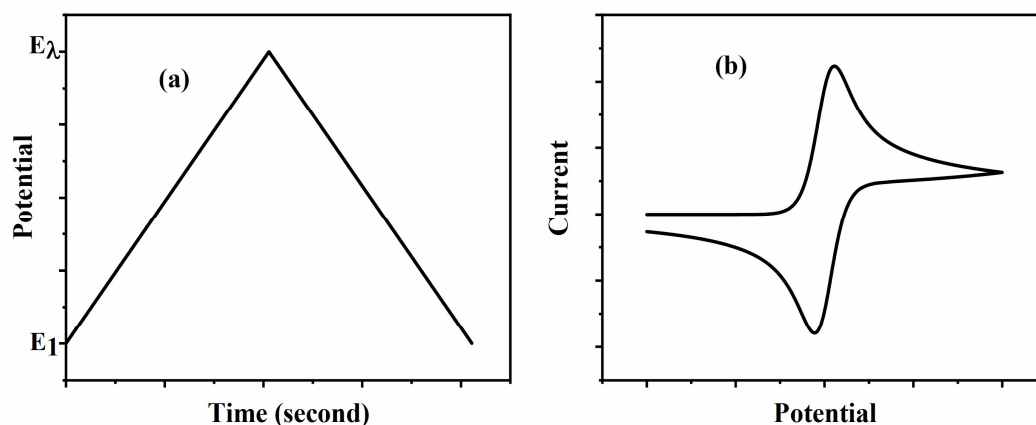
Figure I.7. (a) The triangular potential waveform used in cyclic voltammogram. (b) Cyclic voltammogram profile.

For the quantitative analysis through cyclic and linear sweep voltammetry, important parameters that can be used to distinguish the reversibility of electron transfer reactions are the current peak, the potential peak, the half width peak, peak to peak potential separation and peak to peak current ratio [15, 26].

I.5. Mathematical modeling methods of voltammetry simulation.

Voltammetric experiments can give estimable information on both the kinetics and thermodynamics of electrochemical systems, based on the analysis of the shape and position of LSV and CV voltammograms. In addition to enhance voltammetric analysis, simulation is an insightful tool that helps better understanding the experiments, and by concordance between simulation and experimental results, evidence for a reaction mechanism may be fully achieved [9-10, 29-30].

In the context of voltammetry, the simulation is based on solving the partial differential equations (PDEs) defining diffusion mass transport of the electrochemical system with respect to initial and boundary conditions. The solution of the system is a concentration profile of electroactive species, then the system is given as the current-potential-time response. Three types of simulation method can be used to solve PDEs: analytical, semi-analytical and numerical methods [31].

- The analytical method is an approach that yields exact mathematical solutions for voltammetric responses prediction. It involves direct analysis between the experimental variables and certain conditions. Unfortunately, the analytical solution is not applicable in all

cases due to the complexity of the electrochemical problems. In contrast, numerical method is the preferred approach over analytical ones due to their greater effectiveness [9, 32-33].

- The numerical method provides an approximate solution to solve PDEs in order to predict current-potential relationship. It requires the discretization of the governing equations in both time and space. Therefore, numerical analysis is processed by a computer or computational model to solve problems (PDEs) [7, 33-34].

- The Semi-analytical method is a combination of both analytical and numerical methods used to solve the fully voltammetric problem. In which the analytical method can be used firstly to solve the partial differential equations (PDEs) to obtain an integral equation using an integral transform approach as the Laplace transform, next, the numerical method is required for the discretization the time variable [35, 36]. In the present work, the semi-analytical method is used.

I.6. Literature survey of voltammetric simulation results for soluble-soluble reaction

I.6.1. Some important studies for LSV and CV theories for soluble-soluble system

Electrochemical systems including soluble-soluble, soluble-insoluble systems have been theoretically analyzed via LSV and CV techniques. Subsequently, this section will summarize the important studied on the theoretical linear sweep and cyclic voltammetry related to the electrochemical soluble-soluble systems.

In 1954, **Randles and Ševčík** were the pioneers who studied theoretically the linear sweep voltammetry for reversible reaction [37, 38]. In their study, which is considered as one of the most mentioned publication in electrochemical studies, they developed a well-known relationship describing the voltammetric peak current. **Matsuda and Ayab** (1950) have reported the theory of LSV in the case of quasi-reversible reaction [39]. They have proposed a series of diagrams that analyzed the dependence of the kinetic parameters on the voltammetric peaks, which allows the estimation of heterogeneous rate constants of electrochemical reaction. The results of Matsuda's work will be discussed in the following section. In 1964, **Nicholson and Shain** [40] presented an extensive theoretical study of CV in various coupled reaction types for reversible and irreversible charge transfer. Following **Nicholson's** paper (1965), the theory of CV has been extended for quasi-reversible reaction [41]. In which, their theoretical analysis is based on the relationship between the peak-to-peak potential and the non-

dimensional kinetic rate. Another investigation which has recently studied cyclic voltammetry with the effect of the adsorption was presented by **Samin** [42].

Additionally, the multi-steps systems including electrochemical reaction associated with chemical or adsorption–desorption processes have been studied theoretically through cyclic voltammetry technique [43, 44].

I.6.2. Survey of important theoretical results of LSV and CV for soluble-soluble systems

In what follows, via the application of the theory of LSV and CV for soluble-soluble reaction in three cases of reversibility: reversible, irreversible and quasi-reversible, the reversibility reflects the rate of electrochemical reaction relative to the rate of mass transport. Several criteria are deduced based on the full analysis of the voltammetric peaks of voltammograms with their dependences on scan rates. In reversible process, the electron transfer kinetics is rapid relative to mass transport. The peak current and half peak potential are described in forward oxidation direction (LSV) [37, 38] by the following expression:

$$I_p = 0.4463 \, n \, F \, AC_{Red}^* (D_{Red})^{1/2} \left(\frac{nF}{RT} \right)^{1/2} v^{1/2} \tag{47}$$

$$E_p - E_{p/2} = 2.20 \frac{RT}{nF} \tag{48}$$

The peak potential is given by [10]:

$$E_p = E_{1/2} - 1.109 \frac{RT}{nF} \tag{49}$$

In forward and reversed direction of CV, the peak to peak potential separation ΔE_{pp}, defined as the potential difference between the forward and reverse peak potential and it can be calculated by:

$$\Delta E_{pp} = 2.3 \frac{RT}{nF} \tag{50}$$

It is close to the value $\Delta E_{pp} = 57$ mV at 298 K for reversible process as Nicholson's criteria [41]. The shape of reversible voltammetric curve is presented in Fig. I.8.
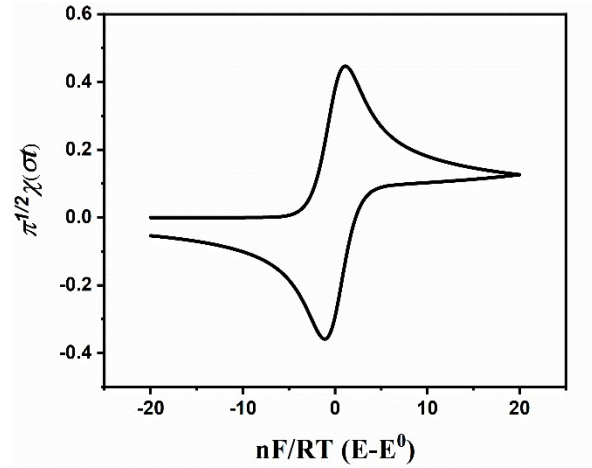
Figure I.8. Illustration of theoretical voltammogram for reversible system, where $\pi^{1/2}\chi(\sigma t)$ is the dimensionless current and $nF/RT(E-E^0)$ is the dimensionless potential.

In irreversible process, the quantification of the linear sweep voltammogram reveals slow electron transfer kinetics compared to mass transport. The current peak, the half peak width and the potential peak are given by the following expressions [10, 40]:

$$I_p = 0.4958 \, nF \, A \, C_{Red}^* (D_{Red})^{1/2} \alpha^{1/2} \left(\frac{nF}{RT}\right)^{1/2} v^{1/2} \tag{51}$$

$$E_p - E_{p/2} = 1.857 \frac{RT}{nF\alpha} \tag{52}$$

$$E_p = E^0 - \frac{RT}{nF\alpha}\left(0.780 + ln\sqrt{D_{Red}b} - \ln k^0\right) \tag{53}$$

$$b = \alpha nFv / RT$$

According to cyclic voltammograms for irreversible system, the peak to peak potential separation ΔE_{pp} is expressed by the expression:

$$\Delta E_{pp} = 2.3 \frac{RT}{\alpha F} \ln(v) + C \tag{54}$$

Where: α is the charge transfer coefficient, v is the scan rate and C is a constant.

Figure I.9 illustrates cyclic voltammograms for irreversible systems.
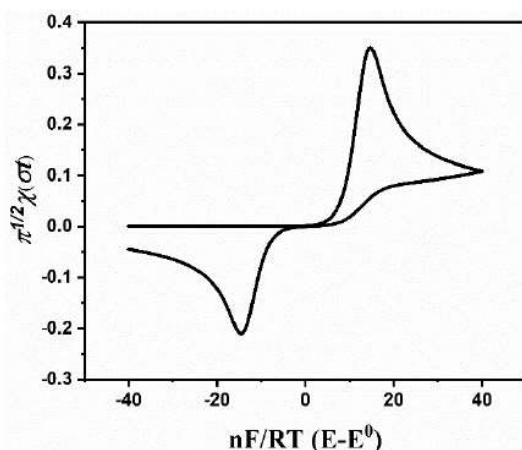
Figure I.9. Illustration of theoretical cyclic voltammogram for irreversible system.

Quasi-reversible process is a system that has intermediate features between both systems reversible and irreversible. In this process, Matsuda and Ayabe [39] have introduced a dimensionless kinetic parameter to evaluate the reversibility of electrochemical reaction.

$$\Lambda = \frac{k^0}{\sqrt{DFv/RT}} \tag{55}$$

According to Matsuda's approach in LSV analysis for quasi-reversible process, the current peak, potential peak and half peak potential are dependent on kinetic parameters. In contrast of CV analysis for quasi-reversible process, Nicholson and shain study have demonstrated that the peak to peak potential separation is also dependent on dimensionless kinetic parameters [41].in Fig. I.10, cyclic voltammetric responses for quasi-reversible system at different values of kinetic parameter (Λ) are shown.
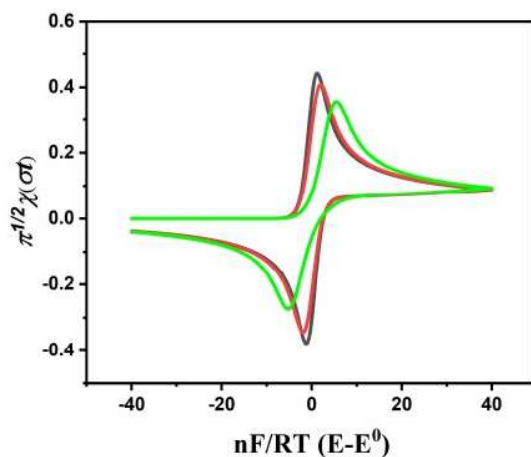
Figure I.10. Theoretical cyclic voltammograms for quasi-reversible system at different values of Λ (10^1, 1, 10^{-1}).

22

I.6.3. Survey of theoretical results for determination of standard rate constant by LSV and CV for soluble-soluble systems

The evaluation of kinetic standard rate constant is a critical step in quantifying the reversibility of electrochemical reaction kinetics. From linear sweep and cyclic voltammetry data, several approaches have been reported for the estimation of k^0 in electrochemical reaction involving soluble species. In this section, the important approaches were discussed.

Matsuda and Ayabe have established three reversibility diagrams for quasi-reversible soluble-soluble systems based on LSV analysis [39]. These diagrams presented the dependence of the voltammetric peaks characteristics: peak current, half peak width and peak potential on the adimensionl kinetic parameter Λ and charge transfer coefficient α as illustrated in Fig. I.11, in which the three diagrams allow an easy estimation of the standard rate constant whatever the degree of the reversibility.
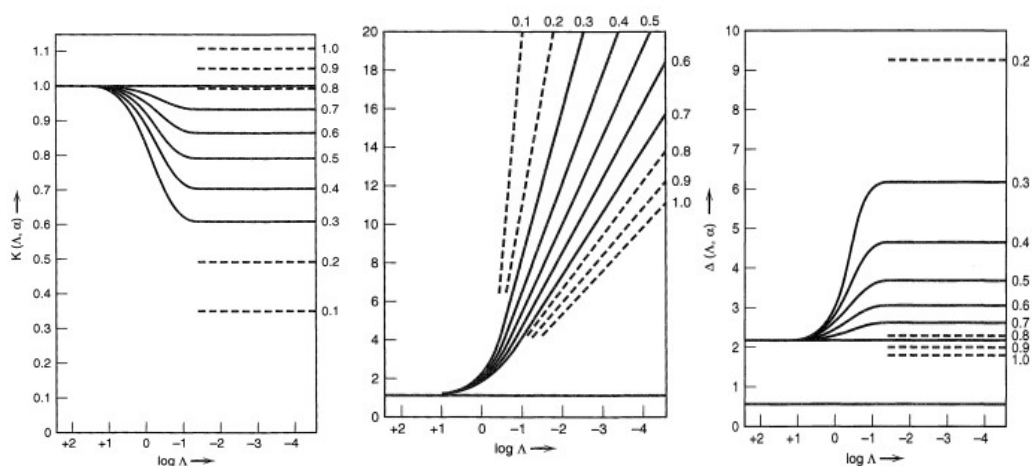
Figure I.11. Matsuda and ayab' diagrams: Variation of adimensionless voltammetric peaks with Λ for different values of α [39].

Matsuda and Ayabe also suggested the limits of three different classification of reversibility based on the kinetic parameter Λ,

For reversible system: $\Lambda \geq 15$

For quasi-reversible system: $10^{-2(1+\alpha)} \leq \Lambda \leq 15$

For irreversible system: $\Lambda \leq 10^{-2(1+\alpha)}$

Another approach has been presented by Gonzalez for electrochemical totally irreversible system using linear sweep voltammetry. In their approach, a new equation based on the half peak potential has been developed and is given as [45]:

$$k^0 = 2.415 \exp\left[-0.02 \frac{F}{RT}\right] D^{1/2} \left(E_p - E_{p/2}\right)^{-1/2} v^{1/2} \tag{56}$$

This equation enables direct determination of k^0.

Laviron [46] also introduced an approach through linear sweep voltammetry analysis in the case of diffusionless systems. He developed practical expressions specifically for irreversible systems to determine the rate constant k^0. One expression based on the peak potential is provided as:

$$E = E^0 + \frac{RT}{\alpha nF} ln\left(\frac{RTk^0}{\alpha nF}\right) + \frac{RT}{\alpha nF} lnv \tag{57}$$

Additionally, he presented another expression based on the peak-to-peak separation potential for $\Delta E_p > 200$ mV as follows:

$$\log k = \alpha \log(1 - \alpha) + (1 - \alpha) \log \alpha - \log\left(\frac{RT}{nFv}\right) - \alpha(1 - \alpha)\frac{nF}{2.3RT}\Delta E_p \tag{58}$$

From cyclic voltammetry analysis, Nicholson developed an approach for determination of standard rate constant in quasi-reversible soluble-soluble systems [41]. In this method, Nicholson established kinetic curves that displayed the peak to peak separation (ΔE_{pp}) as function of dimensionless kinetic parameter only for the value of charge transfer coefficient (α=0.5). Consequently, the determination of standard rate constant is based on the peak potential separation with different scan rates and k^0 can calculated from the following expression:

$$k^0 = \omega \frac{[\pi D_{Ox} v (nF/RT)]^{1/2}}{(D_{Ox}/D_{Red})^{\alpha/2}} \tag{59}$$

Where ω is the dimensionless kinetic parameter, $\omega = \frac{(D_{Ox}/D_{Red})^{\alpha/2} k^0}{[\pi D_{Ox} v (nF/RT)]^{1/2}}$.

The theoretical measured values of ΔE_{pp} to the corresponding value of ω for quasi-reversible systems with constant value of α=0.5, are shown in Table I.1.

Table I.1. Variation of the peak to peak potential separation ΔE_{pp} with dimensionless kinetic parameter ω at 25 °C.

ω	ΔE_{pp}
20	61
7	63
6	64
5	65
4	66
3	68
2	72
1	84
0.75	92
0.5	105
0.35	121
0.25	141
0.1	212

Klingler reported the determination of the heterogeneous rate constants by cyclic-voltammetry (CV) method for totally irreversible system [47]. In their study, an empirical equation as function of alpha for ΔE_{pp} >150 mV is developed, which is available to the determination of k^0.

$$k^0 = 2.18 \sqrt{\frac{\alpha D n v F}{RT}} \, exp\left(-\left(\frac{\alpha^2 nF}{RT}\right)\Delta E_{pp}\right) \tag{60}$$

Gileadi [48] presented a method for the calculation of the heterogeneous rate constants for reversible, quasi-reversible to irreversible electrochemical process , which is based on the the graphical approximation of the critical scan rate v_c from a plot presenting the variation of the peak potential E_p as function of the logarithm of scan rate. The value of v_c is estimated from intersection of the extrapolated lines. Furthermore, a developed equation is introduced that allows the calculation of k^0 and which given as:

$$\log k^0 = -0.48\alpha + 0.52 + \log\sqrt{\frac{nF\alpha v_c D}{2.303RT}} \tag{61}$$

Recently, **Lavagnini** introduced a further approach based on the Nicholson's procedure for quasi-reversible systems. They developed an empirical equation that described the dependence of the peak-to-peak potential separations (ΔE_{pp}) on the dimensionless kinetic

parameter $\omega = k^0[\pi D n v F /RT]^{1/2}$ when the peak separation ranges between 140 to 200 mV. Hence, the k^0 can be determined easily from this equation [49]:

$$\omega = 2.18[\beta\pi]^{1/2} \exp\left[-(\beta^2 F/RT)n\Delta E_{pp}\right] \tag{62}$$

I.7. Conclusion

This chapter has presented a brief overview on the fundamental electrochemistry and techniques necessary to support the discussions in this thesis. The following chapter provides an introduction to the electrochemical detection based on screen-printed electrodes sensor, particularly, their importance in detection of biological molecules.

References

[1] S. Petrovic, Basic Electrochemistry Concepts, In Electrochemistry Crash Course for Engineers, Springer, Cham, 2021.

[2] J. Newman and K.E, Thomas-Alyea, Electrochemical Systems, Third Edition, University of California, Berkeley, 1976.

[3] C. Lin, Doctoral dissertation, University of Oxford, 2017.

[4] P. K. Shen, C. Y. Wang, S. P. Jiang, X. Sun, J. Zhang, Electrochemical Energy: Advanced Materials and Technologies, CRC Press, Boca Raton, 2016.

[5] A. Asthagiri, M. Janik, Computational Catalysis, Royal Society of Chemistry, London, 2013.

[6] A. Rowe, Doctoral dissertation, Memorial University of Newfoundland, 2007.

[7] G. J. Bauer, Doctoral dissertation, Technische Universität München, 2012.

[8] C. Dincer, Doctoral dissertation, University of Freiburg, 2016.

[9] R. G. Compton, E Laborda, K. R. Ward, Understanding voltammetry: simulation of electrode processes, Imperial College Press, London, 2014.

[10] A. J. Bard and L. R. Faulkner, Electrochemical Methods: Fundamentals and Applications, 2nd Edition, Wiley, New York, 2001.

[11] A. Fick, Journal of Science, 1855, 10, 30-39.

[12] J. Philibert, in Diffus. Solids - Past, Present Futur, 2006, 249, 1-6.c

[13] R. Smith, Doctoral dissertation, University of Liverpool, 2018.

[14] A.L. Suherman, Doctoral dissertation, University of Oxford, 2019.

[15] C. M. A. Brett, A. M. O. Brett, Electrochemistry: Principles, Methods, and Applications, Oxford University Press, 1993.

[16] H. le, Doctoral dissertation, University of Oxford, 2021.

[17] E.J.F. Dickinson, A.J. Wain, *Journal of electroanalytical chemistry*, 872 (2020) 114145.

[18] H. Chen, Doctoral dissertation, University of Oxford, 2022.

[19] D. G. Truhlar, B. C. Garrett and S. J. Klippenstein, *Journal of Physical Chemistry*, 100 (1996) 12771- 12800.

[20] R. F. Savinell, K. I. Ota, G. Kreysa, Encyclopedia of Applied Electrochemistry, Springer, New York, 2014.

[21] J. Tafel, *Physikalische Chemie,* 50 (1905) 641-712.

[22] Y. Uchida, E. Kätelhön, R.G. Compton, *Journal Electroanalytical Chemistry*, 801 (2017) 381–387.

[23] N. Elgrishi, K. J. Rountree, B.D. McCarthy, E.S. Rountree, T.T. Eisenhart, J. L. Dempsey, *Journal Chemistry Education*, 95 (2018) 197–206.

[24] P. Khullar, J. Badilla, R. Kelly, *ECS Electrochemistry Letters,* 4(10), 2015.

[25] T. Gueshi, K. Tokuda, H. Matsuda, *Journal of Electroanalytical Chemistry*,101 (1979) 29–38.

[26] G. Bontempelli, N Dossi, and R Toniolo, *Molecular Sciences and Chemical Engineering. Eng.*, 2016.

[27] C. Montellaa , V. Tezyka , E. Efforib , J. Laurencinb , E. Sieberta, *Solid State Ionics*, 359 (2021) 115485.

[28] D. Li, Doctoral dissertation, Doctoral of Oxford, 2022.

[29] C. Batchelor-McAuley, E. K. Atelhon, E.O. Barnes, R.G. Compton, E. Laborda, A. Molina, *Chemistry Open*, 4 (2015) 224–260.

[30] R.G. Compton, E. Laborda, K.R. Ward, Understanding Voltammetry: Simulation of Electrode Processes, *Imperial College Press*, London, 2014.

[31] Keith B. Oldham, Jan C. Myland, *Electrochimca Acta.*, 56 (2011) 10612–10625.

[32] Z. Chen, IOP Conference Series: Materials Science Engineering. C, 711(1), 2020.

[33] S.R. Belding, Doctoral dissertation, University of Oxford, 2012.

[34] L.I. Stephens, J. Mauzeroll, *Journal Chemical Education,* 2019.

[35] N. Kosheva, Alexander Koshevb, Valentina Kuzina, Chemometrics and Intelligent Laboratory Systems, 157 (2016) 78–84.

[36] C. Montella, *Journal of Electroanalytical Chemistry,* 614 (2008)121 - 130.

[37] A. Sevcík, Collection Czechoslovak *Chemistry Communications,* 13 (1948) 349–377.

[38] J.E.B. Randles, *Trans. Faraday Soc.*, 44 (1948) 327–338.

[39] H. Matsuda, Y. Ayabe, *Zeicschrift Elektrochemie*, 59 (1955) 494–503.

[40] R.S. Nicholson, I. Shain, *Analytical Chemistry*, 36 (1964) 706–723.

[41] R.S. Nicholson, *Analytical Chemistry*. 37 (1965) 1351–1355.

[42] A. Samin, AIP Advances. 6 (2016), 055101.

[43] S. Petkovska, R. Gulaboski, *Electroanalysis*, 32 (2020) 1– 14.

[44] P. Schöna , U. Krewer, *Electrochimica Acta*, 373 (2021) 137523.

[45] J.G. Velasco, *Electroanalysis,* 9 (1997) 880–882.

[46] E. Laviron, *Journal of Electroanalytical Chemistry*, 101 (1979) 19-28.

[47] R.J. Klingler and J. K. Kochl, *Journal of Physical Chemistry*, 85 (1981).

[48] U .Eisner, E.Gileadi, *Journal of Electroanalytical Chemistry*, 28 (1970) 81–9

[49] I. Lavagnini, R. Antiochia, F. Magno, *Electroanalysis*, 16 (2004) 505–506.

CHAPTER II

Introduction to sensors and literature review of electrochemical detection of dopamine, uric acid and ascorbic acid

II.1. Introduction

The present chapter offers a general introduction of the sensor basics, specifically electrochemical sensors, then gives information on using the screen-printed electrodes in sensor application. Following this, a literature review will be introduced about the electrochemical determination of dopamine, uric acid and ascorbic acid molecule. Finally, application of voltammetry simulation in electrochemical sensor analysis will be discussed.

II.2. Sensor and Biosensor

The research of sensor and biosensors is an extensive, multidisciplinary field that encompasses several disciplines, including biology, chemistry, and physics. Owing to their numerous application in vital areas such as environmental science, nutrition science, medicine, and agriculture, sensors and biosensor have critical role in academic and industry researchers which offers a better stability and sensitivity compared to the classical methods [1, 2].

A sensor is defined as an analytical device, which can measure and detect different types of analytes (chemical, biologic, physical.......) and converts them into measurable analytical signals (current, potential) [3]. A typical sensor contains two main elements: receptor and transducer. The first element can measure and detect the analyte of interest with high degree of selectivity, and the second element serves as a detector which converts the information of analyte detection into a quantifiable signal [4, 5].

Classification of sensors is based on their receptor elements and transduction mechanism, as well as dependent on the kind of the analyte to be monitored. Sensors can be divided into three important categories [6, 7]:
- **Physical sensor** is a device that detects and measures a physical quantity, then transforms this measurement into a signal that is recognized by the user, which can be identified by the user. This sensor is capable of detecting and monitoring changes in physical parameters including force, mass, volume, density, acceleration, flow rate, and pressure.
- **Chemical sensor** is a sensor used to measure and detect chemical information of analyte such as composition of practical component, concentration, pressure… and transforms it into an analytically measurable signal.
- **Biological sensor** is a specialized device that monitors and measures biological molecules, and converts the biological responses into a measurable signal, which is often referred to as biosensors.

One significant class of sensors is biosensors. The latter contains bio-receptor and bio-transducer elements for sensing biological analytes such as nucleic acid (DNA, RNA), bacterium, protein. The bio-receptors types serve in several types of biosensors, including DNA biosensors, enzymatic biosensors, immunosensors (which use antibodies as their receptors), genosensors (which use nucleic acids as their receptors), and whole-cell biosensors [8]. According to transduction method, biosensors come in a variety types such electrochemical, optical [9-10], thermal biosensor [11].

For developing highly effective sensors, spesific characteristics or parameters are necessary in optimizing and monitored defining their performance. Some of the most important sensor characteristics include [1, 12]:

- **Selectivity** is the capability of the biosensor to detect or respond only to the target analyte within the presence of other compounds in a sample. It is a crucial feature for biosensor selection.

- **Sensitivity** is the ratio between the change in the concentration of the analyte and the signal created by the transducer. This paramater is related to the capability of the sensor to generate a signal in response to the minor variations in the concentration of analyte.

- **Limit of detection (LOD)** represents the minimum concentration that can be relative to a blank sample.

- **Linearity** is an important parameter that determines the accuracy of the measured responses for a series of measurements with varying the analyte concentrations.

- **Response time** is the required time of the output signal of a sensor to stabilize following a change in the analyte concentration.

- **Reproducibility** refers to the capability of sensor to produce similar responses when measuring the same sample multiple times.

- **Stability** relates to the capability of the sensor to maintain its performance over a period of time.

In this context, electrochemical sensors have attracted the interest of researchers owing to their advantages including simplicity, low cost and significant detection limits. Here, we are focused on electrochemical sensors in the following section.

II.3. Electrochemical sensor

In electrochemical sensing, an electrochemical reaction generates an electrochemical signal in the form of potential, current. In this type of sensor, an electrode is used for electrochemical transduction. Depending on the operating principle for signal measurement, electrochemical sensors can be further categorized as potentiometric, amperometric, and voltammetric [13-16].

II.3.1. Potentiometric sensor

Potentiometric sensor is typically utilized in a two-electrode configuration, which contains a sensing electrode and a reference electrode. These sensors are applied to measure the potential signal due to electrochemical reaction that occurs between the working electrode and the reference electrode, wherein no current flows [17].

II.3.2. Amperometric sensor

Amperometric sensor typically requires three electrode system, which are used for current measurement during the electrochemical reaction of electroactive species occurring at electrode surface, over a fixed voltage applied to the working electrode. In quantitative analysis, the generated current is proportional with the concentration of the electroactive species [18, 19].

II.3.3. Voltammetric sensor

Voltammetric sensor operates by measuring the current in response to the applied voltage. During the variation of the applied voltage to the working electrode, the resulting current is measured. The voltammetric measurement also requires a three electrode system. Several voltammetric techniques are used in electrochemical sensing including: the linear sweep voltammetry, cyclic voltammetry, differential pulse voltammetry, square-wave voltammetry [19, 20].

In particular, electrode materials have a pivotal role for improving the analytical performance of electrochemical sensors. Among these, platinum, gold, and carbon-based electrodes are commonly employed for several electrochemical applications owing to their properties [12]. In the following, the carbon based electrodes will be discussed.

II.4. Screen-printed electrodes based sensor

Carbon-based electrodes have attracted significant interest and are extensively used for sensing applications research owing to their excellent sensing characteristics. They are characterized by their low cost, high surface area, chemically inertness, and high electrical conductivity [21-23]. Carbon electrodes include graphite [24], carbon paste electrode (CPE) [25], glassy carbon electrode (GCE) [26] and carbon nanotube [27].

On the development of carbon electrodes based sensor, for providing a high-quality and inexpensive device. Screen printed electrodes (SPEs) are a promising technology device in the electrochemical sensors, presenting excellent advantages in terms of easy fabrication, low cost high conductivity, portable and disposable electrodes [28, 29]. They are extensively used and applicable to the development of analytical detection in various research area including environment, pharmaceutical, clinical and microbiology analysis [29-31].

SPEs are fabricated from different types of inks using the screen printing technique on hard and resistive substrates such as plastic or ceramic [32]. The composition of different inks including carbon [33], graphene [34], gold and platinum [35, 36], for SPEs fabrication determines its selectivity and its sensitivity in different electrochemical analysis. SPEs generally contains three electrodes which are printed as shown in the Fig. II.1.
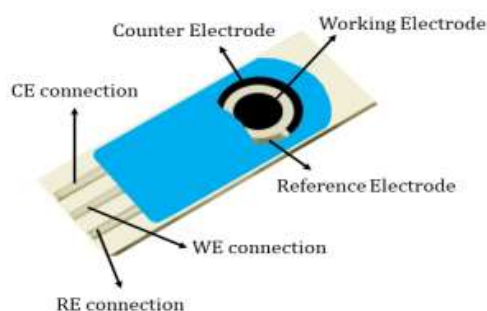
Figure II.1. A representation of screen-printed electrodes scheme [32].

In addition, to enhance their performance, the surface of SPEs has been modified by different material such as carbon materials, metal and metal oxides, enzymes, polymers and

others [32]. These modifications on SPEs surface are achieved through various methods, with electrodeposition serving as the main method in the context of electrochemical sensor [37, 38].

Diverse applications of SPEs, both with and without modification cover various fields including biomedical sensing, environmental and industrial process monitoring [39]. In environment monitoring, sensors based on screen-printed electrodes have been developed for the detection of heavy metals, pollutants, pesticides and used in water quality tests and organic compound analyses [31, 40]. SPEs also have been used in biomedical sensors for detection of biomarkers, drugs, and metabolites in biological samples including blood, urine. SPE-based sensors are employed in industrial process monitoring to detect and quantify various chemicals and compounds in manufacturing processes [29, 39].

II. 5. Dopamine, Uric Acid and Ascorbic Acid compounds: Properties and their functions

II.5.1. Dopamine

Dopamine (DA) is a primary monoamine neurotransmitter in human body, belonging to the catecholamine family. In two step process, Dopamine is synthesized from the amino acid tyrosine occurring in dopaminergic neurons, which are located in specific regions of the brain. Dopamine has a specific chemical structure that includes two hydroxyl (catechol) groups and a monoamine group attached to a benzene ring (**Fig. II.2**). The chemical formula for dopamine is $C_8H_{11}NO_2$, and its systematic name is 3, 4-dihydroxyphenylethylamine [41, 42].
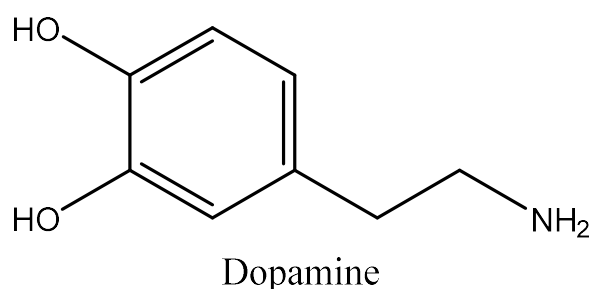
Dopamine

Figure II.2. Chemical structure of Dopamine molecule [41].

Dopamine has several crucial functions that are involved in the central nervous system, cardiovascular, memory, and hormonal systems, including   mood regulation, motor control, and the reward system [43]. DA imbalance level results to several disorders, such as Parkinson's

disease, Schizophrenia [44, 45]. In this regard, it is necessary to detect dopamine levels in human body for diagnosis and treatment of associated disorders.

A variety of methods have been applied for the detection of dopamine, involving the high-performance liquid chromatography [46], fluorescence [47], capillary electrophoresis and electrochemical sensors [48, 49]. With the demand for a method that is selective, sensitive, simple operation, and low cost for DA detection, electrochemical sensors are the most effective alternatives.

The electrochemical oxidation of dopamine is a complex multi-step process involving several intermediates steps and reaction pathways, which depend on different conditions (pH). Therefore, the dopamine is oxidized, releasing two electrons and two protons which resulting in the formulation of dopamine-o-quinone [50]. The typical oxidation of dopamine is presented in **Fig. II.3**.
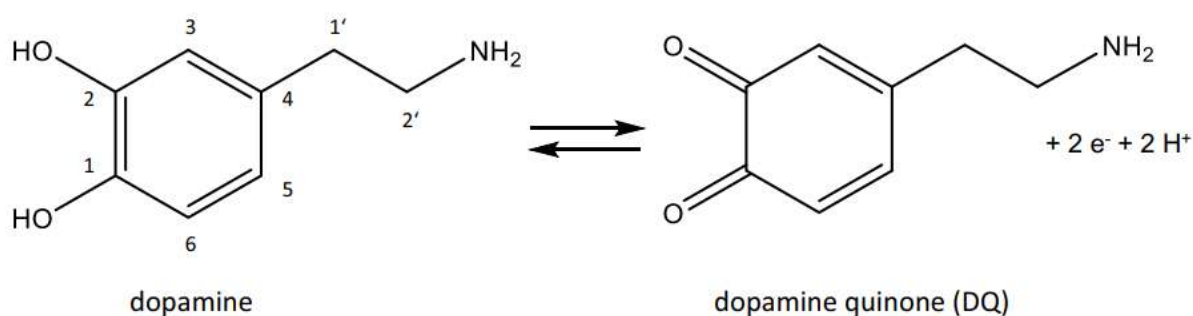
Figure II.3. Oxidation of dopamine in a 2-electron oxidation [50].

II.5.2. Uric acid

Uric acid, a heterocyclic derivative of purine (**Fig. II.4**), represents the end-product of purine nucleotide metabolism in human body. Its chemical structure is represented as 2, 6, 8-trioxypurine ($C_5H_4N_4O_3$) [51].
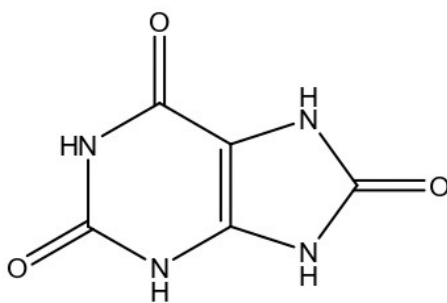
Figure II.4. Structural representation of uric Acid [52].

Uric acid, a major antioxidant exist in urine or serum, playing significant role in human body function [52, 53]. Abnormal levels of UA in the body are also associated with various disorders, such as Lesch-Nyan disease [54], gout [55], hyperuricaemia and heart disease, kidney diseases, and cardiovascular diseases [56, 57]. Therefore, the determination of UA concentration in biological system is very important and occupies a very prominent place in the clinical diagnosis of various diseases [58].

As already mentioned, many analytical techniques have been frequently used for determining UA levels. These include HPLC [59], spectrophotometry [60], chemiluminescence analysis [61] and electrochemical biosensors [62]. Among them, electrochemical biosensors have garnered much interest due to their excellent advantages of low cost, simplicity, high sensitivity, and selectivity [62].

The anodic oxidation pathway of Uric acid was examined under various conditions. In which the anodic oxidation of UA typically proceeds via a two-electron process with transfer of two protons, leading to the formulation of diamine that is very unstable in aqueous solution (**Fig. II.5**) [63, 64].
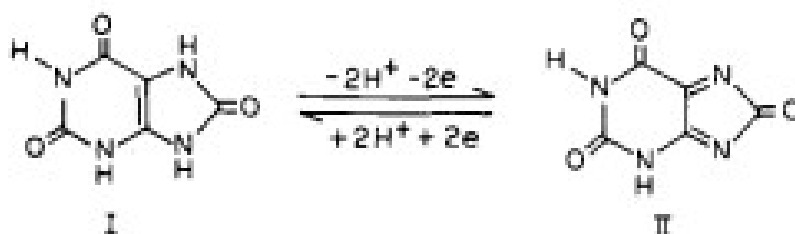
Figure II.5. The pathway oxidation of uric acid [64].

II.5.3. Ascorbic Acid

Ascorbic acid is an organic molecule, with the chemical formula of $C_6H_8O_6$. It represents an enediol structure conjugated with the carbonyl group in the lactone ring [65, 66], as shown in **Fig. II.6**.
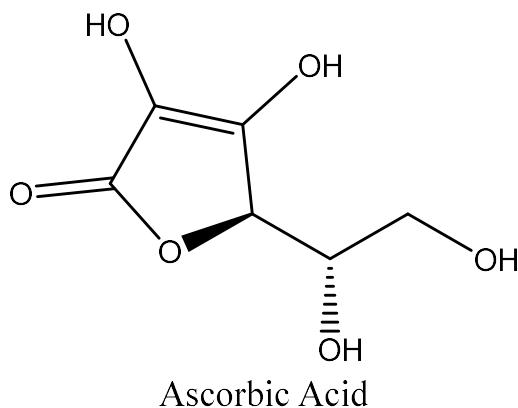
Ascorbic Acid

Figure II.6. Ascorbic acid molecule [65].

Ascorbic acid, a water-soluble vitamin and an important element in human metabolism function, playing a crucial role in collagen production. It acts as a strong antioxidant to prevent the body from oxidative stress responses. Ascorbic acid finds application in the prevention and treatment of several health issues, including diabetes, scurvy, the common cold, infertility, and even cancer [65-67]. Therefore, it is largely employed as an antioxidant in food products, animal nutrition, and medicinal formulations [65, 68]. Several important diseases are related to AA level concentration in body system including: anemia, common cold, scurvy, hepatic diseases and diabetes mellitus [69, 70]. AA determination also presents a great importance in food and pharmaceutical industries [71].

Various analytical methods including Fluorimetry [72], chemiluminescence [73], titrimetry [74] and electrochemical sensors [75], have been used to determine AA. Regarding among these methods, the use of the electrochemical sensors for detecting AA has received significant interest.

The oxidation mechanism of AA includes the loss of 2 electrons and 2 protons to form dehydro-ascorbic acid [76] and is illustrated in **Fig. II.7**.
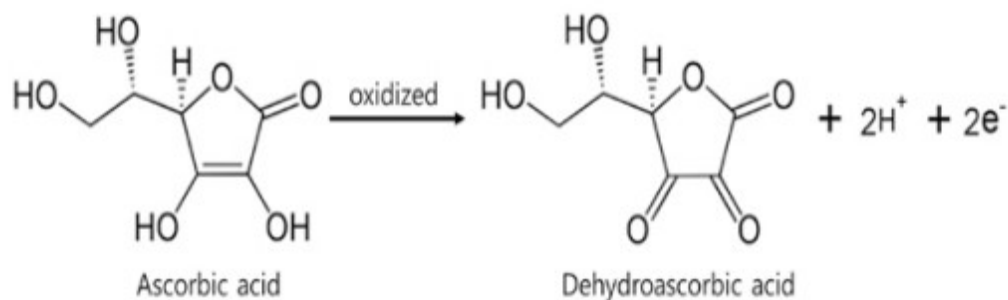
Figure II.7. The oxidation process of Ascorbic acid [75].

II.6. Literature review of DA, UA and AA detection by Screen-printed electrodes based sensors

DA, UA, and AA are vital biomolecules, which also present in biological fluids including blood and urine. These biomolecules have a great importance in the physiological functions of organisms [77-79]. Therefore, evaluation of DA, UA, and AA is highly desirable for diagnostic and pathological research.

In the determination of DA, UA, and AA, amperometric and voltammetric techniques such as LSV, CV, square wave voltammetry and differential pulse voltammetry, have been largely applied for the quantitative detection of these biomolecules using different kinds of working electrodes [80, 81]. Hence, in practice many researchers have used screen printed electrodes due to their reproducibility, mass production, and low cost. Additionally, there is a demand for achieving high selectivity, sensitivity and reproducibility of electrochemical SPEs-sensor for determination of DA, UA and AA. Screen-printed electrodes are often modified with different materials to optimize their advantages, including high stability, excellent electrical conductivity, fast electron transport, and high surface area.

For the determination of DA, ***Calvo et al.*** [81] reported a comparative investigation using screen-printed electrodes modified with reduced graphene oxides (rGO) and the bare SPEs (Dropsens) for the determination of dopamine. Voltammetric measurements showed the lowest peak potential separation that was obtained for rGO-modified electrode, which indicated the highest reversibility (lowest ΔEp) in this modified electrode than the bare electrode. The analytical performance was evaluated using square wave voltammetric, in which the a highest sensitivity (0.259 $\mu A\ \mu M^{-1}$) and a lower limit of detection (0.09 μM) were obtained on SPEs

modified compared to the lower sensitivity (0.09 µA µM^{-1}) and higher limit of detection (0.3 µM) showed with the bare electrode. Similarly, *Sabrine et al.* [83] developed an electrochemical sensor using the Gold nanoparticles (AuNPs) modified on screen printed electrodes to detect DA. Linear sweep voltammetry demonstrated that the AuNPs-SPE sensor achieved a high sensitivity of (550.4 µA.mM^{-1}) with a detection limit (0.2 µM). This study also showed that the Gold nanoparticles based on modified SPEs displayed in the presence of dopamine, a lower anodic peak potential at around (80 mV) and a significantly higher intensity than that on unmodified SPEs revealing that AuNP/SPCE enhanced electron transfer and has a better electro-catalytic effect toward DA compared to the bare electrode. In the same vein, *Singh et al.* [84] used a nanocomposite (MWCNTs/PPDA/Nafion) modified screen-printed electrode to detect dopamine through the use of cyclic voltammetry. Their electrode displayed an excellent performance in determining of DA within a linear range of (1-110 µM), with a detection limit of (0.01µM).

For UA determination, *Wahyuni et al.* [85] fabricated a homemade screen-printed carbon electrode (SPCE) for the detection of uric acid. The homemade SPCE exhibited good analytical performance comparable to that of the commercial SPCE. This sensor showed an excellent reproducibility and a sensitivity of 5 nA µM^{-1} for uric acid determination. It achieved a detection limit of 1.94 µM within a concentration range of 10–80 µM. In another work by *Rasoul et al.* [86], a screen-printed graphite electrode based sensor modified by ZnO/GR nanocomposite was proposed for UA detection via CV and DPV methods. ZnO/GR/SPGEs demonstrated excellent electrocatalytic effect on uric acid oxidation, with higher anodic peak currents and a potential shift of approximately 40 mV towards a less positive potential compared to the unmodified SPE. The modified electrode exhibited a detection limit of 0.43 µM over a concentration range of 1–100 µM. *Cruz et al.* [87] used polymeric films derived from 4-aminosalicylic acid (4-ASA) combined with the enzyme urate oxidase (UOx) on screen printed electrode to quantify of uric acid (UA) in urine samples through amperometric detection. The developed sensor responded to uric acid detection within a linear range of (10 - 200 µM), with a detection limit of 3.0 µM.

In the determination of AA, *Chou et al.* [88] fabricated a screen-printed electrode for detecting ascorbic acid. Using the amperometric technique, their sensor shows a better sensitivity of 13.85 mV/mM in a linear range of (0.02-1 mM), with achieving a detection limit of 0.01 mM for AA detection. In a study, *Gopalakrishnan et al.* [89] presented the modification

of a screen-printed carbon electrodes with cadmium oxide (CdO) nanoparticles for detection of ascorbic acid (AA) under DPV conditions. They reported that CdO nanoparticles based modified SPCEs displayed an excellent achievement toward AA detection, having a good lowest LOD in the nano-molar range of 53.5 nM. The linear concentration range extended from 5 to 150 μM. There is also the study followed by *Uwaya et al.* [90], who developed a voltammetric sensor using a SPCE modified by Iron (III) Oxide Nanoparticles to determine ascorbic acid through square wave voltammetry. The developed sensor showed a good results toward the electrochemical detection of AA that demonstrated a faster electron transport with greater current response to AA oxidation than the unmodified SPCE. The detection limit of 15.7 μM with the linear concentration range of (10 -100) μM were reported. *Ganjali et al. [91]*, proposed the application of a screen printed electrode modified with a ZnO/Al$_2$O$_3$ Nanocomposite for the determination of ascorbic acid, using both CV and differential pulse voltammetry techniques. The proposed sensor exhibited an enhancement on the anodic peak current in comparison to the bare SPE, which showed good electrocatalytic activity towards oxidation of ascorbic acid. Moreover, the ZnO/Al$_2$O$_3$/SPE sensor showed under optimal DPV conditions, a high sensitivity with the lowest detection limit of 0.06 μM for AA detection in the concentration range of 1–100 μM. Similarly, *Raveendran et al.* [92] used copper hydroxide NPs modified screen printed electrodes to detect AA, showing an excellent linearity ranging from 0.0125mM to10 mM and a good sensitivity of 268 μA mM^{-1} cm^{-2}.

In light of simultaneous detection of DA, UA and AA, *Ping et al.* [93] fabricated SPE using graphene with ionic liquid doped screen-printing ink for determining simultaneously of these three molecules via CV and DPV method. The developed SPGNE exhibited enhanced electrochemical response and decreased overpotential for the oxidation reaction of these three molecules DA, UA and AA. The anodic peaks of DA, UA and AA are well separated under DPV conditions. Results highlighted the good reproducibility and stability of the SPGNE in determining these species. The SPGNE exhibited also linear responses to the detection of DA, UA and AA in concentration ranges of (0.5–2000) μM, (0.8–2500) μM, and (4.0–4500) μM, respectively. The corresponding detection limits for dopamine, uric acid, and ascorbic acid were determined to be 0.12 μM, 0.20 μM and 0.95 μM, respectively. *Kunpatee et al.* [94] modified SPCE for highly sensitive and selective simultaneous detection of DA, UA, and AA by synthesizing graphene quantum dots (GQDs) with ionic liquid (IL), using DPV. The GQDs/IL-SPCE offered good electro-activity to the oxidation of these three compounds, yielding distinct and well-separated oxidation peaks for dopamine, uric acid, and ascorbic acid. This modified

electrode also exhibited an excellent performance in determining DA, UA, and AA, showing low detection limit of 0.03 μM, 0.06 μM and 6.64 μM, respectively, with linear response ranges of 0.2–10 μM for DA, 0.5–20 μM for UA, and 25–400 μM for AA. ***Qin et al.*** [95] presented a new sensor by applying electropolymerization of a conductive β-CD polymer onto the rGO modified screen-printed electrode to detect simultaneously DA, UA, and AA. The proposed sensor showed significant electro-catalytic activity to the oxidation of DA, UA, and AA, effectively resolving their anodic peaks responses into three distinct and well-defined peaks. The resulting modified electrode provided the detection limits for DA (0.017 μM), UA (0.026 μM) and AA (0.067 mM) within linear detection ranges of (0.05 - 50) μM, (0.08 - 150) μM and (0.2 - 2) mM for DA, UA and AA, respectively. In a work by ***Kanyong et al***. [96], they studied a sensor using a modified screen-printed carbon electrode with reduced graphene oxide (rGO) for the simultaneous evaluation of UA, AA, and DA through differential pulse voltammetry. The sensor demonstrated a linear concentration range of (10-3000) μM for UA, (0.1-2.5) μM and (5.0 to 2×10^4) μM for AA, and (0.2-80.0) μM and (120.0- 500) μM for DA. The detection limits were obtained as 0.1, 50.0, and 0.4 μM, respectively. This developed sensor represented an excellent analytical performance in simultaneously determining UA, AA and DA.

II.7. Application of voltammetry simulation in electrochemical sensor analysis

Voltammetry stands out as a powerful distinguished technique in the electrochemical detection, which offers valuable insights about the mechanistic and kinetic of different electroactive analytes on electrode surface [97]**.** In development of understanding electroanlytical experiments, computer modeling and simulation serve as one necessary approach to obtain more detailed information for comprehending and developing electrochemical process and sensors [98, 99].

It is worth mentioning that few papers deal with the use of simulation for developing diverse electrochemical sensors through the voltammetry techniques highlighting the determination of different kinetic parameters.

Kaffash et al. [100] used the numerical simulation to analyse an electrochemical nano-biosensor for phenol reaction in horseradish peroxidase enzyme by using COMSOL Multiphysics. In their study, the oxidation of phenol enzymatic was studied via cyclic voltammetry. Numerical simulation was performed for CVs related to the enzymatic reaction

of phenol. From a kinetic point of view, the rate constant k^0, as well as the charge transfer coefficient α, were estimated by comparing the simulation and experimental results of cyclic voltammetric experiments. The diffusion coefficient of phenol enzymatic oxidation was determined through experimental chronoamperograms. **Flexer et al.** [101] have studied experimentally the cyclic voltammetry of the homogeneous reaction involving glucose oxidase and osmium bipyridine–pyridine carboxylic acid in the presence of glucose as well as digital simulation in order to extract kinetic parameters. Based on combining simulation and experiment analysis, the kinetic proprieties for the substrate–enzyme reaction were extracted. **Adesokan et al.** [102] reported an investigation into the electrochemical micro-sized sensors using cyclic voltammetry measurement and numerical simulation. In their study, through the simulation of cyclic voltammetry a rigorous analysis of systems was performed. In particular, they examined the effects of flow rates, scan rates, variation of electrolyte concentration, changes in supporting electrolyte, and reaction rate constants.

II. 7. Conclusion

The chapter provides a general description of sensor and biosensor devices highlighting on the electrochemical sensor. It also reviews the development and the utility of screen printed electrode in electrochemical sensing. Following that, we summarized a relevant literature on the electrochemical detection of dopamine, uric acid and ascorbic acid using screen-printed electrode sensor. In another part, we have given a brief survey on the use of simulation in voltammetry for electrochemical sensor.

Within this framework, the present thesis seeks to conduct both experimental and theoretical investigations of electrochemical sensors utilizing the cyclic voltammetry technique. The important objective is to determine various kinetic parameters for electrochemical sensor reactions.

References

[1] N. Bhalla, P. Jolly, N. Formisano, P. Estrela, *Essays in Biochemistry*, 60 (2016) 1-8.

[2] H. Altug, Sang-Hyun Oh, S.A. Maier, J. Homola, *Nature Nanotechnology*, 17 (2022) 5–16.

[3] A.A. Ensafi,. In Electrochemical Biosensors, 1st ed.; Ensafi, A.A., Ed.; Elsevier: Cambridge, MA, USA, (2019) 1–10.

[4] D.R. Thévenot, K. Toth, R.A. Durst, G.S. Wilson, *Biosensors and Bioelectronics*, 16 (2001) 121-13.

[5] A. Rudnitskaya, Sensors | biomimetic sensor arrays, in: P. Worsfold, C. Poole, A. Townshend, M. Miró (Eds.) Encyclopedia of analytical science (third edition), Academic Press, Oxford, (2019) 154-160.

[6] R.M. White, IEEE Trans. Ultrason. Ferroelectr. Freq. Control., 34(1987)124–126.

[7] V. Naresh, N. Lee, *Sensors*, 21 (2021) 1109.

[8] C.I.L. Justino, A.C. Freitas, R. Pereira, A.C. Duarte, T.A.P.R. Santos, *Trends in Analytical Chemistry*, 2015.

[9] S. Mittal, H. Kaur, N. Gautam, A.K. Mantha, Biosens Bioelectron., 88 (2017) 217-231.

[10] A. Touhami, *Nanomedicine*, (2004) 374-403.

[11] B.D. Malhotra, Md.A. Ali, Chapter 1-Nanomaterials in Biosensors: Fundamentals and Applications, *Nanomaterials for Biosensors*, (2018) 1-74.

[12] C. Dincer, R. Bruch, E. Costa-Rama, M.T. Fernández-Abedul, A. Merkoçi, A. Manz, G.A. Urban, and F. Güder, *Advanced Materials*, (2019) 1806739.

[13] G. Hanrahan, D.G. Patila, J. Wang, *Journal of Environmental Monitoring*, 6 (2004) 657–664.

[14] M.A. Rahman, P. Kumar, D.S. Park, Y. Shim, *Sensors*, 8 (2008) 118–141.

[15] E.B. Bahadir, M.K. Sezginturk, *Biosensors and Bioelectronics*, 68 (2015) 62-71.

[16] H.R.S. Lima, J.S. da Silva, E.A. de Oliveira Farias, P.R.S. Teixeira, C. Eiras, L.C.C. Nunes, *Biosensors and Bioelectronic*, 108 (2018) 27-37.

[17] E. Zdrachek, E. Bakker, *Journal of analytical Chemistry,* 91 (2019) 2−26.

[18] J. Baranwal, B. Barse, G. Gatto, G. Broncova, and A. Kumar, *Chemosensors*, 10 (2022) 363.

[19] N.J. Ronkainen, H.B. Halsallb, W.R. Heineman*, Chemical Society Reviews,* 39 (2010) 1747–1763.

[20] D. Grieshaber, R. MacKenzie, J. Voros and E. Reimhult, *Sensors*, 8 (2008) 1400-1458.

[21] A.V. Kolliopoulos, Doctoral dissertation, University of Manchester Metropolitan, 2014.

[22] P.T. Lee, Doctoral dissertation, University of Oxford, 2015.

[23] S.A. Wring, J.P. Hart, *Analyst*, 117 (1992) 1215-1229.

[24] D. A. C. Brownson and C. E. Banks, *Analyst*, 2010, 135, 2768–2778

[25] I. Švancara, K. Vytřas, J. Barek, J. Zima, *Critical Reviews in Analytical Chemistry*, 31 (2001) 311-345.

[26] W. Geremedhin, M. Amare and S. Admassie, *Electrochimica Acta*, 87 (2013) 749-755.

[27] C.E. Banks, A. Crossley, C. Salter, S.J. Wilkins, R.G. Compton, Angewantdte Chemie Edition, 45 (2006) 2533–2537.

[28] A.G-M. Ferrari, S.J. Rowley-Neale, C.E. Banks, *Talanta Open*, 3 (2021) 100032.

[29] Z. Taleat, A. Khoshroo, *Microchimica Acta*, 181 (2014) 865–891.

[30] K. Yamanaka, M.C. Vestergaard, E. Tamiya, *Sensors*, 16 (2016) 1761.

[31] M. Li, Y. Li, D. Li, Y. Long, *Analytica Chimica Acta*, 734 (2012) 31–44.

[32] G. Paimard, E. Ghasali, M. Baeza, *Chemosensors*, 11 (2023) 113.

[33] J.M. Petroni, B.G. Lucca, V.S. Ferreira, *Analytica Chimica Acta*, 954 (2017)88–96.

[34] E.P. Randviir, D.A.C. Brownson, J.P. Metters, R.O. Kadara, and C.E. Banks, *Physical Chemistry Chemical Physics*
, 16 (2015) 4598–4611.

[35] J.P. Metters, F. Tan, R.O. Kadara, C.E. Banks, *Analytical Methods*, 4 (2012) 1272–1277.

[36] J.P. Metters, R.O. Kadara, C.E. Banks, *Analyst*, 137 (2012) 896–902.

[37] N. Sandhyarani, , *Electrochemical Biosensors, Elsevier*, (2019) 45-75.

[38] A.K.M.S. Inam, M.A.C. Angeli, B. Shkodra, A. Douaki, E. Avancini, L. Magagnin, L. Petti, and P. Lugli, *ACS Omega*, 6 (2021) 33523−33532.

[39] J.P. Hart, A. Crew, E. Crouch, K.C. Honeychurch, R.M. Pemberton, *Analytical Letters*, 37 (2004) 789-830.

[40] A. Hayat, J.L. Marty, *Sensors*, 14 (2014) 10432-10453.

[41] L. Cruickshank, A.R. Kennedy, N. Shankland, *Journal of Molecular Structure*, 1051 (2013) 132–136.

[42] M.O. Klein, D.S. Battagello, A.R. Cardoso1, D.N. Hauser, J.C. Bittencourt, R.G. Correa, *Cellular and Molecular Neurobiology*, (2019) 39:31–59.

[43] X. Liu, J. Liu, *VIEW*, (2020) 20200102.

[44] S. Sansuk, E. Bitziou, M. B. Joseph, J. A. Covington, M. G. Boutelle, P. R. Unwin, and J. V. Macpherson, *Analytical Chemistry*, 85 (2012) 163.

[45] C. Bucolo, G.M. Leggio, F. Drago, S. Salomone, *Pharmacology & Therapeutics*, 203 (2019) 107392.

[46] X. Hou, W. Huang, Y. Tong, M. Tian, Microchimicta Acta, 2019.

[47] Y. Liu, X. He, P. Ma, Y. Huang, X. Li, Y. Sun, X. Wang, D. Song, *Talanta*, 217 (2020) 121081.

[48] M. Schoening, M. Jacobs, A. Muck, D. Knobbe, J. Wang, M. Chatrathi, S. Spillmann, *Sensors and Actuators B*, 108 (2005) 688–694.

[49] A. Pandikumar, G.T.S. How, T.P. See, F.S. Omar, S. Jayabal, K.Z. Kamali, Y. Norazriena, A. Jamil, R. Ramaraj, S.A. John, H.N Lim, N.M. Huang, *RSC Advances*, 4 (2014) 63296–63323.

[50] S. Schindler, T. Bechtold, *Jornal of Electroanalytical Chemistry*, 836 (2019) 94–101.

[51] J. Maiuolo, F. Oppedisano, S. Gratteri, C. Muscoli, V. Mollace, *International Journal of Cardiology*, 2015.

[52] R. El Ridi, H. Tallima, *Journal of Advanced Research,* 2017.

[53] S. Jain, S. Verma, S.P. Singh, S.N. Sharma, *Biosensors and Bioelectronic,* 127 (2019) 135–141.

[54] K.L. Rock, H. Kataoka, J.J. Lai, *Nature reviews, Rheumatology*, 9 (2013)13–23.

[55] W.L. Nyhan, Journal of Inherited Metabolic Disease, 20 (1997) 171–178.

[56] M. Jin, F. Yang, I. Yang, Y. Yin, J.J. Luo, H. Wang, X.F. Yang, Frontiers in Bioscience, 17 (2012) 656–669.

[57] R.J. Johnson, D.H. Kang, D. Feig, S. Kivlighn, J. Kanellis, S. Watanabe, K.R. Tuttle, B. Rodriguez-Iturbe, J. Herrera-Acosta, M. Mazzali, *Hypertension*, 41 (2003) 1183–1190.

[58] Q. Yan1 , N. Zhi, L. Yang, G. Xu, Q. Feng, Q. Zhang, S. Sun, *Scientific Reports* , 10 (2020) 10607.

[59] D. Swinson, J. Snaith, J. Buckberryc, M. Brickley, *International Journal of Osteoarchaeology*, 20 (2010) 135–143.

[60] D.L. Rocha, F.R.P. Rocha, *Microchemical Journal*, 94 (2010) 53–59.

[61] S. Zhao, X. Lan, Y.M. Liu, *Electrophoresis*, 30 (2009) 2676–2680.

[62] H. Dai, N. Wang, D. Wang, X. Zhang, H. Ma, M. Lin, *Microchimica Acta*, 183 (2016) 3053–3059.

[63] L. F. Cavalieri, G. B. Brown, *Journal American Chemistry Society.*, 70 (1948) 1242–1243.

[64] H.A. Marsh, Jr. and G. Dryhurst, *Journal Electroanalytical Chemistry*, 95 (1979) 81—90.

[65] S. J. Devaki and R. L. Raveendran, IntechOpen, 2017.

[66] F. J. Barba, M. Esteve, A. Frıgola, *Studies in Natural Products Chemistry*, 41(2014) 321–346.

[67] K. Iqbal, A. Khan, M. Khattak, *Pakistan Journal of Nutrition*, 3 (2004) 5–13.

[68] K. Pallauf, J. Bendall, C. Scheiermann, K. Watschinger, J. Hoffmann, T. Roeder and G. Rimbach, *Food and Chemical Toxicology*, 58 (2013) 255–263.

[69] Zelalem Bitew and Meareg Amare, *International Journal of Organic & Medicinal Chemistry*, 2019.

[70] A. Ambrosi, A. Morrin, M.R. Smyth, A.J. Killard, *Analytica Chimica acta*, 609 (2008) 37-43.

[71] S. Yilmaz, M. Sadikoglu, G. Saglikoglu, S. Yagmur, G. Askin, *International Journal Electrochemical Science*, 3 (2008) 1534–1542.

[72] X. Wu, Y. Diao, C. Sun, J. Yang, Y. Wang, and S. Sun, *Talanta*, 59 (2003) 95–99.

[73] A.A. Alwarthan, Analyst, 118 (1993) 639–642.

[74] L. Suntomsuk, W. Gritsanapun, S. Nilkamhank, and A. Paochom, *Journal of Pharmaceutical and Biomedical Analysis*, 28 (2002) 849–855.

[75] M. Motahary, S.M. Ghoreishi, M.M. Behpour, Golestaneh, *Journal of Applied Electrochemistry*, 40 (2010) 841-847.

[76] A.M. Macan, T.G. Kraljević, S. Raić-Malić, *Antioxidants*, 8 (2019) 247.

[77] H. Bagheri, N. Pajooheshpour, B. Jamali, S. Amidi, A. Hajian, H. Khoshsafar, *Microchemical Journal*, 131 (2017) 120–129.

[78] B. Yang, H. Wang, J. Du, Y. Fu, P. Yang, Y. Du, *Colloids and Surfaces A: Physicochemical and Engineering Aspects,* 456 (2014) 146–152.

[79] C.V.D. Horsta, V, Somerseta, *Russian Journal of Electrochemistry*, 58 (2022) 341–359.

[80] N. Tukimin, J. Abdullah, and Y. Sulaiman, *Journal of The Electrochemical Society*, 165 (2018) B258-B267.

[81] S. Qi, B. Zhao, H. Tang, X. Jiang, *Electrochimica Acta*, 161 (2015) 395–40.

[82] A.S. Calvo, C. Botas, D. Martin-Yerga, P. Alvarez, R. Menendez and A. Costa-Garcia, *Journal of The Electrochemical Society*, 162 (2015) 282-290.

[83] S. Chelly, M. Chelly, R. Zribi, R. Gdoura, H. Bouaziz-Ketata, and G. Neri, *ACS Omega*, 6 (2021) 23666−23675.

[84] M. Singh, I. Tiwari, C.W. Foster, C.E. Banks, *Materials Research Bulletin*, 101 (2018) 253-263.

[85] W. T. Wahyuni, B.R. Putra, R. Heryanto, E. Rohaeti, D. H.Y. Yanto, A. Fauzi, *International Journal Electrochemical Science*, 16 (2021) 210221.

[86] R. Rezaeia, M.M. Foroughia, H. Beitollahib, and R. Alizadehc , *Russian Journal of Electrochemistry*, 54 (2018) 860–866.

[87] F.S.d. Cruz, F.d.S. Paula, D.L. Franco, W.T.P.d. Santos, L.F. Ferreira, *Journal of Electroanalytical Chemistry*, (2017).

[88] J.C. Chou, Y.His. Tsai, and C.C. Chen, *IEEE Sensors Journal*, 8 (2008) 1571-1577.

[89] A. Gopalakrishnan, R. Sha, N. Vishnu, R. Kumar, S. Badhulika, *Nano-Structures & Nano-Objects*, 16 (2018) 96-103.

[90] G.E. Uwaya, O.E. Fayem, *Journal of Cluster Science*, 2021.

[91] M.R. Ganjali, F.G. Nejad, H. Beitollahi, S. Jahani, M. Rezapour, B. Larijan, *International Journal Electrochemical Science*, 12 (2017) 3231 – 3240.

[92] J. Raveendran, R.G. Krishnan, B.G. Nair, T.G. Satheesh Babu, *Microchimica Acta*, 184 (2017) 3573–3579.

[93] J. Ping, J. Wu, Y. Wang, Y. Ying, *Biosensors and Bioelectronics*, 34 (2012) 70–76.

[94] K. Kunpatee, S. Traipop, O. Chailapakul, S. Chuanuwatanakul, *Sensors and Actuators B: Chemical*, 314 (2020) 128059.

[95] Q. Qin, X. Bai, Z. Hua, *Journal of Electroanalytical Chemistry*, 782 (2016) 50-58.

[96] P. Kanyong, S.Rawlinson, J. Davis, *Chemosensors*, 2016.

[97] C. Batchelor-McAuley, E. K. atelhon, E.O. Barnes, R.G. Compton, E. Laborda, A. Molina, *ChemistryOpen*, 4 (2015) 224–260.

[98] R.G. Compton, E. Laborda, K.R. Ward, Understanding Voltammetry: Simulation of Electrode Processes, *Imperial College Press*, London, 2014.

[99] R. Baronas, F. Ivanauskas, J. Kulys, *Springer Science & Business Media*, New York, 2009.

[100] A. Kaffash, K. Rostami, H.R. Zare, *Enzyme and Microbial Technology*, 121 (2019) 23-28.

[101] V. Flexer, M.V. Ielmini, E.J. Calvo, P.N. Bartlett, *Bioelectrochemistry*, 74 (2008) 201–209

[102] B.J. Adesokan, X. Quan, A. Evgrafov, A. Heiskanen, A. Boisen, M.P. Sørensen, *Journal of Electroanalytical Chemistry*, 763 (2016) 141-148.

CHAPTER III

Simulation and experimental method

III.1. Introduction

This chapter presents first the simulation method and outlines different analysis tools used for theoretical calculations. Second, it describes the chemical reagents used and details the electrochemical measurements performed.

III.2. Simulation and analysis tools

III.2.1. Semi-analytical Method

Semi-analytical modeling is a common method for simulating electrochemical systems, providing insights into mass transport and kinetics through techniques such as linear sweep or cyclic voltammetry. The approach involves defining the system under study, taking into consideration factors such as the type of redox reaction, mass transport mechanisms, kinetic reactions, and the scanning applied potential method. By specifying these parameters, which provide a full access over defining the voltammetry problem, allowing the use of semi-analytical simulations to effectively address and solve the given electrochemical problem.

In this approach, the semi-analytical solution to the voltammetry problem is divided into two parts, an analytical solution followed by a numerical solution integrating both to compute theoretically voltammetric current–time response. As shown in **Fig. III.1**:

Part I: an analytical method is applied to solve the partial differential equation resulting from the mass transport equation with specified boundary conditions using the Laplace transform. The analytical solution to PDEs re-transformed and subjected to the convolution theorem. Then, the obtained expressions are combined with specific equations from the kinetics and the potential sweep, as well as with boundary conditions, giving the voltammetry integral equation.

Part II: numerical solution of the integral equation (IE) involves a multi-steps process, using the integral subdivision and the method of integration by parts. This approach yields a model that enables to compute voltammetric responses.

Throughout this thesis, the Nicholson and Shain method [1] is employed to utilize the semi-analytical solution.
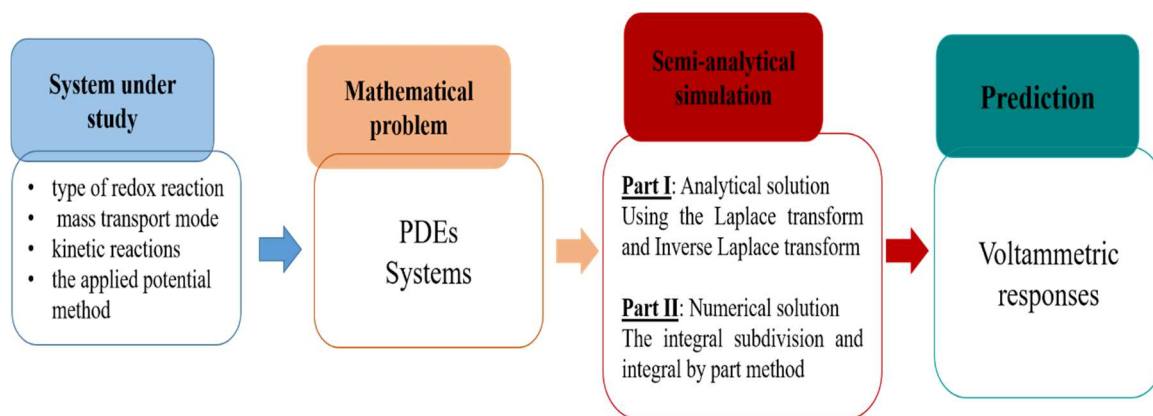
Figure III.1. Representation of semi-analytical strategy for LSV simulation.

III.2.2 Semi-integral method

Semi-integration (SI) method stands as a powerful approach in the analysis of LSV and CV operating to the electrochemical reaction that proceeds under semi-infinite linear diffusion conditions for planar electrodes. This approach is used for quantitative determination of the concentration and the diffusion coefficient. The semi-integrative voltammetry can be described as the semi-integration of the current observed in the voltammogram over time, producing a novel function M(t) termed semi-integrated current. This derived function is related to the concentration of the electroactive species [2-4].

In this thesis, the determination of the diffusion coefficient was achieved by applying the semi-integral (SI) method, using the algorithm proposed by Oldham and Saila [5, 6].

III.2.3 Other Computational details

The developed algorithm for LSV responses were written in Fortran 90. The calculation of charge transfer coefficients was conducted using the Tafel plots. The data analysis and graphing (Analysis and visualization of data) were implemented with Origin 2018.

III.3. Experimental method

III.3.1 Chemical Reagents

All analytical grade chemical reagents used throughout this thesis were bought from Sigma-Aldrich Company, without requiring any purification. The specific reagents included potassium ferrocyanide (K_4FeCN_6), sodium hydroxide (NaOH), potassium chloride (KCl), sodium phosphate monobasic (NaH_2PO_4), sodium phosphate dibasic (Na_2HPO_4), dopamine hydrochloride (1mM), uric acid (1mM), and ascorbic acid (1mM). All aqueous solutions were prepared using double-distilled water.

Phosphate buffer solution (PBS) with a concentration of 0.1 M and a pH=7.4 was prepared from a mixture of NaH_2PO_4 and Na_2HPO_4. The aqueous NaOH was used to adjust the pH of 0.1 M PBS. The solutions containing dopamine (1mM), uric acid (1mM) and ascorbic acid (1mM) were prepared by dissolving the appropriate amount of them in 100 ml phosphate buffer solution.

III.3.2. Electrochemical measurements

Electrochemical experiments were conducted using a VersaSTAT 3 Potentiostat at room temperature. All electrochemical measurements were performed within a single cell setup employing screen-printed graphite electrodes (SPEs) obtained from Manchester Micropolitan University, without any preparation. The SPEs comprise of three electrodes, a graphite working electrode with a surface area of 7.07 mm^2, a graphite auxiliary electrode, and an Ag/AgCl reference electrode.

In this thesis, both LSV and CV techniques were used for different studies. First, the LSV experiments were carried out using a solution containing 5 mM potassium ferrocyanide and 0.1 M KCl as the supporting electrolyte in the potential range between -0.4 V to 0.8 V versus a Ag/AgCl with scan speeds varying from 0.03 V s^{-1} to 0.2 V s^{-1}. Second, cyclic voltammetry experiments were investigated for quantitative analysis of dopamine (1mM), uric acid (1mM) and ascorbic acid (1mM) by sweeping the potential from -0.4 V to 0.6 V in 0.1 M of phosphate buffer solution with a pH of 7.4. The CVs were obtained at various selected scan rates ranging from 0.01 V s^{-1} to 0.2 V s^{-1}.

III.4. Conclusion

       In this chapter, the principle of semi-analytical simulation has been discussed. More details regarding semi-analytical simulation strategy for computing the current response to a single wave potential for soluble-soluble reactions, are well described in the subsequent chapter. The essentials of the electrochemical experimental information were provided.

References

[1] R.S. Nicholson, I. Shain, *Journal of Analytical Chemistry*, 36, 706– 723, 1964.

[2] J.M. Pedrosa, M.T. Martin, J.J. Ruiz, Luis Camacho, *Journal of Electroanalytical Chemistry*, 523 (2002) 160–168.

[3] A.M.P. Sakita, R.D. Noce, C.S. Fugivara, and A.V. Benedetti, *Analytical Chemistry*, 89, 16, (2017)8296–8303.

[4] R. Klicka, *Journal of Electroanalytical Chemistry*, 455 (1998) 253–257.

[5] K.B. Oldham, *Journal of Electroanalytical Chemistry*, 121 (1981) 341.

[6] A. Saila, Doctoral dissertation, University of Badji Mokhtar-Annaba, 2010.

CHAPTER IV

Simulation and analysis of linear sweep voltammetry for soluble-soluble quasi-reversible systems

IV.1. Introduction

This chapter begins by outlining the details of establishment of theoretical linear sweep voltammetry with semi-analytical method. Secondly, we provide an in-depth examination of the linear sweep voltammetry responses for establishing the standard speed constant for soluble redox couples. Following that, the validity of the theoretical results will be discussed through electrochemical oxidation of ferrocyanide.

IV.2. Simulation and calculation procedures

To simulate the LSV for a redox system with soluble-soluble components, the key steps in defining the system are as follows:

An electron exchange process involving soluble reduced (Red) and oxidized (Ox) species was considered:

$$Red \rightleftarrows Ox + ne^- \tag{1}$$

The system was considered to be quasi-reversible, and the electrode kinetics is governed by the well-known Butler-Volmer relationship [1]:

$$I(t) = nFAk^0 \left[C_{red}(0,t)\exp\left[\frac{\alpha nF}{RT}(E - E^0)\right] - C_{ox}(0,t)\exp\left[\frac{-(\beta)nF}{RT}(E - E^0)\right] \right] \tag{2}$$

Where $C_{red}(0,t)$ and $C_{ox}(0,t)$ represent the Red and Ox species concentrations at electrode surface (x=0) at time t.

Via the use of linear sweep voltammetry, E, which is the electrode potential, is linearly scanned in the positive direction beginning from an Ei, which represents the initial potential:

$$E = E_i + vt \tag{3}$$

The initial state is regarded as being in equilibrium, thus the initial potential is determined by the Nernst relationship.

$$E_i = E_{eq} = E^0 + \frac{RT}{nF}\ln\left(\frac{C^*_{Ox}}{C^*_{Red}}\right) \tag{4}$$

In this system, the movement of electroactive species to the electrode surface is governed by diffusion. Therefore, the transport of the analyte is represented by the one-dimensional diffusion relationship, which is ruled by the second equation of Fick:

$$\frac{\partial C(x,t)}{\partial t} = D \frac{\partial^2 C(x,t)}{\partial x^2} \tag{5}$$

With assuming that the bulk solution initially contains just Red species, the initial and boundary conditions can be written as:

$$t = 0, x \geq 0, C_{Red}(x,0) = C_{Red}^*, \quad C_{Ox}(x,0) = 0 \tag{6}$$

$$t > 0, x \rightarrow \infty, C_{Red}(\infty,t) = C_{Red}^*, C_{Ox}(\infty,t) = 0 \tag{7}$$

$$t > 0, x \rightarrow 0, J_{Red}(0,t) = \frac{I(t)}{nFA} = D_{Red}\left[\frac{\partial C_{Red}(x,t)}{\partial x}\right]_{x=0} \tag{8}$$

Here, $J_{Red}(0,t)$ represents the flux of reduced species at the electrode (x=0).

Using Laplace's transform on the first side of Eq. (5), yields:

$$s\bar{C}_{Red}(x,s) - C_{Red}(x,0) = D_{Red}\frac{\partial^2 C(x,t)}{\partial x^2} \tag{9}$$

Where s represents the Laplace variable, the over-bar symbolizes the Laplace transform.

Using the boundary condition in eq. (6), Eq. (9) becomes:

$$\frac{s}{D_{Red}}\bar{C}_{Red}(x,s) - \frac{C_{Red}^*}{D_{Red}} = \frac{\partial^2 C(x,t)}{\partial x^2} \tag{10}$$

Then, eq. (10) can be written as follows:

$$\frac{\partial^2 C_{Red}(x,t)}{\partial x^2} = \left[\sqrt{\frac{s}{D_{Red}}}\right]^2 \bar{C}_{Red}(x,s) - \frac{C_{Red}^*}{D_{Red}} \tag{11}$$

By supposing $a = \sqrt{\frac{s}{D_{Red}}}$, The Laplace transform of eq. (11) is given as:

$$\bar{C}_{Red}(s)(s^2 - a^2) = sC_{Red}(x,0) + C_{Red}(x,0) - \frac{C_{Red}^*}{D_{Red}} \tag{12}$$

By rearranging, it gives:

$$\bar{C}_{Red}(s) = \frac{s^2 C_{Red}(0) + sC_{Red} - \frac{C_{Red}^*}{D_{Red}}}{s(s^2 - a^2)} \tag{13}$$

By decomposing the second side of eq. (13) into fractional equation, it can be rewritten as:

$$\bar{C}_{Red}(s) = \frac{A'(s)}{s+a} + \frac{B'(s)}{s-a} + \frac{D'(s)}{s} \tag{14}$$

A'(s), B'(s), D'(s) represent the decomposition factors.

By multiplying eqs. (13), (14) by s, and supposing s=0. Through comparison between eq. (13) and eq. (14), the value D'(s) is expressed as:

$$D'(s) = \frac{C_{Red}^*}{a^2 D_{Red}}.$$

Hence, formulating equation (14) into a general solution form:

$$\overline{C}_{Red}(x,s) = A'(s) \exp\left[-\sqrt{\frac{s}{D_{Red}}}x\right] + B'(s) \exp\left[\sqrt{\frac{s}{D_{Red}}}x\right] + \frac{C_{Red}^*}{s} \tag{15}$$

Taking into account the first boundary condition Eq. (7) into Eq. (15), the constant B'(s) can be determined.

$$\lim_{x\to\infty} \overline{C}_{Red}(x,s) = \lim_{x\to\infty} \left[A'(s)exp\left[-\sqrt{\frac{s}{D_{Red}}}x\right] + B'(s) \exp\left[\sqrt{\frac{s}{D_{Red}}}x\right] + \frac{C_{Red}^*}{s}\right] = C_{Red}^* \tag{16}$$

Yielding to: B'(s) = 0, we get:

$$\overline{C}_{Red}(x,s) = A'(s)exp\left[-\sqrt{\frac{s}{D_{Red}}}x\right] + \frac{C_{Red}^*}{s} \tag{17}$$

Then, the second boundary condition used to found the constant A'(s) :

$$x \to 0, \left[\frac{\partial C_{Red}(x,t)}{\partial x}\right]_{x=0} = \frac{I(t)}{nFAD_{red}} \tag{18}$$

According to eq. (18), the equation (17) derived to get:

$$\frac{\partial C_{Red}(x,s)}{\partial x} = -\sqrt{\frac{s}{D_{Red}}}A'(s)exp\left[-\sqrt{\frac{s}{D_{Red}}}x\right] \tag{19}$$

For x =0, the equation (19) can be reduced to:

$$\left[\frac{\partial C_{Red}(x,s)}{\partial x}\right]_{x=0} = -\sqrt{\frac{s}{D_{Red}}}A'(s) \tag{20}$$

Then, by setting the equations (18) and (20) equal to each other, A'(s) can be determined as:

$$A'(s) = -\frac{I(s)}{nF\sqrt{D_{Red}}\sqrt{s}} \tag{21}$$

Upon substituting equation (21) into equation (17), and subsequently applying inverse Laplace-transforming, we arrive at the time evolution relationship [1].

$$C_{Red}(0,t) = C_{Red}^{*} - \frac{1}{nFA\sqrt{D_{Red}}} \frac{1}{\sqrt{\pi}} \int_0^t \frac{I(\tau)}{\sqrt{t-\tau}} d\tau \tag{22}$$

Using the same procedure, we obtain the equation of $C_{OX}(0,t)$:

$$C_{Ox}(0,t) = \frac{1}{nFA\sqrt{D_{ox}}} \frac{1}{\sqrt{\pi}} \int_0^t \frac{I(\tau)}{\sqrt{t-\tau}} d\tau \tag{22'}$$

To drive to the voltammetry integral, we first replace the eq. (3) into eq. (2) to obtain the function of current-potential in linear sweep voltammetry:

$$I(t) = nFAk^0 C_{red}(0,t) \left[ex^{\frac{nF}{RT}(E_i - E^0)} e^{\frac{nF}{RT}vt} \right]^{\alpha} - nFAk^0 C_{ox}(0,t) \left[e^{\frac{nF}{RT}(E_i - E^0)} e^{\frac{nF}{RT}vt} \right]^{-\beta} \tag{23}$$

Before deriving the solution to voltammetry model, a normalization of the parameters used within the system is necessary to provide general and easier applicability under different electrochemical systems. Furthermore, the conversion of dimensional parameters into dimensionless forms is employed. Hence, the different adimensionl parameters are defined in the following **Table IV.1.**

Table IV.1. Adimensionl parameters.

Adimensionl Parameter	Equation	Eq. Nº
Initial potential INIT	$INIT = \frac{nF}{RT}(E_i - E^0)$	(24)
final potential LIMIT	$LIMIT = \frac{nF}{RT}(E - E^0)$	(25)
Applied potential Φ	$\Phi = \frac{nF}{RT}(E(t) - E^0) = INIT - \sigma t$	(26)
Scan rate σ	$\sigma = \frac{nF}{RT}(v)$	(27)

By substituting equations (22), (22'), (24), (25), (26) and (27) into equation (23), and by rearranging, we get:

$$I(t) = nFAk^0 \left[C^*_{Red}[\theta S(t)]^{\alpha} - \frac{1}{nFA\sqrt{\pi D_{red}}}[\theta S(t)]^{\alpha} \int_0^t \frac{I(\tau)}{\sqrt{t-\tau}} d\tau - \frac{1}{nFA\sqrt{\pi D_{ox}}}[\theta S(t)]^{-\beta} \int_0^t \frac{I(\tau)}{\sqrt{t-\tau}} d\tau \right] \tag{28}$$

Where $S(t)$, θ are defined as:

$$S(t) = \exp(\sigma t) \tag{29}$$

$$\theta = \exp\left[\frac{nF}{RT}(E_i - E°)\right] \tag{30}$$

With supposing $D_{red}=D_{Ox}$ and after rearrangement, yields:

$$\int_0^t \frac{I(t)}{\sqrt{t-\tau}}d\tau = \left[\frac{n\,FAC_{Red}^*\sqrt{\pi\,D_{Red}}}{1+[\theta S(t)]^{-(\alpha+\beta)}}\right]\left[1 - \frac{I(t)\,[\theta S(t)]^{-\alpha}}{n\,FAC_{Red}^*K^0}\right] \tag{31}$$

Herein, the solution of equation (31) requires a numerical resolution.

In numerical resolution, the equation (31) is adimensionalized using the following redefinitions:

$z = \sigma\tau$, $I(\tau) = g(z)$.

So, equation (31) can be written as:

$$\int_0^{\sigma t} \frac{g(z)}{\sqrt{\sigma t - z}\,\sqrt{\sigma}}dz = \left[\frac{n\,FAC_{Red}^*\sqrt{\pi\,D_{Red}}}{1+[\theta S(\sigma t)]^{-(\alpha+\beta)}}\right]\left[1 - \frac{I(t)\,[\theta S(\sigma t)]^{-\alpha}}{n\,FAC_{Red}^*K^0}\right] \tag{32}$$

After dividing both sides of eq. (32) by $nFAC_{Red}^*\sqrt{\pi D_{Red}}$, the dimensionless current is defined as:

$$\chi(z) = \frac{g(z)}{nFAC_{Red}^*\sqrt{\pi D_{Red}\sigma}} \tag{33}$$

Eq. (32) becomes:

$$\int_0^{\sigma t} \frac{\chi(z)}{\sqrt{\sigma t - z}}dz = \left[\frac{1}{[1+[\theta S(\sigma t)]^{-(\alpha+\beta)}]}\right]\left[1 - \frac{I(t)}{nFAC^*{}_{Red}k^0}[\theta S(\sigma t)]^{-\alpha}\right] \tag{34}$$

By multiplying the right-hand term from the second side of Eq. (34) by $\frac{\sqrt{\pi D_{Red}\sigma}}{\sqrt{\pi D_{Red}\sigma}}$, and defining the dimensionless heterogeneous rate constant Λ [2]:

$$\Lambda = \frac{k^0}{\sqrt{D_{Red}\sigma}} \tag{35}$$

Thus, we get:

$$\int_0^{\sigma t} \frac{\chi(z)}{\sqrt{\sigma t - z}}dz = \left[\frac{1}{[1+[\theta S(\sigma t)]^{-(\alpha+\beta)}]}\right]\left[1 - \chi(\sigma t)\sqrt{\pi}\frac{1}{\Lambda}[\theta S(\sigma t)]^{-\alpha}\right] \tag{36}$$

Chapter IV

Solving equation (34) requires partitioning the integration domain into a number of segments of equal width δ.

By using the following definitions: $z = \delta k$, $\sigma t = \delta N$, Eq. (36) is rewritten as follows:

$$\sqrt{\delta} \int_0^{\delta N} \mathcal{X}(\delta k) \frac{1}{\sqrt{N-k}} dk = \left[\frac{1}{[1+[\theta S(\delta N)]^{-(\alpha+\beta)}]}\right]\left[1 - \mathcal{X}(\delta N)\sqrt{\pi}\frac{1}{\Lambda}[\theta S(\delta N)]^{-\alpha}\right] \qquad (37)$$

Then, upon applying the integration by parts on the left side of the expression (37), we find:

$$2\sqrt{\delta}\chi(0)\sqrt{N} + 2\sqrt{\delta}\int_0^{\delta N}\sqrt{N-k}(\mathcal{X}(\delta k)) = \left[\frac{1}{[1+[\theta S(\delta N)]^{-(\alpha+\beta)}]}\right]\left[1 - \mathcal{X}(\delta N)\sqrt{\pi}\frac{1}{\Lambda}[\theta S(\delta N)]^{-\alpha}\right] \qquad (38)$$

The left-hand part of Equation (38) can be written as a summatioxn :

$$\chi(1)\sqrt{N} + \sum_{i=1}^{N-1}\sqrt{N-i}[\chi(i+1)-\chi(i)] = \frac{1}{2\sqrt{\delta}}\left[\frac{1}{[1+[\theta S(\delta N)]^{-(\alpha+\beta)}]}\right]\left[1 - \mathcal{X}(\delta N)\sqrt{\pi}\frac{1}{\Lambda}[\theta S(\delta N)]^{-\alpha}\right] \qquad (39)$$

Where: $\chi(i) = \chi(\delta i)$

Taking the development of the summation expression for eq. (39) yields to the following expression:

$$\chi(1)\sqrt{N} + \sqrt{N-1}[\chi(2)+\chi(1)] + \sqrt{N-2}[\chi(3)-\chi(2)] + \sqrt{N-3}[\chi(4)\chi(3)]+......+\sqrt{N-(N-2)}$$
$$+[\chi(N-1)-\chi(N-2)] + \sqrt{N-(N-1)} + [\chi(N)-\chi(N-1)] = A(N) - B(N)\chi(N) \qquad (40)$$

Where,

$$A(N) = \frac{1}{2\sqrt{\delta}}\left[\frac{1}{1+[\theta S(\delta N)]^{-(\alpha+\beta)}}\right] \qquad (41)$$

$$B(N) = A(N)\sqrt{\pi}\frac{1}{\Lambda}[\theta S(\delta N)]^{-\alpha} \qquad (42)$$

Hence, the equation defines N equations for $\chi(i)$.

$$\chi(N) + \sum_{i=1}^{n-1}\left[\sqrt{N-(i-1)} - \sqrt{N-i}\right]\chi(i) = A(N) - B(N)\chi(N) \qquad (43)$$

The numerical resolution of equation (43) allows us to formulate dimensionless curves of the current $\chi(k)$ over the potential pot(k), where, the developed expressions for calculating the dimensionless curves of current $\chi(k)$ and potential $\Phi(k)$ are as follows:

$$\chi(k) = \frac{\left(A(k) - \sum_{i=1}^{k-1}\left[\sqrt{k-(i-1)} - \sqrt{k-i}\right]\chi(i)\right)}{(1+B(k))}$$

(44)

$$\Phi(k) = \frac{nF}{RT}(E - E^0) = init + \delta k$$

(45)

With:

$$A(k) = \frac{1}{2\sqrt{\delta}}\left[\frac{1}{1+[\theta exp(\delta k)]^{-(\alpha+\beta)}}\right]$$

(46)

$$B(k) = A(k)[\sqrt{\pi}\frac{1}{\Lambda}[\theta exp(\delta k)]^{-\alpha}$$

(47)

A developed algorithmic was implemented coded in Fortran language. It allows calculating the theoretical linear sweep voltammograms by inputting values of the following parameters: INIT, LIMIT, Λ and α.

The general flowchart for LSV algorithm is illustrated in Fig. IV.1.

```
                    ┌─────────────────────┐
                    │   LSV algorithm     │
                    │  Program Sol-Sol    │
                    └─────────────────────┘
```

Parameter (nmax=5000)
Implicit double precision (a-h,o-z)
Double precision INIT, LIMIT
Character*12Fich1
Character*12Fich2
Dimension Y(0: NMAX) , PHI(0: NMAX),
 PHId(0:NMAX), Yd(0:NMAX), X(0:NMAX)
Equivalence (PHI (0), INIT)

```
                    ┌─────────────────────┐
                    │  Open Results File  │
                    └─────────────────────┘
```

Pi=3.1416
R=8.314
F=96485.31
Delta=0.1
INT1=IT
INT2=2*IT
C=1.d0/2.d0*dsqrt(DELTA)
IT= ((INIT-LIMIT)/DELTA)
F_1=2*(LIMIT-INIT)
F_2=R*T/n*F
C_2=n*F*$\sqrt{D * \dfrac{v}{F_2}}$
TETHA=dexp (INIT)

```
                    ┌─────────────────────┐
                    │  DO 10 k=1 , INT₁    │
                    └─────────────────────┘
```

$$\text{DO 10 k=1 , INT}_1$$

(A)

$A=C*[(THETA*exp(DELTA*k)^{(\alpha+\beta)})/(1+THETA*exp(DELTA*k)^{(\alpha+\beta)})]$
$B=A*\sqrt{\pi}\frac{1}{\Lambda}/(THETA*exp(DELTA*k))^{\alpha}$

Sigma=0.d0

Yes

No

K=1

Do 20 j=1 , k-1

$SIGMA=SIGMA-[\sqrt{k+1-j}-\sqrt{k-j}].X(j)$

X(K)=(A+SIGMA)/(1+B)

Y(K)=(X(K)*dsqrt(PI))

Write on File Fich 1 PHI(k) , Y(k)

Continue

B

No

Yes

Rep=0

Open File Fich2

Read n,T ,D,v

Do11 k=1,INT1

$PHId(k)=F_2*pot(k)$
$Yd(k)=y(k)*C_2$

Write on File Fich2 PHId (k) ,Yd(k)

Continue

Close   File Fich2

Stop End

Close File Fich2

Figure IV.1. Flowchart for the implemented LSV algorithm.

IV.3. Results and discussion

IV.3.1. Theoretical results

In the analysis of LSV, the peak current, half-peak width, and peak potential are crucial characteristics for assessing the electron transfer reversibility. The LSV responses are affected upon various variables, comprising the charge transfer coefficient α and k^0. The joint influence impact of k^0 and v is quantified by means of adimensionl kinetic parameter, Λ, defined by Eq. (35). In this section, the effects of varying Λ and α on the positioning and shape of peak are studied.

Fig. IV.2. presents a standard theoretical LS voltammograms of a reversible redox couple computed with Λ=10^3 and α=0.5 in the corresponding directions of cathodic and anodic potential sweeps. The voltammograms exhibit symmetry, showing identical characteristics in both form and magnitude of peak current. The characteristics of voltammograms are independent on the sweep direction of the potential for soluble-soluble systems.
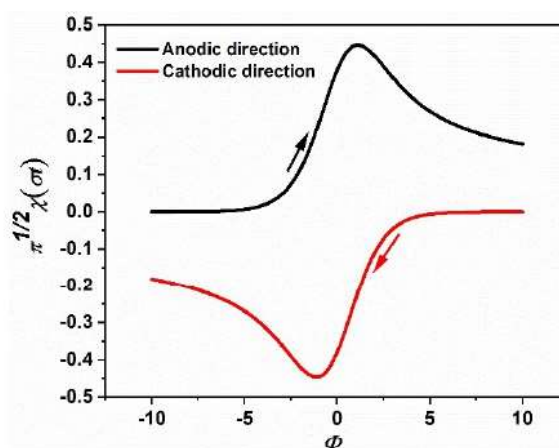
Figure IV.2. Simulated linear sweep voltammograms for reversible soluble-soluble reaction in both anodic (black) and cathodic (red) sweep potential directions.

IV.3.1.1. Influence of kinetic rate

The variation of Λ was inspected at a fixed value of α and results are shown in **Fig. IV.3**. Furthermore, **Table IV.2** presents the development of dimensionless peak current values corresponding to adimensionl rate constants at α=0.5. Through quantitative data analysis, three distinct regions can be identified:

1) For $\Lambda \geq 10^3$

The theoretical voltammograms are not affected by the dimensionless kinetic parameter Λ. Additionally, the value of the dimensionless peak current $\pi^{1/2}\chi_p$ remains constant at a value of 0.4463, which is identical with that reported in literature concerning the soluble redox reversible couples [3-5].

2) For $\Lambda \leq 10^{-3}$

In this zone, simulated linear sweep voltammograms maintain identical shapes with the peak potential position shifting towards anodic direction as Λ value drops. The adimensional peak current remains unchanged where $\pi^{1/2}\chi_p = 0.4958\ \alpha^{1/2}$, corresponding to the value previously reported for irreversible charge transfer process [5].

3) For $10^{-3} < \Lambda < 10^3$

Within this intermediate zone, the peak characteristics of voltammograms are strongly influenced by the adimensionl rate constant Λ. Therefore, the reduction of Λ results to a reduction in $\pi^{1/2}\chi_p$. As well as Λ decreases, the peak potential moves marginally towards anodic values. This zone is defined as quasi-reversible systems region [2, 6].
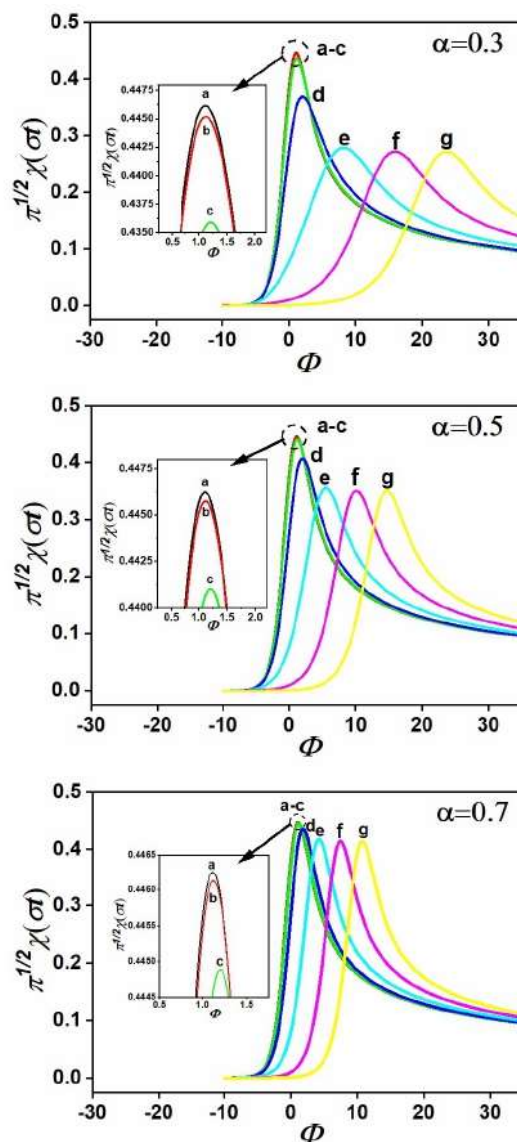
Figure IV.3. Theoretical linear sweep voltammatric responses calculated for different value of Λ at α=0.3 (top), 0.5 (middle) and 0.7 (bottom) a) $\Lambda = 10^3$, b) $\Lambda = 10^2$, c) $\Lambda = 10^1$, d) $\Lambda = 1$, e) $\Lambda = 10^{-1}$, f) $\Lambda = 10^{-2}$, g) $\Lambda = 10^{-3}$.

Table IV.2. The variation of dimensionless peak current $\pi^{1/2}\mathcal{X}_p$ with dimensionless rate constant Λ for different curves presented for α=0.5 in **Fig. IV.3** (middle).

Λ	$\pi^{1/2}\mathcal{X}_p$	Λ	$\pi^{1/2}\mathcal{X}_p$	Λ	$\pi^{1/2}\mathcal{X}_p$
10^6	0.4463	10^2	0.44575	10^{-3}	0.3505
10^5	0.4463	10^1	0.4410	10^{-4}	0.3505
10^4	0.4463	10^0	0.4069	10^{-5}	0.3505
10^3	0.44625	10^{-1}	0.3559	10^{-6}	0.3505
		10^{-2}	0.3507		

Chapter IV

IV.3.1.2. Influence of the charge transfer coefficient

In Fig. IV.4, a number of adimensionl voltammograms obtained for various charge transfer coefficients α with different adimensionl rate constants Λ are displayed. For Λ= 10^3, the voltammograms remain unaffected by α. For Λ=1 and Λ=10^{-1}, an increase in α leads a minor rise in the peak current. For Λ= 10^{-3}, the dependence of the peak current and peak potential on α is evident, wherein, the peak current rises and the peak potential moves towards more anodic potentials as α increases and voltammograms are completely distinct. The deductions drawn from these instances support the ones outlined in section **IV.3.1.1**.

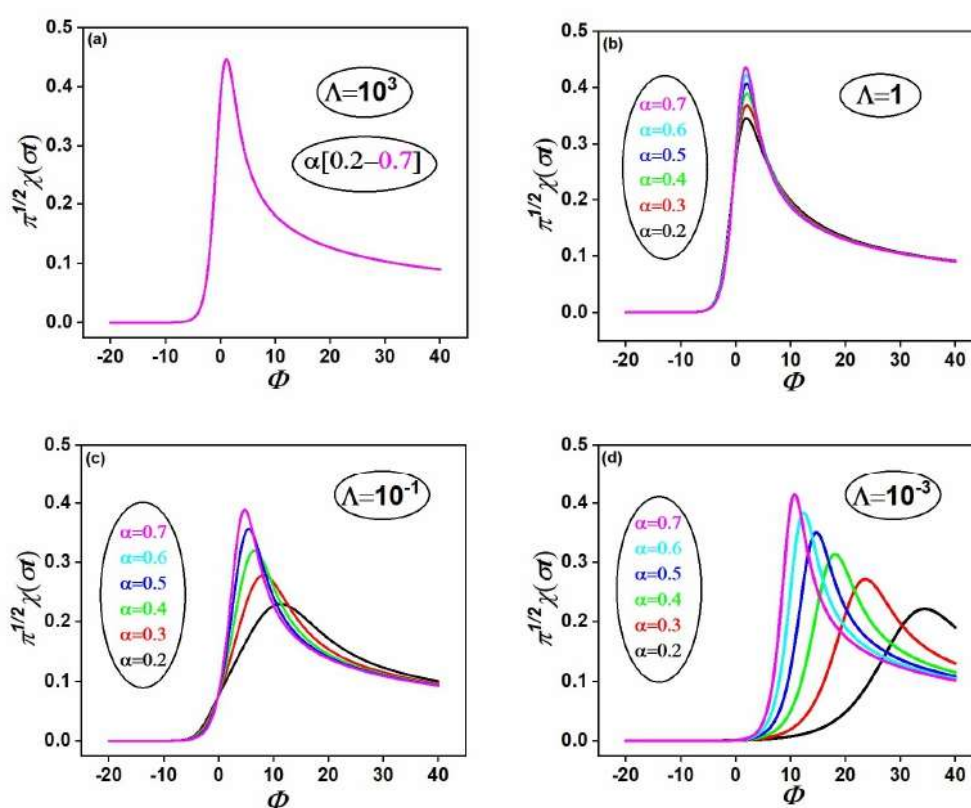***Figure IV.4.*** The influence of charge transfer coefficient on theoretical linear sweep voltamograms for Different values of the dimensionless rate constant.

From results presented in **Fig. IV.3** and **Fig. IV.4**, revealing clearly coupled effect of (Λ) and (α) on the linear sweep voltammograms characteristics. Consequently, a change in peak parameters are dependent on the values of Λ and α.

IV.3.1.3. Kinetic curves and interpolation relationships
Kinetic curves

Matsuda and Ayabe have conducted an investigation into the impact of Λ and α on peak quantities of LS voltammograms, resulting in the establishment of three diagrams illustrating the relationship between the adimensionl peak current, half-peak width, and peak potential with respect to the normalized heterogeneous rate constant Λ and the electron transfer coefficient α [6]. In this segment, we've reconstructed the three diagrams of Matsuda in the broad intervals of $\Lambda = [10^{-6} - 10^{6}]$ and $\alpha = [0.2 - 0.7]$. Subsequently, four additional diagrams were derived for designated Λ ranges. Following this, different characteristic equations were established by interpolation in order to determine the standard speed constant from experimental curves, particularly in the context of non reversible redox couples.

Fig. IV.5 displays the variation of different peak characteristics, including

$$\Psi_p/\left(\Psi_p\right)_{rev} = \pi^{\frac{1}{2}} \chi_p / \left(\pi^{\frac{1}{2}} \chi_p\right)_{rev}, \ \Delta\Phi_{p/2} = \frac{nF}{RT}\left(E_p - E_{p/2}\right) \text{ and } \eta_p = \frac{nF}{RT}\left(E_p - E^0\right) \text{ varying}$$

with $log\ \Lambda$ and α. The two-dimensional illustration is depicted on the left-hand side of **Fig. IV.5** meanwhile, the three-dimensional illustration is shown on the right. $\left(\Psi_p\right)_{rev}$ represents the reversible adimensionl peak current , which is equal to 0.4463. At a cursory look, one can deduce that the characteristics' of peaks are closely identical to the ones documented by Matsuda. The 1st 2D diagrams in Fig. IV.5 (a, b), corresponding to the peak current, and the half peak width exhibit a sigmoidal dependency. However, a quadratic dependency is shown in the last diagram (Fig. IV.5 (c)). The 3D diagrams provide a clear representation of the distinction between the varied regions unlike in 2D diagrams. The shift from a reversible to an irreversible system is more distinct. Then, the linear portions of the diagrams exposed in **Fig. IV.5** is depicted in **Fig. IV.6**. This simplified presentation makes it easy to produce a linear interpolation within the specified ranges of Λ.
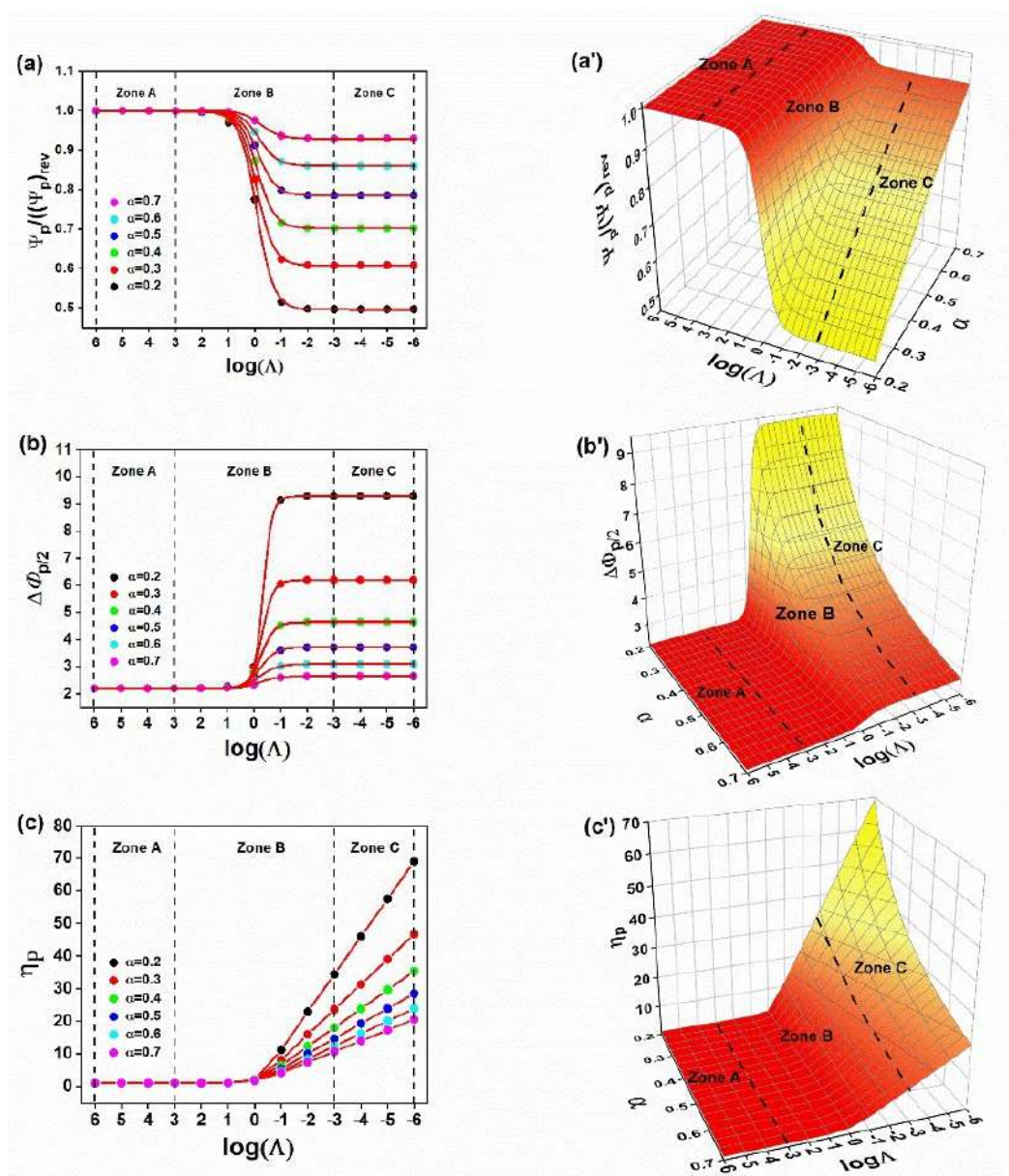
Figure IV.5. The effect of the kinetic rate constant Λ and charge transfer coefficient α on the peak current ratio $\Psi_p/\left(\Psi_p\right)_{rev}$ (a, a'), the half peak width $\Delta\Phi_{p/2}$ (b, b'), and the peak potential η_p (c, c') in 2D (left) and 3D (right) representations.
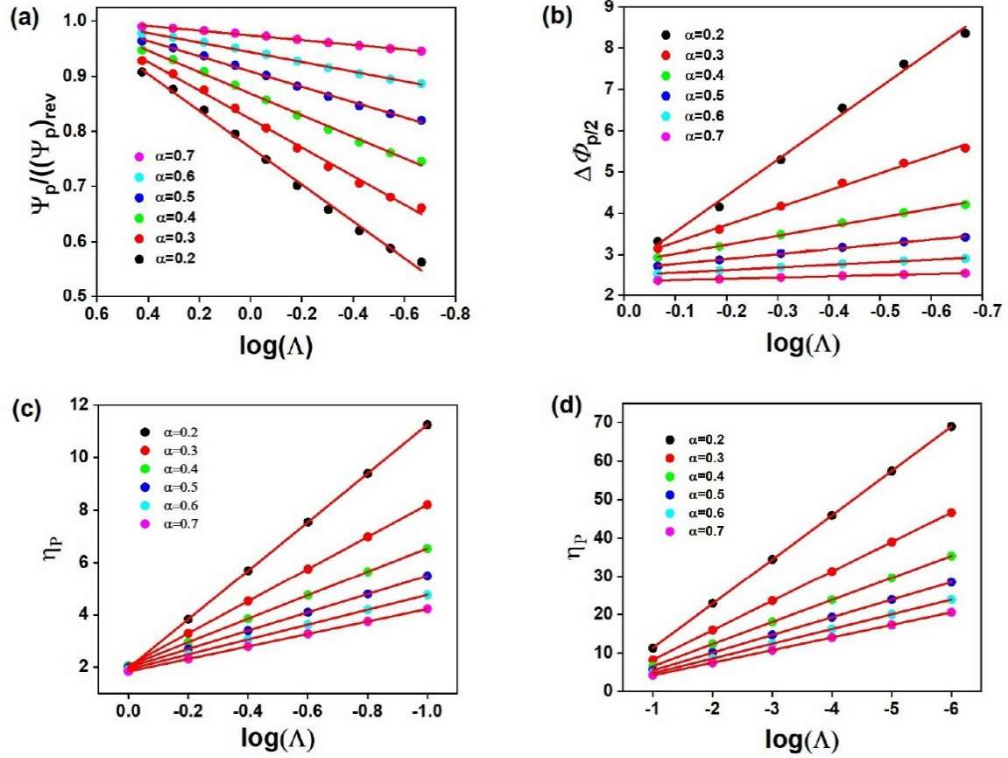
Figure IV.6. Linear effects of the peak current ratio $\dfrac{\Psi_p}{(\Psi_p)_{rev}}(a)$, the half peak width $\Delta\Phi_{\frac{p}{2}}$ (*b*), and

the peak potential η_p (c, d) on the restricted ranges of Λ for different α values.

Despite the fact that the form of the diagrams in **Fig. IV.5** vary significantly, their alignment can be identified in 3 clearly defined kinetic regions, as stated bellow:

Zone A: for $\Lambda \geq 10^{+3}$. The dimensionless kinetic rate Λ and α have no influence on the peak parameters. The adimensional kinetic speed Λ and α do not impact the peak characteristics. The current peak, the half peak width, and the potential peak expressions are similar with those of the reversible charge transfer reaction [3-5, 7]. The units of different parameters are indicated in the Nomenclature section.

$$I_p = 0.4463 \; n \; F \; A \; C_{Red}^* (D_{Red})^{1/2} \left(\frac{nF}{RT}\right)^{1/2} v^{1/2} \tag{48}$$

$$E_p - E_{p/2} = 2.20 \frac{RT}{nF} \tag{49}$$

$$E_p = E_{1/2} - 1.109 \frac{RT}{nF} \tag{50}$$

Zone B: Lies within the interval of ($10^{-3} < \Lambda < 10^3$), where *quasi*-reversible behaviour is observed. Notably, significant variations in peak characteristics are evident as functions of both of Λ and α. It's evident that there was a significant alteration in peak parameters in terms of Λ

and α. To best of our knowledge, no particular kinetics relationships have been found to describe this *quasi*-reversible attitude.

Zone C: characterized for $\Lambda \leq 10^{-3}$. This zone of curves exhibit irreversible features. For a constant value of α, both the peak current and the half peak width remain unchanged as Λ decreases. As, the peak potential keeps increasing. The following relationships describing the irreversible systems [5] can be acquired as follows:

$$I_p = 0.4958 \, nF \, A \, C^*_{Red}(D_{Red})^{1/2} \, \alpha^{1/2} \left(\frac{nF}{RT}\right)^{1/2} v^{1/2} \tag{51}$$

$$E_p - E_{p/2} = 1.857 \frac{RT}{nF\alpha} \tag{52}$$

$$E_p = E^0 - \frac{RT}{nF\alpha}\left(0.780 + ln\sqrt{D_{Red}b} - \ln k^0\right) \tag{53}$$

Where $b = \alpha nFv/ RT$

Interpolation relationships

The graphics of **Fig. IV.5** (a) and (b) exhibit sigmoidal patterns. The data interpolation was fitted excellently by the sigmoidal Boltzmann function:

$$y = A2 + \left\{\frac{[A1-A2]}{\left[1 + \exp\left(\frac{x-x0}{dx}\right)\right]}\right\} \tag{54}$$

A1, A2, x0 and dx are the parameters of the sigmoid Boltzmann function.
Furthermore, the fitted relationships were found:

$$\frac{\Psi_p}{(\Psi_p)_{rev}} = 0.999 + \frac{(1.112\alpha^{0.5}-0.999)}{1+\exp\left[\frac{\log(\Lambda)-(-0.489\alpha^3 - 0.0589)}{0.111\alpha^3 + 0.322}\right]} \tag{55}$$

$$\Delta\Phi_{p/2} = 2.214 + \frac{(1.859\alpha^{-1}-2.214)}{1 + \exp\left(\left[\frac{\log(\Lambda)-(-0.208\alpha^{-0.327})}{0.440\alpha^{0.608}}\right]\right)} \tag{56}$$

The coefficient of correlation of equations (55) and (56) are 0.99980 and 0.99988, respectively

The developed relationships allow the determination of standard rate constant k^0 using I_p, E_p or $E_{p/2}$ values obtained from the experimental data, whatever the process is reversible, *quasi*-reversible or irreversible, provided that α is known.

According to the relationships (55) and (56), which are longs and somewhat complex. Nevertheless and as presented in **Fig. IV.6**, a linear form is observed in the regions of $log \wedge = $ [-0.66, 0.42] of the curves of **Fig. IV.5** (a) and those of **Fig. IV.5** (b) within the $log \wedge = $ [-0.66, -0.06] range. After fitting the data in these two $\wedge$ regions, the following equations were obtained:

$$\frac{\Psi_p}{(\Psi_p)_{rev}} = (1.039\alpha^{0.19}) + (0.436 - 0.578\alpha)\log(\Lambda) \tag{57}$$

$$\Delta\Phi_{p/2} = (3.401 - 1.493\alpha) + (3.481 - 2.392\alpha^{-1})\log(\Lambda) \tag{58}$$

The R^2 of relationships (57) and (58) are 0.99436 and 0.99912, correspondingly.

In conclusion, achieving a straightforward fit for the plots depicted in **Fig. IV.5 (c)** across the entire Λ region is unattainable. Nonetheless, the subsequent approximate equations linearly depict the variations of η_p with Λ and α.

For $-1 \leq log \wedge \leq 0$,

$$\eta_P = (2.379\alpha^{-0.694}) + (-1.288\alpha^{-0.999})\log(\Lambda)) \tag{59}$$

For $log \wedge \leq -1$,

$$\eta_P = (1.222 - 0.189\alpha^{-1}) + (-2.296\alpha^{-1})\log(\Lambda) \tag{60}$$

The R^2 of the equations (59) and (60) is 0.99833.

The relationships (55), (56), and (60) exhibit similar forms to those of the quasi-reversible soluble-insoluble systems derived by Atek et al. [8]. Meanwhile, equations (57) and (58) bear resemblance to the ones that were acquired by Krulic [9] for (SCV). Using these relationships, the determination of k^0 is notably more suitable and accurate than relying on Matsuda's diagrams. Additionally, Matsuda's diagrams were designed for specific α values, making it difficult to predict intermediate values in constant-rate kinetics. For example, when $\alpha = 0.22$ or $\alpha = 0.57$, the influence of α on the voltammogram features (like peak current, half-peak width, and peak potential) does not follow a linear trend.

IV.3.2. Theory-experiment validation

Fig. IV.7 (a) and (b) show CV and LS voltammograms which were conducted by employing varying scan rates, to investigate at a screen-printed electrodes (SPE) the oxidation of ferrocyanide in a potassium chloride electrolyte. The redox reaction between Ferrocyanide and Ferricyanide is extensively studied in electrochemistry literature [10-14]. This system involves a straightforward one-electron transfer reaction between soluble species which can be outlined according to the subsequent equation:

$$Fe(CN)_6^{4-} \rightleftharpoons Fe(CN)_6^{3-} + 1\,e^- \tag{61}$$

In Fig. IV.7 (b), linear sweep voltammetry experiments are presented, we can observe that as the scanning speed goes up, the peak current also goes up. Additionally, the peak potential moves to anodic potentials as the scan speed rises, suggesting that the transmission of charge isn't reversible. The current peaks increase linearly with $v^{1/2}$, as depicted in Fig. IV.7 (c), implying that the anodic oxidation of Fe $(CN)_6^{4-}$ on SPEs was controlled by diffusion.

Hereafter, we will elaborate extensively on the computation of the voltammogram acquired at 50 mV s^{-1}. After that, we'll summarize the important findings for the remaining scan rates.
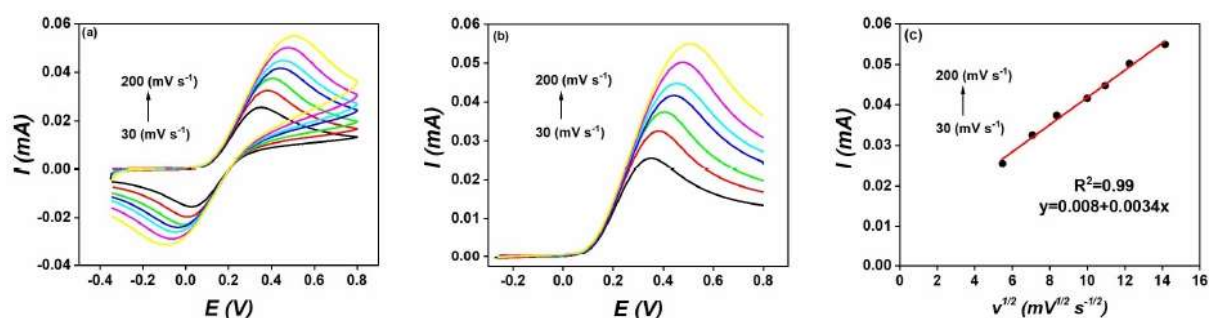
Figure IV.7. (a) Cyclic voltammograms (b) linear sweep voltammograms plots representing the oxidation of 5 mM potassium ferrocyanide on a screen-printed graphite electrode with 0.1 M potassium chloride at various scan rates. (c) The anodic peak currents variation with the square root of the scan rate.

IV.3.2.1. Charge transfer coefficient and diffusion coefficient calculation

The Tafel curve derived from experimental LS voltammetry is shown in **Figure IV.8 (a)**, obtained at a scan speed of 50 mVs^{-1}. By determining the anodic slope of Tafel curves, we calculated the α value as 0.259, which is then noted in **Table IV.2**. Moreover, an alternative analysis of the voltammogram in **Figure IV.8 (a)** was conducted using the semi-integral approach. The voltammogram accompanied by its semi-integral plot, labeled as *m*, was displayed in **Figure IV.8 (b)**. The values obtained from semi-integration converge toward a threshold, indicated as m*, as a result of diffusion constraints on mass transfer. The diffusion coefficient $D_{Fe(CN)_6^{4-}}$ can be derived from this threshold value using the subsequent equation [15, 16]:

$$m^* = n \, FA \, C^*_{Red}(D_{Red})^{1/2} \tag{62}$$

The determined value for the diffusion coefficient $D_{Fe(CN)_6^{4-}}$ is 6.45×10^{-6} cm^2 s^{-1}. Previous studies have reported a diffusion coefficient range between 6.10×10^{-6} and 8.0×10^{-6} cm^2 s^{-1} in the aqueous solutions [11, 17-19], consistent with our finding.
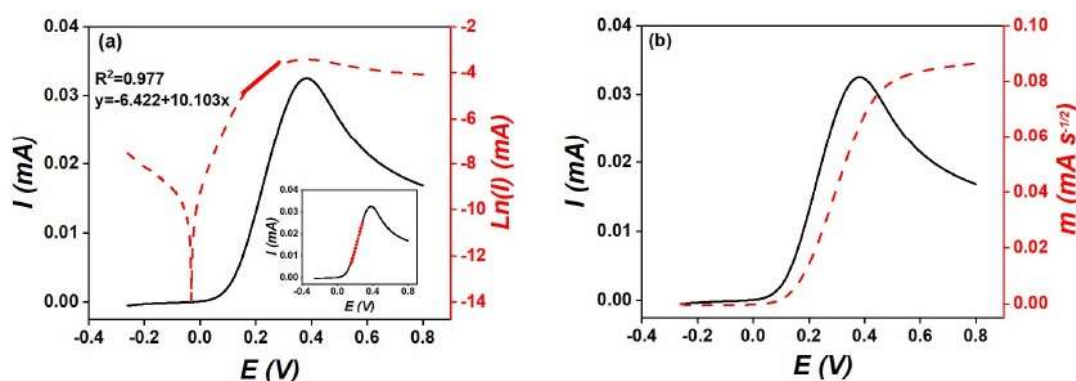
Figure IV.8. (a) Linear sweep voltammetry and Tafel plots at scan rate of 50 mVs^{-1} (b) LSV response at scan rate 50 mVs^{-1} (black line), with its convoluted curve (red lines).

IV.3.2.2. Determining standard rate constant through the use of interpolation relationships

The LSV curve in **Fig. IV.8 (a)** yields peak current *Ip*, peak potential *Ep*, and half-peak potential $Ep - E_{p/2}$ values of 0.0325 mA, 0.3828 V, and 0.1613 V correspondingly. To convert these values into dimensionless units, we proceed as follows:

$$\frac{\Psi_p}{(\Psi_p)_{rev}} = \frac{I_P}{0.4463 \ n \ FA \ C^*_{Red}(D_{Red})^{1/2} \left(\frac{nF}{RT}\right)^{1/2} v^{1/2}} = 0.603 \tag{63}$$

$$\Delta\Phi_{p/2} = \frac{nF}{RT}\left(E_p - E_{p/2}\right) = 6.278 \tag{64}$$

$$\eta_p = \frac{nF}{RT}\left(E_p - E^0\right) = \frac{nF}{RT}(0.3828 - 0.1337) = 9.696 \tag{65}$$

The E^0 value utilized in this computation is 0.1337 V versus Ag/AgCl [20].

Equations (55-60) facilitate the determination of Λ. Employing relationship (35), the standard rate constant k^0 values are derived, which are then documented in **Table IV.3.**

Table IV.3. The parameters of electrochemical kinetics for the oxidation reaction of ferrocyanide extracted from the voltammogram recorded at a scan rate of 50 mV s^{-1}.

	α		$D_{Fe(CN)_6^{-4}}$, 10^{-6} cm^2 s^{-1}	Λ		k^0, 10^{-4} cm s^{-1}	
Tafel	0.259	SI	6.45	Eq. 55	0.1464	Eq. 55	5.1854
Fit	0.260	Fit	6.50	Eq. 56	0.2426	Eq. 56	8.5956
				Eq. 57	0.1987	Eq. 57	7.0414
				Eq. 58	0.2709	Eq. 58	9.5988
				Eq. 59	0.1866	Eq. 59	6.6115
				Eq. 60	0.0916	Eq. 60	3.2444
				Fit	0.1646	Fit	5.8543

Initially, it is observed that the Λ values, ranging from 0.09 to 0.24, fall within the quasi-reversible region defined in **section IV.4.1.3** ($10^{-3} < \Lambda < 10^3$), and align with the ranges suggested by Matsuda ($10^{-2(1+\alpha)} < \Lambda < 15$) [2] and Kwak ($10^{-1.7} < \Lambda < 10^{1.7}$) [21]. Studies show that the standard rate constant (k^0) values for the oxidation of ferrocyanide on carbon material electrodes typically vary between 4.9×10^{-4} and 2.0×10^{-2} cm s^{-1} [22, 23]. The calculated values here fall within this range, suggesting that the performance of ferrocyanide at SPEs is quasi-reversible. This highlights an easier and more interesting way to figure out rate constants from specific points on linear sweep voltammetry graphs.

IV.3.2.3. Simulation and fitting

Here, we show how the developed equations can be applied. To begin with, we utilized the values of D, α, and k^0 determined in **sections IV.3.2.1** and **IV.3.2.2** to simulate the voltammograms. Furthermore, we conducted a fitting test, utilizing a range of values for D, α, and k^0, to obtain the most accurate alignment between the computed and experimental curves.

Fig. IV.9 displays the simulated voltammograms. Notably, those generated using k^0 values derived from equations (55-60) closely match the experimental voltammogram, especially when equations (55), (57), and (59) pertaining to peak current and peak potential are employed. The minor differences observed while applying equations (56) and (58) could stem from the effect of ohmic drop. However, in the case of equation (60), these variations can be ascribed to the adimensional rate constant Λ falling beyond the applicable range for this equation.

A strong match (shown in **Fig. IV.10**) was achieved between the experimental Linear Sweep Voltammetry curves and simulated curves using these values:

$D=6.5\times10^{-6}$ cm^2 s^{-1}, α=0.26 and $k^0=5.854\times10^{-4}$ cm s^{-1}.

The k^0 derived from fitting falls within the spectrum of k^0 values derived from equations (55-60), particularly showing strong similarity to those calculated by equations (55), (57), and (59).

In **Figure IV.10**, we have juxtaposed the simulated, the fitted and the experimental curves. The simulated curve was obtained utilizing the average value of k^0, which measures 6.7129×10^{-4} cm s^{-1}. The strong similarity among the three curves suggests that employing the average value of k^0 could reconcile the minor discrepancies observed in the various k^0 values calculated by equations (55-60).

We used the same method to examine the acquired voltammograms at varying scan rates. **Table IV.4** summarizes the distinct k^0 values calculated employing distinct relationships for every scan speed. Exceptional agreements were replicated between the experimental LSVs and simulated counterparts across different scan speeds, as depicted in **Fig. IV.11.** The simulated curves were generated employing the average value of k^0 for every scanning rate. These findings affirm the earlier findings and demonstrate that the interpolation equations presented in the present study can effectively analyze experimental linear sweep voltammograms for soluble/soluble system of quasi-reversible regime.
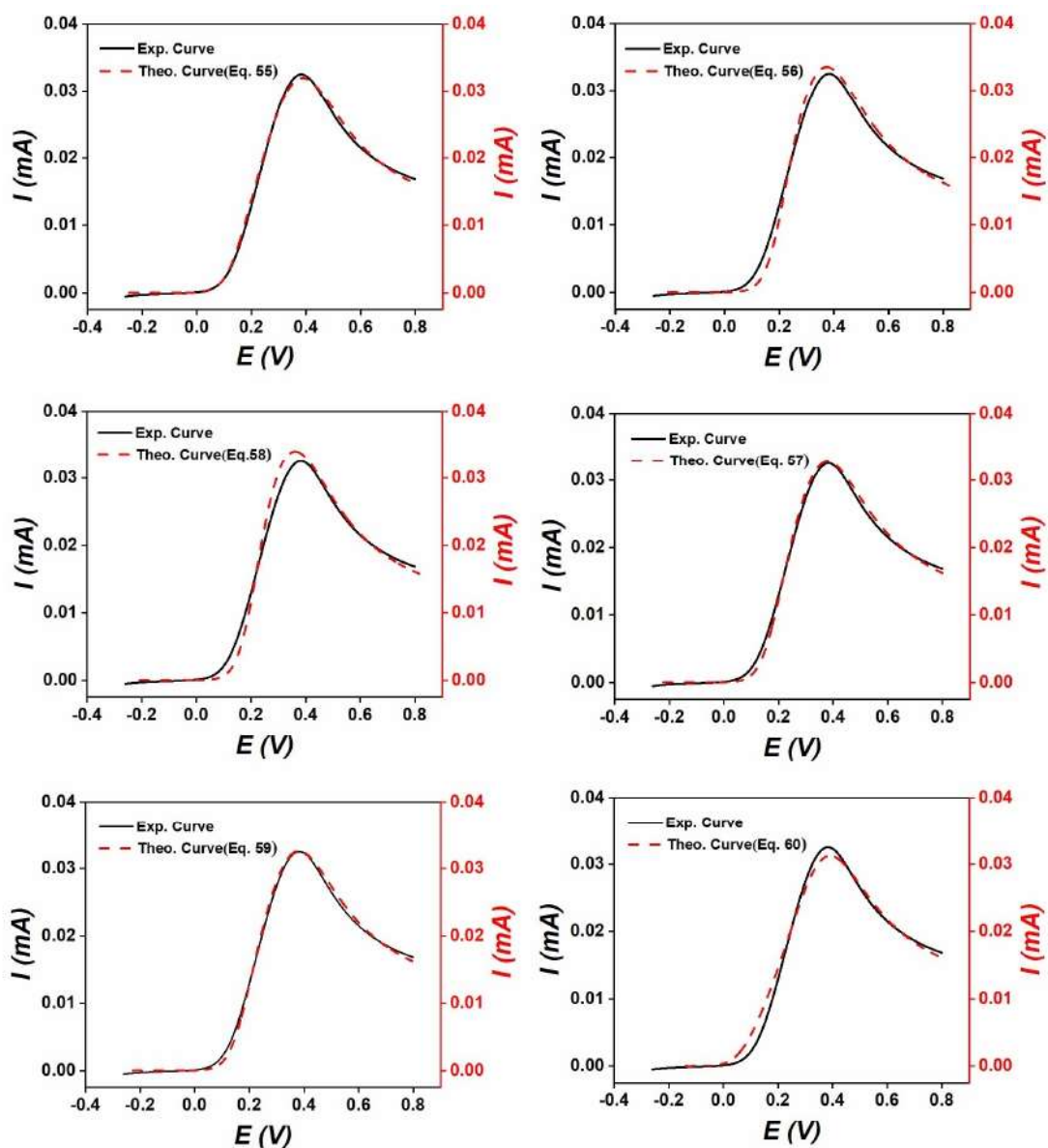
Figure IV.9. Comparing the theoretical LSV curves generated using k^0 values from equations (55), (56), (57), (58), (59), and (60) to the experimental voltammogram obtained at a scan rate of 50 mVs^{-1}.
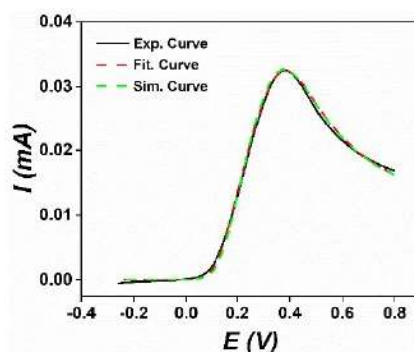
Figure IV.10. Comparison among the fitted, simulated, and experimental voltammograms. The simulated voltammogram was generated using the mean value of k^0.

Table IV.4. The electrochemical standard rate constant k^0 for the oxidation reaction of ferrocyanide, obtained from the voltammograms recorded at various scan rates.

v	k^0, 10^{-4} cm s^{-1}							
mV s^{-1}	Eq. 55	Eq. 56	Eq. 57	Eq. 58	Eq. 59	Eq. 60	Mean value of k^0	fit
20	4.0005	12.094	4.8449	8.1107	9.8435	3.2714	7.0271	4.2575
30	4.6203	9.1586	5.7654	9.6403	9.0564	3.4565	6.9496	4.9075
50	5.1854	8.5956	7.0414	9.5988	6.6115	3.2444	6.7129	5.8543
70	5.1462	9.2838	7.8476	10.6512	6.2719	3.4123	7.1022	5.3640
100	4.9108	10.531	8.7916	12.0350	6.3537	3.8051	7.7393	6.2153
120	3.5750	8.0777	8.9398	11.4859	5.5540	3.6733	6.8843	6.5343
150	6.5218	9.6474	10.9634	12.9617	5.4971	3.8707	8.2437	8.2779
200	2.6182	6.5977	10.8614	13.6003	5.2846	4.0730	7.1725	6.9932
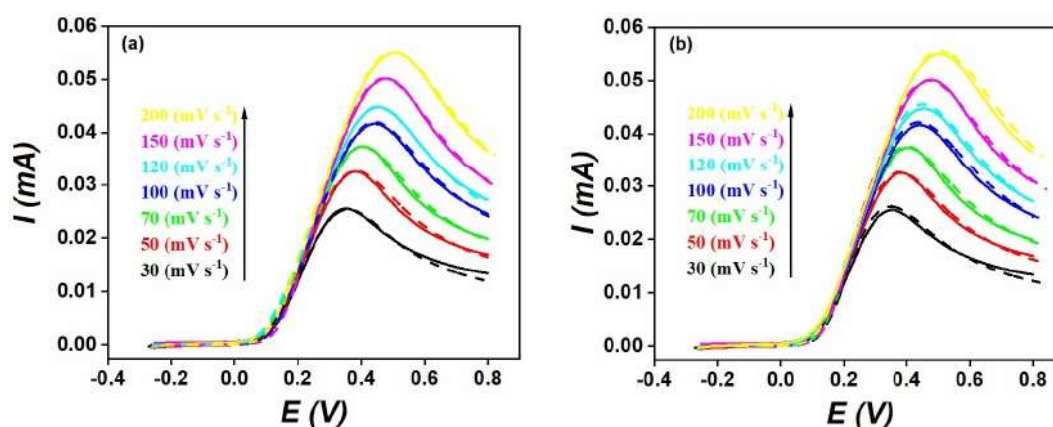
Figure IV.11. Fitted voltammograms (dashed curves, (a)) and simulated voltammograms (dashed curves, (b)) in comparison to experimental voltammograms (solid curves) at different scan rates.

IV.4. Conclusion

This chapter presented first the use of the semi-analytical method for the simulation of LSV corresponded to electrochemical systems involving soluble species. Through the simulation study, a rigorous analysis of LSV responses was introduced in which the dependence of the shape and position of LSVs to the adimensional kinetic rate constant Λ and charge transfer coefficient α were examined. Based on the quantitative analysis of characteristics peaks via the variation of both Λ and α, different kinetics diagrams were established. In particular, according to these kinetics diagrams a series of practical equations were developed, which enable to the easy and direct calculation of the standard speed constant for quasi-reversible soluble redox couples.

On other hand, the electro-oxidation of ferrocyanide at SPGEs has chosen to verify the theoretical results. The standard speed constant of the ferrocyanide oxidation on SPEs was determined using the developed equations. Comparison of the simulation and experimental voltammograms was perfomed, and an excellent agreement was obtained.

References

[1] A. J. Bard and L. R. Faulkner, Electrochemical Methods: Fundamentals and Applications, 2nd Edition, Wiley, New York, 2001.

[2] H. Matsuda, Y. Ayabe, *Zeitschrift Für Elektrochemie, Berichte Der Bunsengesellschaft Für Physikalische Chemie.*, 59 (1955) 494–503.

[3] A. Ševčík, Collection of Czechoslovak Chemical Communications, 13 (1948) 349–377.

[4] J.E.B. Randles, *Transactions of Faraday Society*, 44 (1948) 327–338.

[5] R.S. Nicholson, I. Shain, *Analytical chemistry*. 36(1964)706–723,

[6] R.S. Nicholson, *Analytical chemistry,* 37 (1965) 1351–1355.

[7] Angela M. Keightley, Jan C. Myland, Keith B. Oldham and Peter G. Symons, *Journal ElectroanalyticaL chemistry*, 322 (1992) 25-54.

[8] I. Atek, S. Mayeb , H. H. Giraultb , A.M. Affoune, P. Peljo, *Journal of Electroanalytical Chemistry,* 818 (2018) 35-43.

[9] D. Krulic, N. Fatouros, D. Liu, *Journal of Electroanalytical Chemistry,* 754(2015)30–39.

[10] M. Stieble and K. Jiittner, *Journal of Electroanalytical Chemistry*, 290 (1990) 163-180.

[11] Krzysztof Winkler, *Journal of Electroanalytical Chemistry*, 388 (1995) 151- I59.

[12] W.J. BlaedeL, G.W. Schieffer, *Journal of Electroanalytical Chemistry*, 80 (1977) 259-271.

[13] Kneten, McCreery RL, Analytical Chemistry, 64(1992) 2518–2524.

[14] J. Wang, Ü.A. Kirgöz, J.W. Mo, J. Lu, A.N. Kawde, A. Muck, *Electrochemistry Communications,* 3 (2001) 203–208.

[15] K.B. Oldham, *Journal of Electroanalytical Chemistry*, 121 (1981) 341.

[16] A. Saila, Univ. Badji Mokhtar, Annaba, 2010.

[17] T. Singh, *Journal of Electroanalytical Chemistry,*., 238 (1987) 33-41.

[18] L. Daruhbzi, K. Tokuda, *Journal of Electroanalytical Chemistry,* 264 (1989)77-89.

[19] M. Stieble ,K. Jiittne, *Journal of Electroanalytical Chemistry,* 290 (1990)163-180.

[20] Ball, D. and J. Key, *Introductory Chemistry – 1st Canadian Edition*. Victoria, B.C.: BCcampus, (2014).

[21] J. Kwak, *Bull. Korean, Chemistry Society*, 15 (1994).

[22] W.C. Chen, H. M. Lin, C. A. Chang, *Analytical and Bioanalytical Chemistry,* 383 (2005) 532–538.

[23] L. Xiong, C. B-McAuley, k. R. Ward, C. Downing, R. S. Hartshorne, N. S. Lawrence, R. G. Compton, *Journal of Electroanalytical Chemistry,* 661 (2011) 144–149.

CHAPTER V

Experimental and modelling study of electrochemical sensor for Dopamine Uric acid and ascorbic Acid detection

V.1. Introduction

This chapter investigates firstly the use of cyclic voltammetry on SPEs to determine the presence of dopamine, uric acid, and ascorbic acid. Secondly, the modelling of LSVs responses related to the oxidation of these three molecules is presented.

V.2. Voltammetric study of DA, UA, AA detection on SPEs

Dopamine, uric acid and ascorbic acid sensing necessitates high sensitivity and selectivity techniques. Electrochemical methods like voltammetry offer a valuable advantage in identifying dopamine (DA), uric acid (UA), and ascorbic acid (AA) due to their ease of use and speed [1]. In this section, cyclic voltammetry analysis was performed in evaluating the influence of both scan speed and concentration on the three molecules oxidation on screen-printed graphite electrodes.

V.2.1. Scan rate effect

The speed scan impact on oxidation peak current and potential of dopamine, ascorbic acid and uric acid was examined at screen-printed electrodes in 0.1 M Phosphate Buffered Saline (pH 7.4) through CV.

Figure. V.1 presents the CVs of the oxidation of 0.5 mM of dopamine, ascorbic acid and uric acid on SPEs for various scan speeds ranging between 10 and 200 mV s^{-1}. For the three molecules that are illustrated in **Fig. V.1** (a, c, e), the currents of the anodic peaks increase with the raise of scan rate. Additionally, the oxidation peak potentials of these three molecules shift to more positive potentials with increasing the scan rate, suggesting that the charge transfer kinetics is not reversible. As observed in **Fig. V.1** (b, d, f) anodic peak currents depend ($v^{1/2}$) linearly, suggesting that the oxidation of DA, UA and AA are diffusion-controlled process [2].
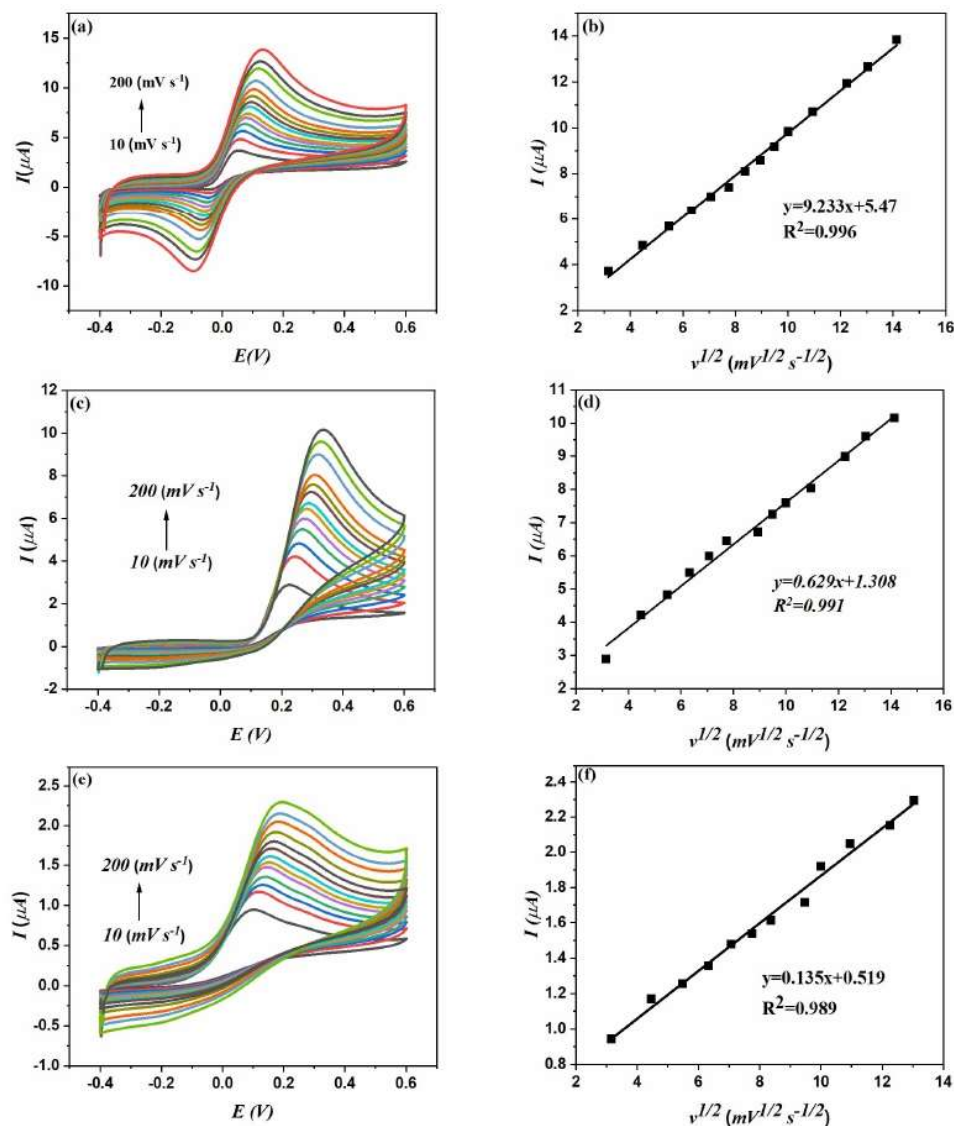
Figure V.1. CVs of 0.5 mM DA (a), 0.5 mM UA (c), 0.5 mM AA (e) on screen-printed electrodes at different scan rates (10–200 mV/s) in 0.1 M PBS solution (pH 7.4). Linear plots of anodic peak current (I_{pa}) *vs.* square root of scan rate $v^{1/2}$ (b, d, f).

V.2.2. Effect of concentration

The individual detection of three analytes was carried out in 1.10^{-1} M Phosphate Buffered Saline (pH 7.4) at screen-printed electrodes as presented in **Fig. V.2** (a), (b), (c). Dopamine A, Urea A and Ascorbic A peak currents were linear with the raise of there concentrations (**Fig. V.2** (d), (e) and (f)). The corresponding linear equations are outlined below:

For Dopamine: I_{pa} (μA) = 0.4273 + 0.0145C (μM) (R^2 = 0.9875),

For Urea acid, I_{pa} (μA) = 0.2072 + 0.0153C (μM) (R^2 = 0.984),

And for Ascorbic Acid, I_{pa} (μA) = 0.0893 + 0.0029C (μM) (R^2 = 0.988),

The linear intervals for Dopamine, Urea Acid, Ascorbic Acid ranged from 1 to 500 μM, 1 to 200 μM and 5 to 500 μM, in that order. The threshold of detection of DA, UA and AA were calculated as follows 0.89 μM, 3.22 μM, and 9.19 μM in their respective order.
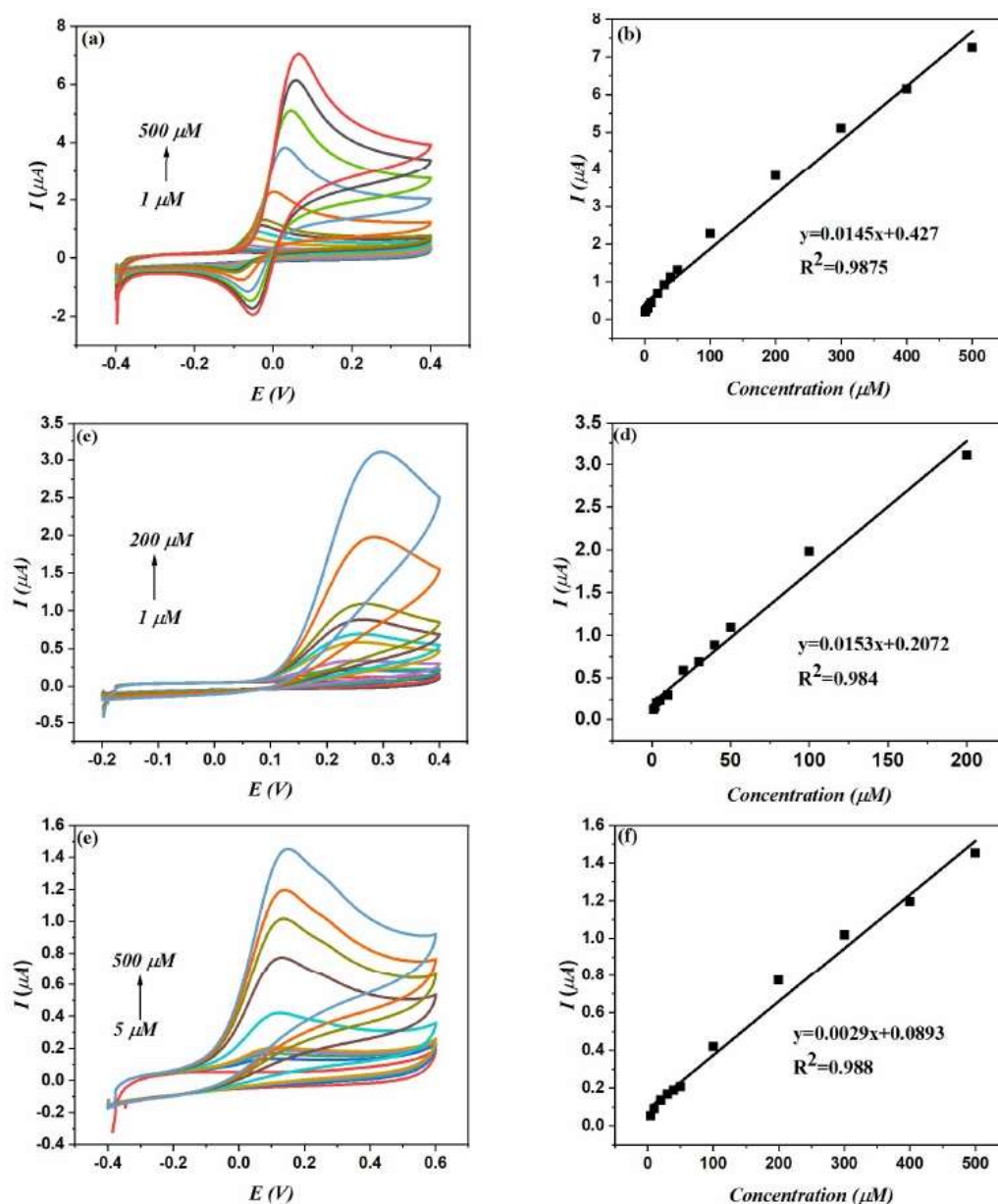
Figure V.2. Cyclic voltammetric responses for different concentrations of DA (a), UA(c) and AA(e) on screen-printed electrodes at scan rate of 50 mV s⁻¹ in 0.1 M PBS. Plots of peak currents as function of DA (b), UA (d), and AA concentrations (f).

Table V.1. Comparison of various DA, UA and AA determination of some properties of the present work with other studies.

Dopamine			
Electrode	**Linearity (µM)**	**LOD (µM)**	**Reference**
DropSens SPCE	1-500	0.3	[3]
ERGO1pr-SPCE	1-100	0.09	[3]
AuNP/SPCE	2−100	0.22	[4]
SPGEs(Graphite)	1-500	0.89	This work
Uric Acid			
Electrode	**Linearity (µM)**	**LOD (µM)**	**Reference**
The homemade SPCE	10 − 80	1.94	[5]
ZnO/GR/SGPE (Graphite)	1-110	0.43	[6]
Poly(4-ASA)-PB-SGPE(Graphite)	10 − 200	3.0	[7]
SPGEs (Graphite)	1-200	3.22	This work
Ascorbic Acid			
Electrode	**Linearity (µM)**	**LOD (µM)**	**Reference**
Cu/ CSPEs	1-250	0.5	[8]
CV-Fe3O4NP/ SPCE	10-100	15.7	[9]
ZnO/Al2O3/ GSPE	10-100	0.06	[10]
SPGEs (Graphite)	5-500	9.19	This work

Analytical findings obtained from the determining of DA, UA, and AA using the screen-printed electrodes were contrasted with that of earlier published studies which are condensed into Table V.1. The findings suggest that even without modification, the screen-printed electrodes demonstrate good performance in detecting DA, UA, and AA.

V.3. LSV Simulation of electrochemical oxidation of Dopamine (DA), Uric Acid (UA) and Ascorbic Acid (AA)

V.3.1. Determination of charge transfer coefficient

The oxidation charge transfer coefficient α of dopamine, uric acid and ascorbic acid, was determined using Tafel analysis. **Fig. V.3** (a, b, c) is an illustration the plots of Tafel derived from experimental Linear Sweep Voltammetry data for DA, UA and AA where the scan speed is 100 mV s^{-1}. By employing the anodic Tafel slope, α values of Dopamine, Urea Acid and

Ascorbic Acid were calculated, taking into consideration that the number of electron used are n=2 (DA), n=2 (UA), n=1(AA). The obtained result is reported in Table V.2. Clearly, it is observed that α value for DA, uric acid UA, and AA ranges between 0.2 and 0.27. The value of α obtained for DA is lower than that reported in a previously published work [3], due to the use of a different electrolyte. Conversely, the obtained value of α for UA aligns well with that reported in literature [6]. While the α value obtained for AA is significantly higher than that reported in the previous study [11] as listed in **Table V.2**, the discrepancy is attributed to the different number of electrons *n* used in the calculation of α. In our calculation, we used *n*=1 while in literature the value *n*=2 was used. This point will be discussed in the section V.3.4.
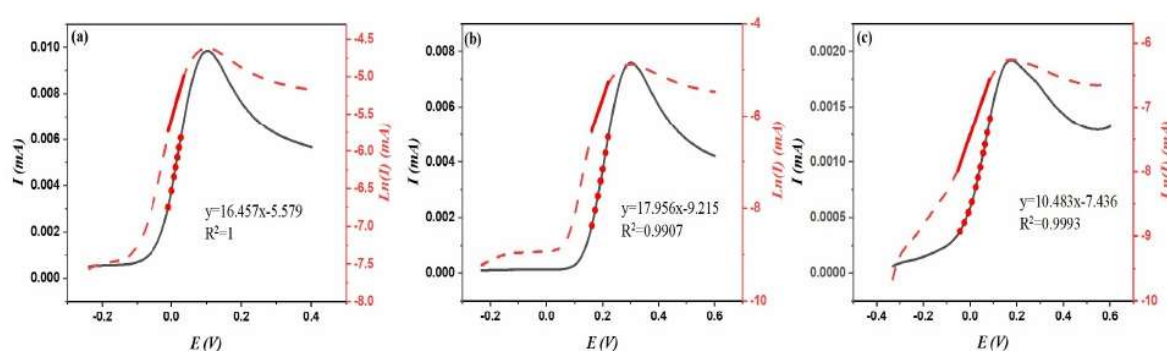
Figure V.3. Linear sweep voltammograms (black line) with Tafel plots (dashed red line) for the oxidation of 0.5 mM DA (a) , 0.5 mM UA (b) and 0.5 mM AA (c) on SPEs recorded at scan rate of 100 mV s^{-1}in 0.1 M PBS (pH 7.4).

Table V.2. The calculated values of the charge transfer coefficient α for DA, UA and AA from the Tafel plots presented in Fig. V.3.

Molecule	Charge transfer coefficient, α	
	Our results	Literature
DA	0.20	0.5 [3]
UA	0.24	0.28 [6]
AA	0.27	0.15 [11]

V.3.2 Determination of diffusion coefficient

A semi-integral voltammetry was employed to determine the diffusion coefficient of DA, UA, and AA,. The principle of semi-integral voltammetry, developed by Oldham [12], involves the semi-integration of the current observed in the voltammogram with respect to time. This process generates a novel function, denoted as M(t), characterized by a well-defined plateau representing the limiting semi-integral current m* [13]. The diffusion coefficient could be calculated by using the equation below:

$$m^* = n F A C^*_{Red} (D_{Red})^{1/2}$$

Fig.V.4. presents the semi-integral plots obtained from the experimental voltammetric data of DA, UA, and AA oxidation recoded at scan rate of 100 mV s⁻¹. Furthermore, it is apparent that the semi-integration responses are not limited by a well-defined plateau due the influence of electrolyte. In the calculation of diffusion coefficient of DA, UA and AA, the m* values were extracted at where the potential corresponds to the third of peak current as indicated in Fig.V.4. The calculated values of diffusion coefficient for DA, UA and AA are shown in **Table V.3**.
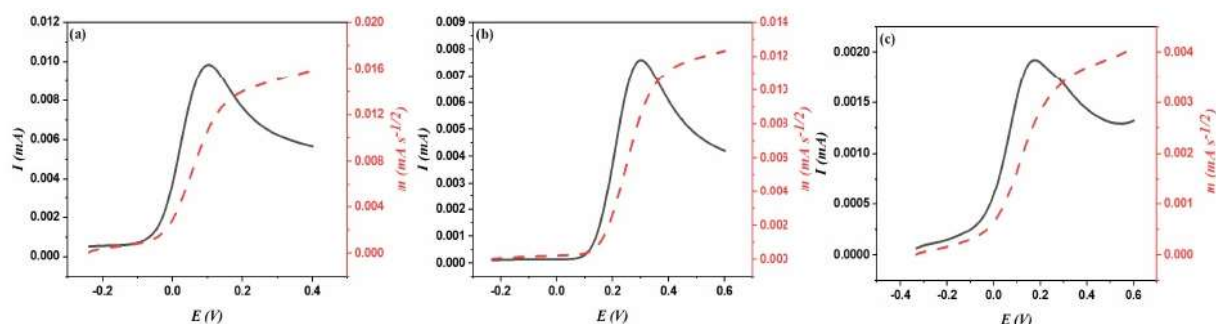
Figure V.4. LSV responses (black line) and their semi-integrated curves (dashed red line) for the oxidation of 0.5 mM DA (a) , 0.5 mM UA (b) and 0.5 mM AA (c) on SPEs at scan rate of 100 mV s⁻1 in 0.1 M PBS (pH 7.4).

In comparison to the literature, the obtained D_{DA} value (4.85×10^{-6} cm² s⁻¹) aligns with the reported range (0.650×10^{-6} cm² s⁻¹ to 6.07×10^{-6} cm² s⁻¹) for DA oxidation at different carbon electrodes: ERGO1pr-SPCE [3], AuNPs·PTAP/GCE [14] and poly-film/ GCE [15]. As well as the diffusion coefficient of UA (2.6×10^{-6} cm² s⁻¹) is close to 1.54×10^{-6} cm² s⁻¹ published by Ardakani [16]. Diffusion coefficient of ascorbic acid was obtained and is 1.195×10^{-6} cm² s⁻

[1], this value is lower compared to that reported by Ernst [11]. This difference is attributed mainly in the number of electrons used as mentioned in the section V.3.1.

Table V.3. The diffusion coefficient α values obtained for DA, UA and AA using semi-integrative voltammetry.

Molecule	diffusion coefficient, D, 10^{-6} cm^2 s^{-1}	
	Our results	Literature
DA	4.85	6.07 [3]
		0.607 [14]
		0.650 [15]
UA	2.6	1.54 [16]
AA	1.195	6.48 [11]

V.3.3 Determination of the kinetic standard rate constant k^0

By means of determining the standard rate constant k^0 form CV and LSV measurements, different approaches were used. Form CV data, the Nicholson's approach is a conventional approach based on the peak-peak separation which is used in several studied in the quantitative determination of DA, UA and AA [17]. Another approach was presented by Laviron, and mainly used for irreversible systems [18].

Herein, from LS Voltammetry analysis, the standard rate constant k^0 of DA, UA and AA determination is based on the use of the developed kinetics equations that was reported in the precedent chapter. The developed kinetics equations related to the characteristics of voltammetric peaks: the peak current, peak width potential, the peak potential, are as follows [19]:

$$\frac{\Psi_p}{(\Psi_p)_{rev}} = 0.999 + \frac{(1.112\alpha^{0.5}-0.999)}{1+\exp\left[\frac{\log(\Lambda)-(-0.489\alpha^3 - 0.0589)}{0.111\alpha^3 + 0.322}\right]} \tag{1}$$

$$\Delta\Phi_{p/2} = 2.214 + \frac{(1.859\alpha^{-1}-2.214)}{1 + \exp\left(\left[\frac{\log(\Lambda)-(-0.208\alpha^{-0.327})}{0.440\alpha^{0.608}}\right]\right)} \tag{2}$$

$$\frac{\Psi_p}{(\Psi_p)_{rev}} = (1.039\alpha^{0.19}) + (0.436 - 0.578\alpha)\log(\Lambda) \tag{3}$$

$$\Delta\Phi_{p/2} = (3.401 - 1.493\alpha) + (3.481 - 2.392\alpha^{-1})\log(\Lambda) \tag{4}$$

The first two equations (1) and (2) characterize a sigmoidal function, while equations (3) and (4) represent linear functions. Both of eq. (1) and (3) describe the change in the adimensional peak current $(\Psi_p)/\left(\Psi_p\right)_{rev}$, whereas eq. (2) and (4) describe the change the adimensional half peak width ($\Delta\Phi_{p/2}$). Furthermore, we have developed two linear equations, under distinct range, relative to the change in the adimensional peak potential (η_p), which are:

When $-1 \geq \log \Lambda \leq 0$,

$$\eta_p = (2.379\alpha^{-0.694}) + (-1.288\alpha^{-0.999})\log(\Lambda)) \tag{5}$$

When $\log \Lambda \leq -1$,

$$\eta_p = (1.222 - 0.189\alpha^{-1}) + (-2.296\alpha^{-1})\log(\Lambda) \tag{6}$$

Where Λ is the dimensionless kinetic parameter.

These equations (1-6) allow quantifying the k^0 for DA, UA, and AA by using measurements of peak current, peak potential and half-peak potential form the experimental LS voltamograms, while α value is known.

Results of the peak current *Ip*, half peak width $Ep - E_{p/2}$ and peak potential *Ep* that were extracted from LS voltammograms of DA, UA and AA oxidation recoded at 100 mV s^{-1} are converted into dimensionless values as follows:

$$\frac{\Psi_p}{\left(\Psi_p\right)_{rev}} = \frac{Ip}{0.4463nFA\,C_{Red}{}^*D^{1/2}\left(\frac{nF}{RT}\right)^{1/2}v^{1/2}} \tag{7}$$

$$\Delta\phi_{p/2} = \frac{nF}{RT}\left(E_p - E_{p/2}\right) \tag{8}$$

$$\eta_p = \frac{nF}{RT}\left(E_p - E^0\right) \tag{9}$$

We didn't not find in literature the E^0 values for DA, UA and AA in PBS media. We have used the simulation calculation presented in section V.3.4. to determine the values of E^0. From equation (9), the expression of E^0 is as follows:

$$E^0 = E_p - \frac{RT}{nF}\eta_p$$

Where Ep is the potential of experimental curve.

η_p is the dimensional peak potential of simulated curve.

The standard potential values E^0 for DA, UA, and AA we have obtained are as follows:

$E^0(DA) = -0.037$ V

$E^0(UA) = 0.1331$ V

$E^0(AA) = -0.1449$ V

Using equations 7-9, we have calculated the different dimensionless parameters for the three molecules and the obtained values are given in the **Table V.4.**

Table V.4. Dimensionless parameters for DA, UA and AA.

	DA	UA	AA
$\dfrac{\Psi_p}{(\Psi_p)_{rev}}$	0.5262	0.5541	0.5846
$\Delta\phi_{p/2}$	7.0327	7.4126	4.9417
η_p	10.86	12.86	12.31

Using the developed equations (1-6), the kinetic parameter Λ can be easily calculated, and the standard rate constant k^0, is determined by applying the equation associated with Λ [20]:

$$\Lambda = \frac{k^0}{\sqrt{\sigma D_{Red}}} \tag{11}$$

In our calculation, we used α coefficients and the diffusion coefficients for DA, UA and AA, previously determined in **section V.3.1** and **section V.3.2**. The corresponding results of k^0 are shown in **Table V.5**. In the same table, we have also calculated the two following values of k^0:

Mean value 1 = (k^0 (Eq.1) + k^0 (Eq.3) + k^0 (Eq.5/6))/3

Mean value 2 = (k^0 (Eq.1) + k^0 (Eq.2) + k^0 (Eq.3) + k^0 (Eq.4) + k^0 (Eq.5)+ k^0 (Eq.6))/6

Table V.5. The obtained kinetic parameter k^0 for the oxidation of DA, UA and AA.

	Dopamine			Uric acid			Ascorbic acid		
	$log\Lambda$	Λ	k^0, 10^{-3} cm s^{-1}	$log\Lambda$	Λ	k^0, 10^{-4} cm s^{-1}	$log\Lambda$	Λ	k^0, 10^{-4} cm s^{-1}
Eq. (1)	-0.9676	0.1077	0.6620	-1.3141	0.048	2.1826	-1.3905	0.0407	0.8778
Eq. (2)	-0.4770	0.3334	2.0487	-0.8389	0.1449	6.5198	-0.3864	0.4108	8.8593
Eq. (3)	-0.7471	0.1790	1.0999	-0.8013	0.1580	7.1095	-0.8053	0.1566	3.3765
Eq. (4)	-4.6354	0.3439	2.1132	-0.6738	0.2119	9.5349	-0.3614	0.4351	9.3833
Eq. (5)	-0.5585	0.2764	1.6982	-1.2044	0.0624	2.8094	-1.3449	0.0452	0.9746
Eq. (6)	-0.9219	0.1197	0.7356	-1.2988	0.0502	2.2609	-1.3862	0.0411	0.8863
Mean Value1	-0.7265	0.1877	1.1533	-1.0676	0.0856	3.8506	-1.0999	0.0794	1.7133
Mean Value2	-0.6054	0.2481	1.5244	-0.91104	0.12273	5.5215	-0.66386	0.21684	4.6766

Overall **Table V.5**, it is remarkably observed that the k^0 values for DA are higher than those obtained for UA and AA. The k^0 values obtained for dopamine oxidation are close to those reported in the works of Emad *et al*. [14] and Calvo *et al* [3], wherein they obtained 3.78×10^{-3} cm s^{-1} and 0.36×10^{-3} cm s^{-1}. For uric acid oxidation, the k^0 results are in the range between 2.1826×10^{-4} cm s^{-1} and 9.5345×10^{-4} cm s^{-1}. According to Ardakani [16], the k^0 value was determined to be 8.460×10^{-4} cm s^{-1} which falls in the obtained range of k^0. It was reported that the k^0 is 2.7×10^{-2} cm s^{-1} for the oxidation of AA on platinum electrode [11], which is higher than those calculated in our study and ranging between 0.8778×10^{-4} cm s^{-1} and 9.3833×10^{-4} cm s^{-1}. This significant difference in values could be attributed to the effect of working electrodes.

Based on the kinetic curves presented in precedent chapter, the Λ values (0.04 – 0.43) corresponding to DA, UA, and AA are situated in the range of Zone B ($10^{-3} < \Lambda < 10^3$), which is defined for quasi-reversible systems. These values are also situated in both ranges ($10^{-2\,(1+\alpha)} < \Lambda < 15$) and ($10^{(-1.7)} < \Lambda < 10^{(1.7)}$) suggested by Matsuda and Kwak respectively for quasi-reversible systems [20, 21]. As a result, electrochemical behaviour of these three compounds on screen-printed electrodes are characterized as quasi-reversible systems.

V.3.4. Voltammetry simulation

With the aim to examine the applicability of the developed equations in chapter IV, a simulation study was performed to calculate theoretical voltammograms related to dopamine, uric acid and ascorbic acid oxidation. Using the determined values of the parameters α, D and k^0.

In the dopamine (DA), uric acid (UA) and ascorbic acid (AA) oxidation mechanisms, a two-electrons oxidation process is typically reported in the literature. In our simulation calculations, we specifically applied a two-electrons oxidation for DA and UA. However, In for ascorbic acid (AA), we have tested both one-electron and two-electrons processes.

In Figs. V(5-8), simulated LS voltammograms using k^0 of equations listed in **Table V.5** with the experimental curves of DA, UA and AA oxidation at 100 mV s^{-1} are presented. The results of the simulation indicate an accord with the experimental voltammograms. However, the better agreement are obtained with eq. (2), (4) and (6/7) compared than to eq. (3) and (5). The remarkable discrepancies seen with eq. (3) and (5) may be attributed to the influence of ohmic drop, while for eq. (5) may be explained by Λ values that were outside the limits of these equations' applicability. This remark corroborate with that mentioned in chapter VI.

The simulated voltammograms of DA, UA and AA using the mean values of k^0 reveal that the best agreement with the experimental voltammograms is generally that obtained with Mean Value 1.

Furthermore, comparison between voltammograms of **Fig. V.7 and Fig. V.8** indicates that the use of one electron gave better-simulated voltammograms for AA oxidation [22].
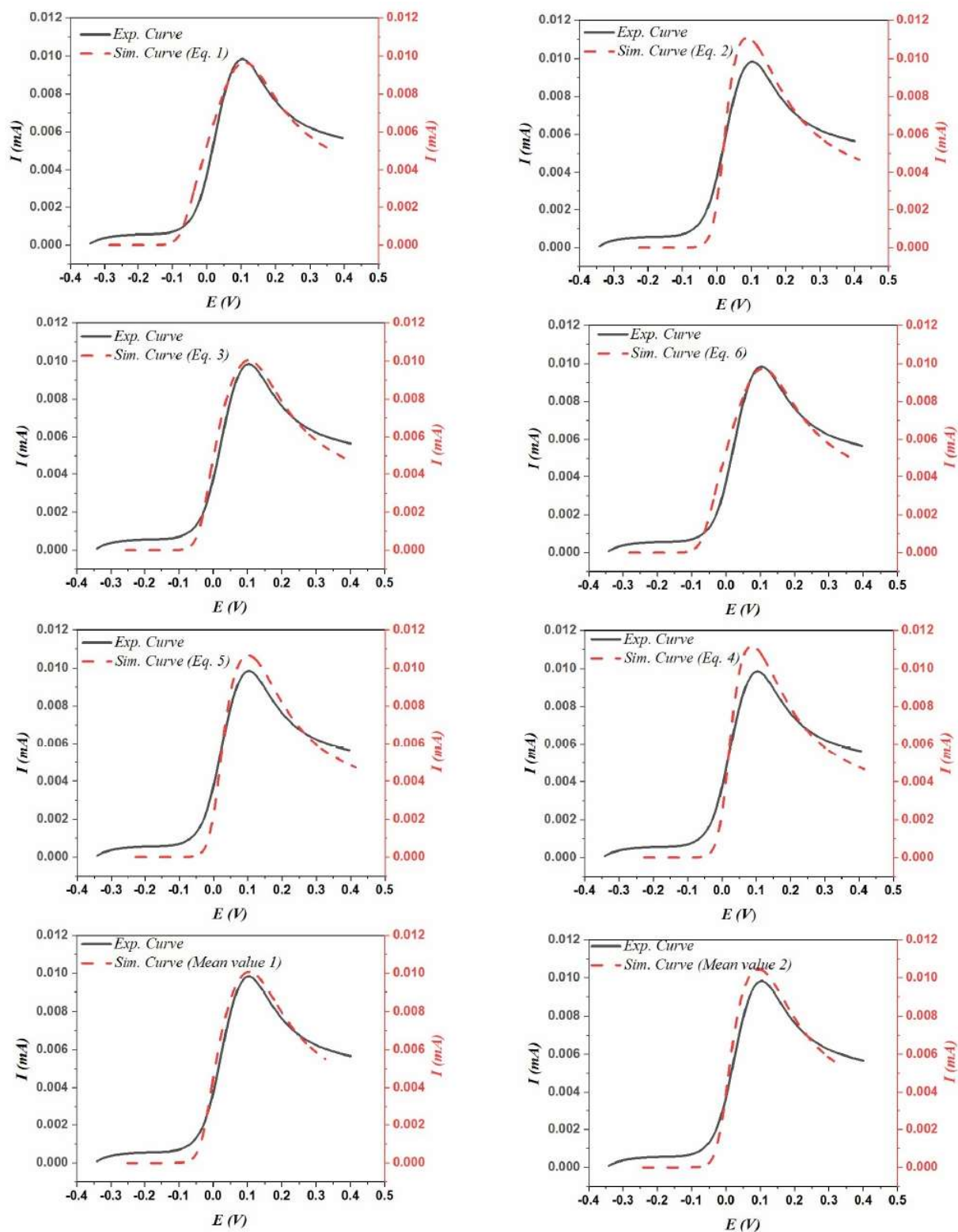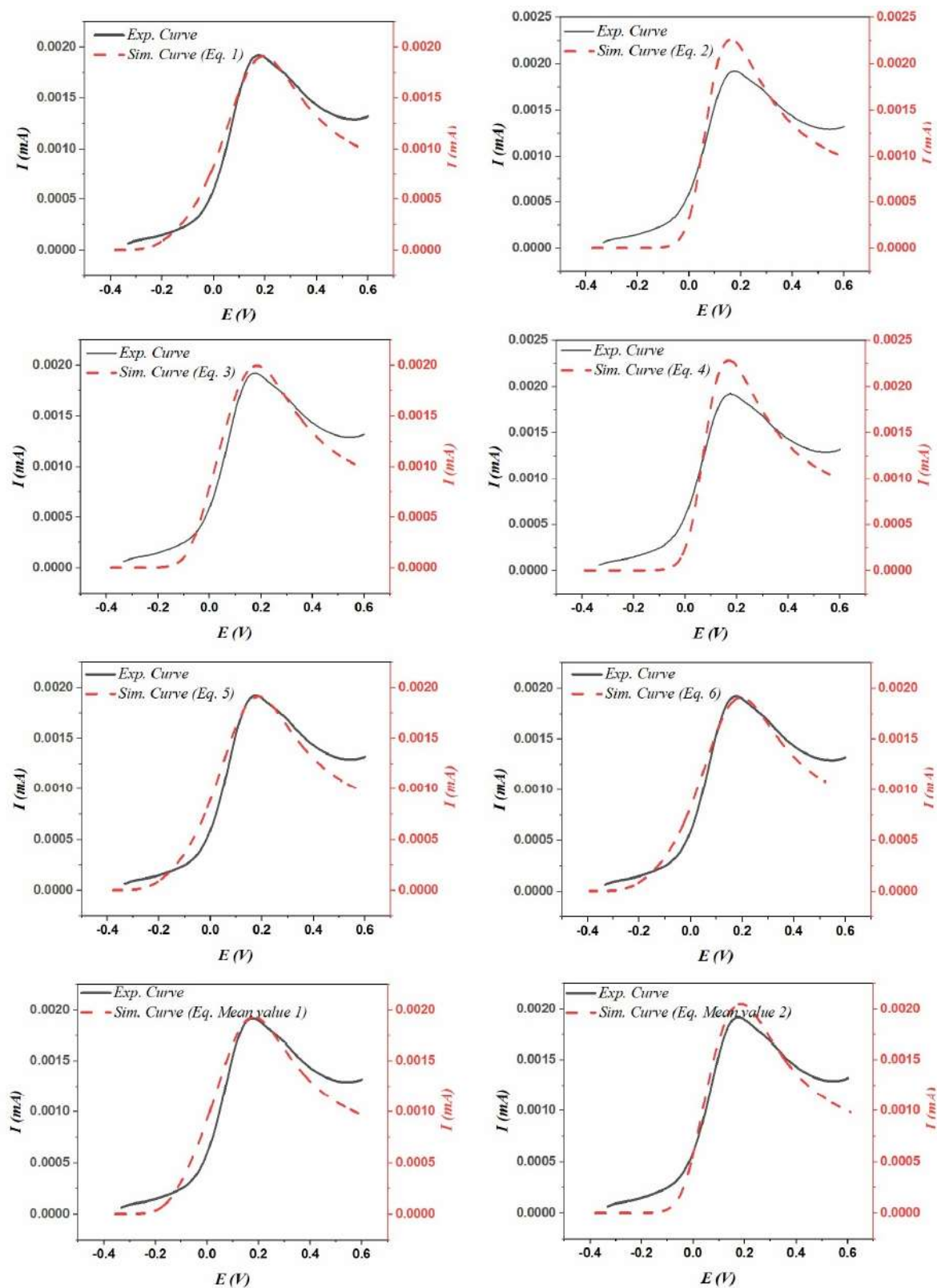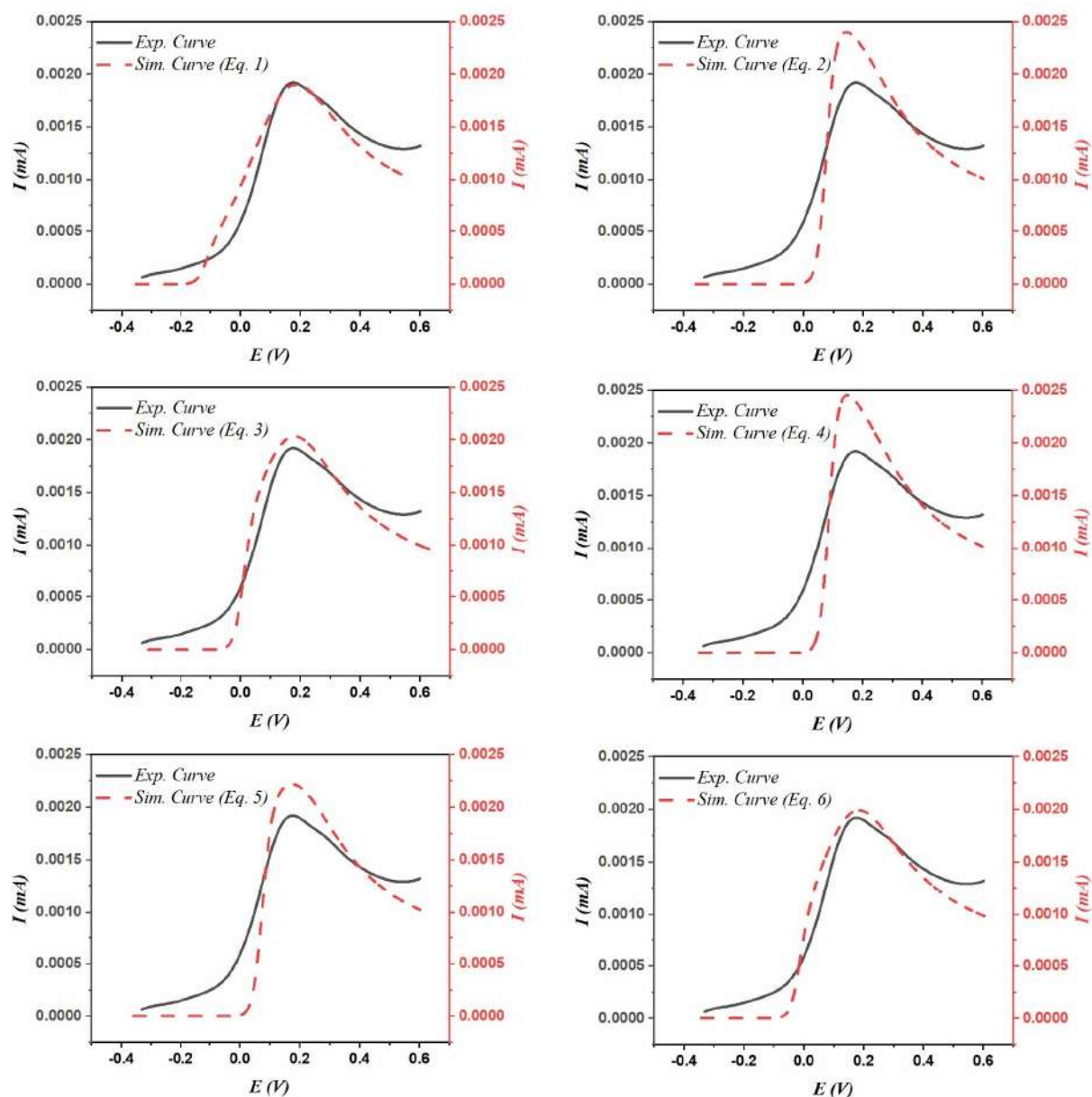
Figure V.5. Comparison between simulated and experimental LS voltammograms for 0.5 mM DA recoded at 100 mV s^{-1} scan rate.
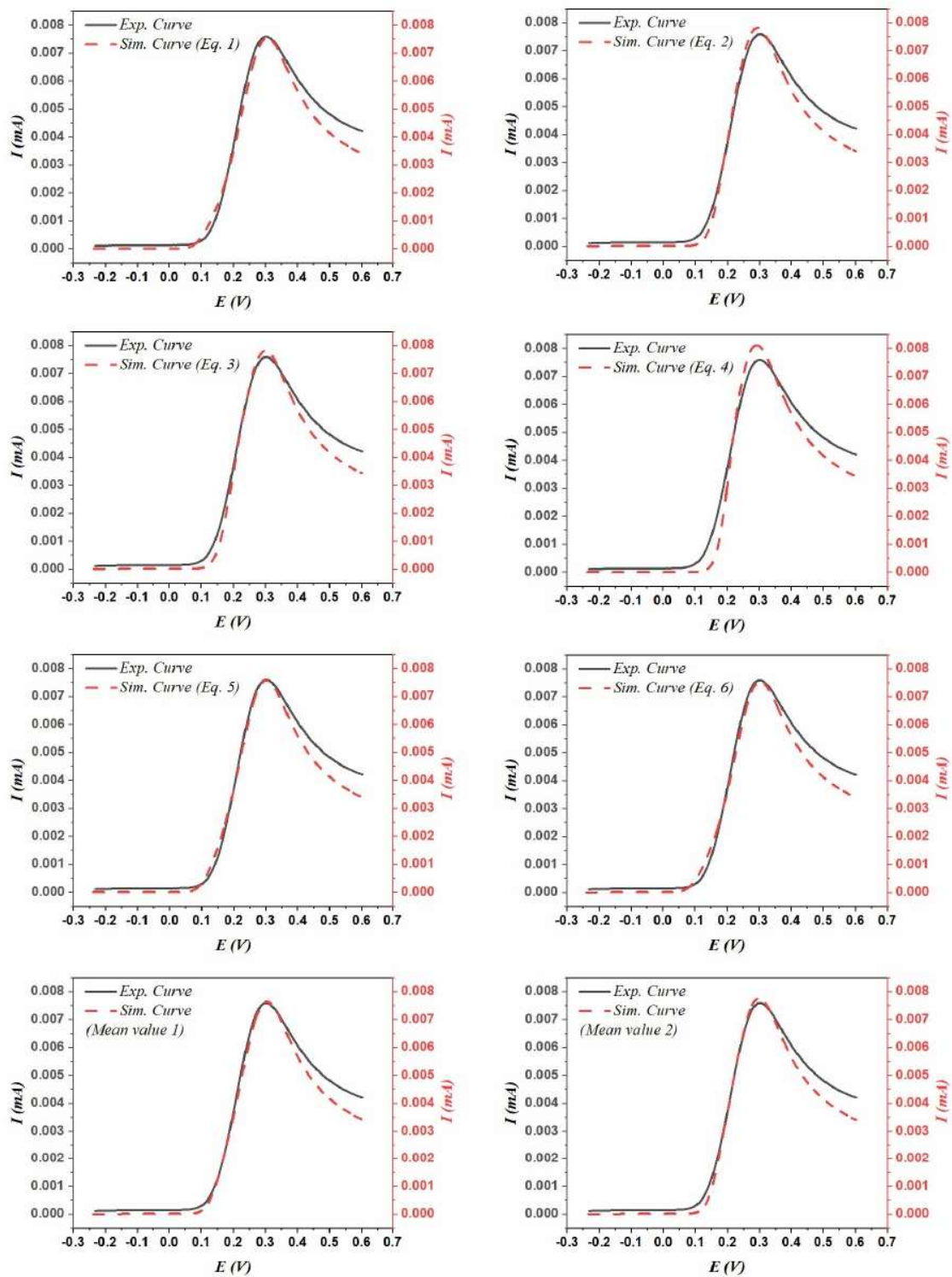
Figure V.6. Comparison between simulated and experimental LS voltammograms for 0.5 mM UA recoded at 100 mV s^{-1} scan rate.

Figure V.7. Comparison between theoretical and experimental LS voltammograms for 0.5 mM AA recoded at 100 mV s^{-1} scan rate using n=1.

Figure V.8. Comparison between theoretical and experimental LS voltammograms for 0.5 mM AA recoded at 100 mV s^{-1} scan rate using n=2, α=0.13 and D= 2.98×10^{-7}.

V.3.5. Scan rate analysis

In **Fig.V.(9-11)**, the LS voltammograms for DA, UA and AA at different scan speeds of 30, 50, 100 and 150 mV s-1 were calculated using the parameter k^0 acquired from Eq. (1) for each scan rate. Simulated and experimental LSVs reproduced best fits under different scan rates.

All these results of simulation show that the equations developed in chapter IV provide a good values of k^0 (Table V.2). Furthermore, the values calculated from equations (1), (3), (5) or Mean Value 1 are the best ones.
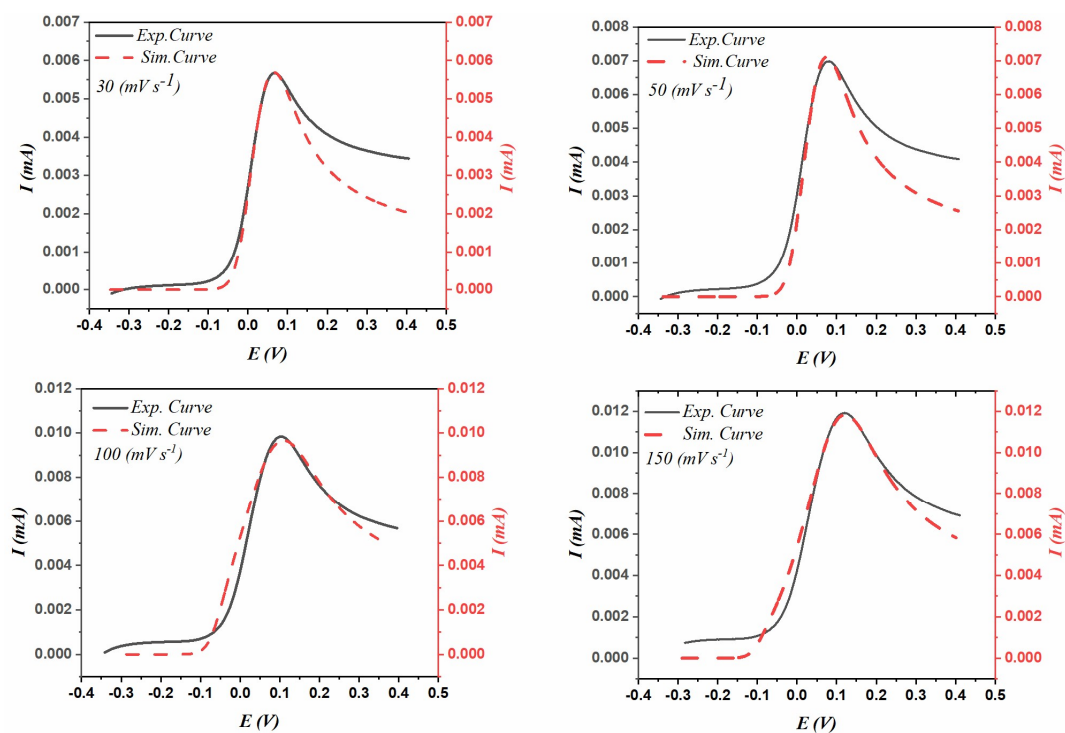
Figure V.9. Fitted and experimental LS voltammograms for 0.5 mM DA on screen-printed electrodes at different scan rates (30, 50, 100, 150) mV s^{-1}.
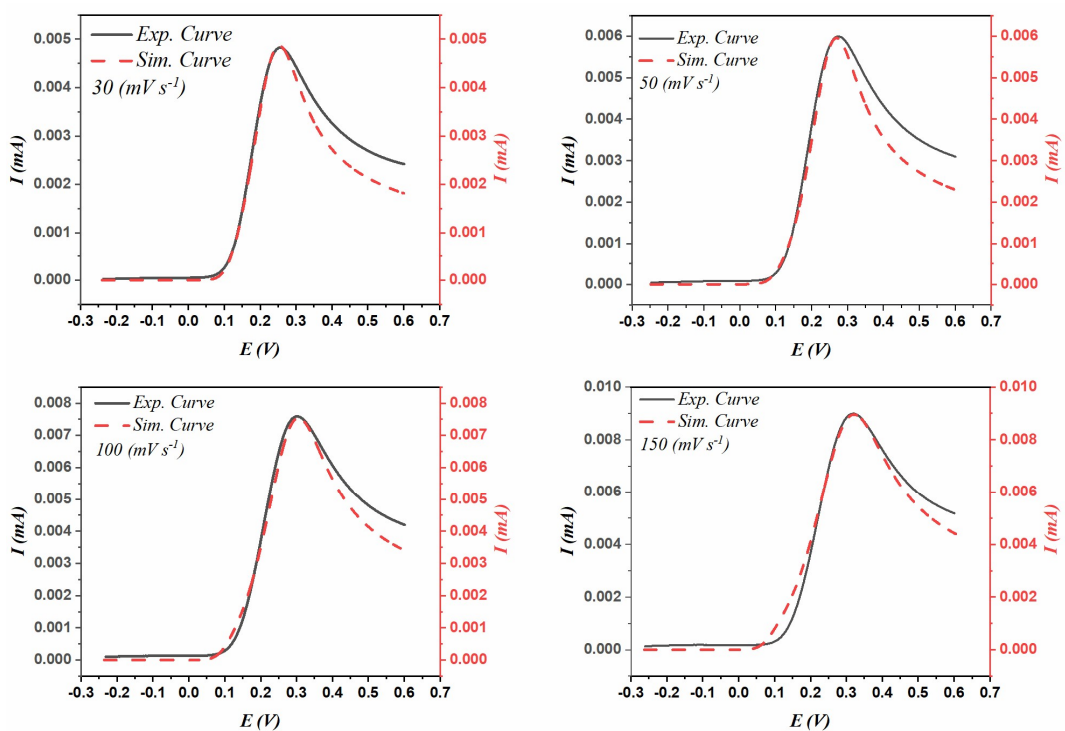
Figure V.10. Fitted and experimental LS voltammograms for 0.5 mM UA on screen-printed electrodes at different scan rates (30, 50, 100, 150) mV s^{-1}.
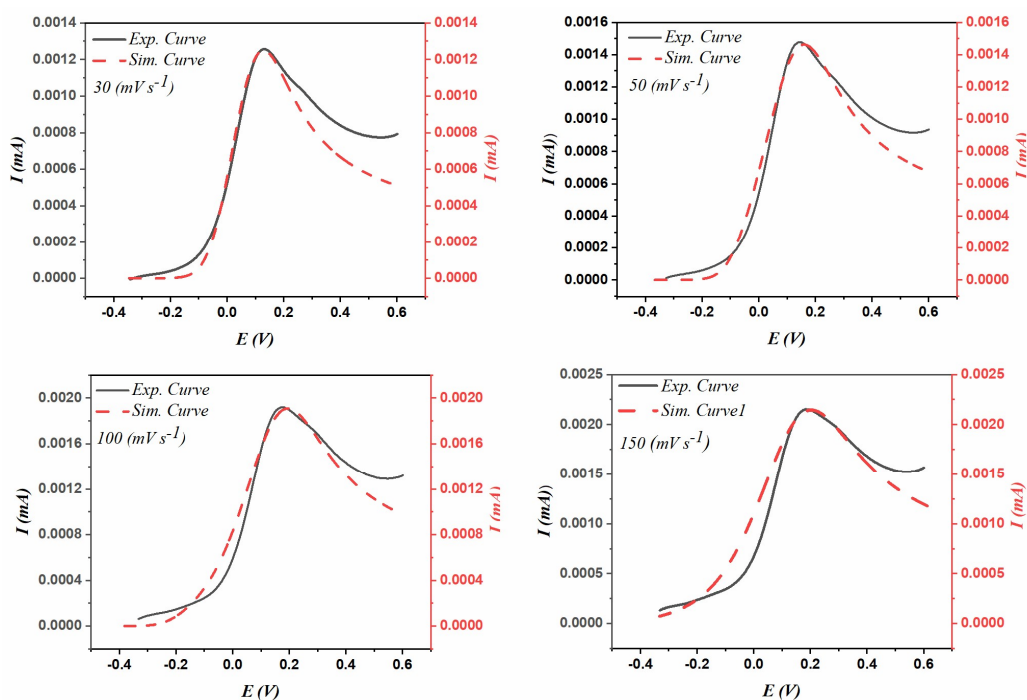
Figure V.11. Fitted and experimental LS voltammograms for 0.5 mM AA on screen-printed electrodes at different scan rates (30, 50, 100, 150) mV s⁻¹.

V.3.6. Concentration analysis

In order to estimate theoretically the analytical parameters for detection of DA, UA and AA at screen-printed electrodes, variation in concentrations of DA, UA and AA was examined by using simulation method. Fig. V.12 (a, c, e) presents experimental linear sweep voltammogrames with simulated LS voltammograms for different concentration of DA, UA and AA. The simulated voltammograms for each concentration were calculated using the k^0 value of eq. (1). Consequently, a good accord was observed between the simulated and experimental ones under different concentrations.

Next, in Fig. V.12 (b, d, f.) plots of calibration of the oxidation peak currents corresponding to the different DA, UA and AA concentrations obtained from simulated voltammograms of Fig. V.12 (a, c, e) are illustrated. A linear dependence for DA (Fig. V.12 (b)) was noticed over the concentration interval of 10-500 μM according to the equation I (μA) = 0.0138C (μM) + 0.6170 and a coefficient of correlation equal to 0.984. Then, Fig. V.12 (d) showed a linear current response with UA concentrations in the interval of 3 μM to 200 μM according to the equation of I (μA) = 0.0153 C (μM) + 0.24436 and R^2 = 0.983. For AA

concentrations, a linear relationship was obtained as presented in Fig. V.12 (f) in the concentration spectrum from 20 to 500 µM according to the equation I (µA) = 0.00281C (µM) + 0.10826 with R² =0.9862. These results confirm again that the calculated values of k0 could generate theoretical curves very close to corresponding experimental ones.
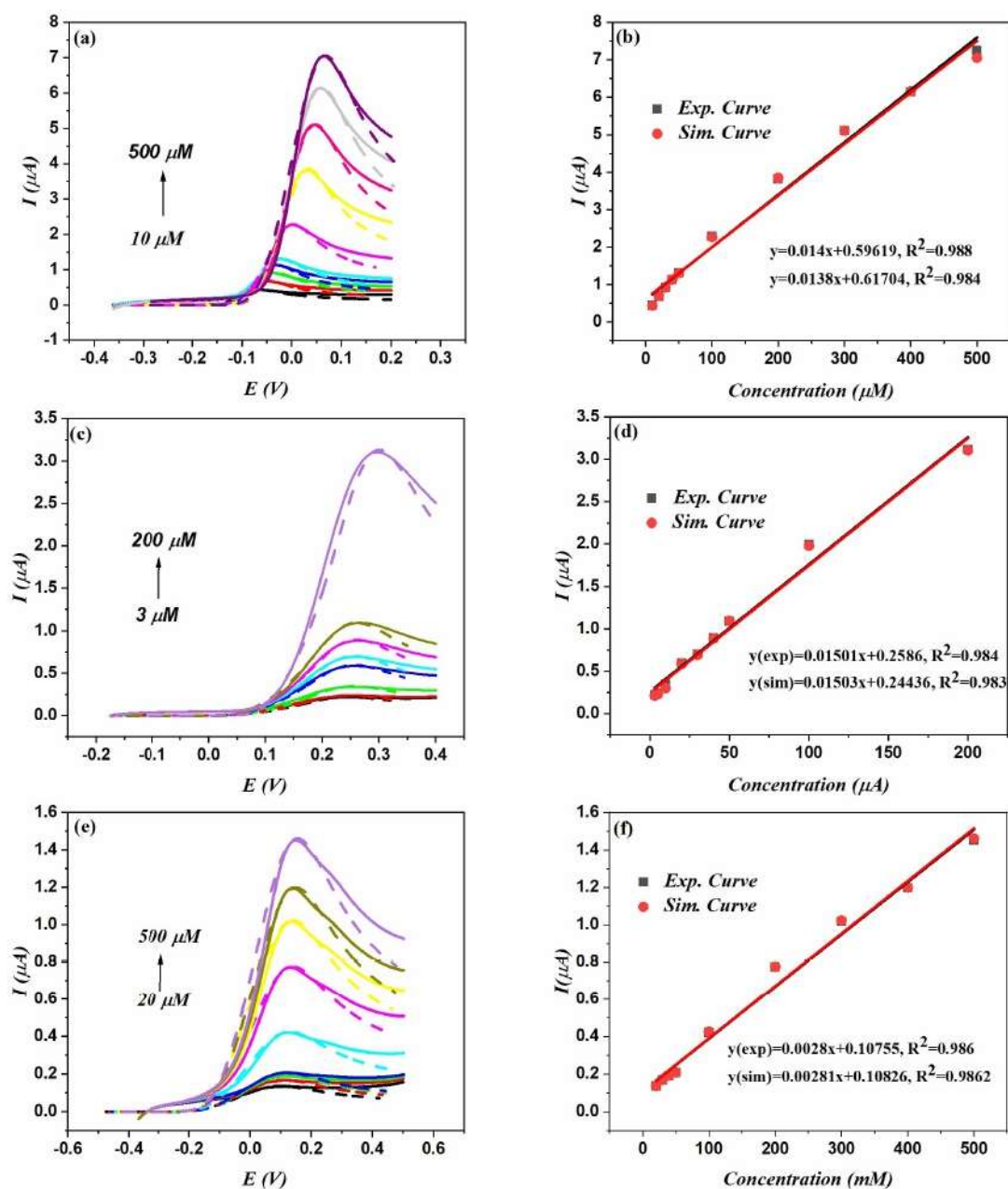
Figure V.12. Experimental and simulated LS voltammograms corresponding to the different concentrations of DA (a), UA (c), AA (e). Calibration plots of the experimental and simulated peak currents of DA (b), UA (d), AA (f).

V.4 Conclusion

This chapter is firstly focused on the study of detection by electrochemical method of three biomolecules: dopamine, uric acid and ascorbic acid, on screen-printed electrode using cyclic voltammetry. Voltammetric results demonstrated a good performance of SPEs for DA, UA and AA determination in concentration range of 1-500 µM, 1-200 µM, and 5-500 µM, respectively, with corresponding limit detection of 0.89 µM, 3.22 µM, 9.19 µM for DA, UA, and AA in order. These results showed good analytical performance for the unmodified SPE compared to other modified SPEs.

Tafel plots were employed to calculate the transfer charge coefficient while the diffusion coefficients of DA, UA and AA were determined through the semi-integral method. The standard rate constants k^0 of DA, UA and AA were determined using the equations developed in chapter IV. The obtained results indicate that the electro-oxidation of dopamine, uric acid, and ascorbic acid is quasi-reversible processes, and confirm that the calculated values of k^0 could generate theoretical curves very close to corresponding experimental ones. We consider these results as a very good validation for the obtained theoretical equations of k^0.

Chapter V

References

[1] C.V.D. Horsta, V, Somerseta, *Russian Journal of Electrochemistry*, 58 (2022) 341–359.

[2] J. Ping, J. Wu, Y. Wang, Y. Ying, *Biosensors and Bioelectronics*, 34 (2012) 70–76.

[3] A.S. Calvo, C. Botas, D. Martin-Yerga, P. Alvarez, R. Menendez and A. Costa-Garcia, *Journal od Electrochemical Society*, 162 (2015) 282-290.

[4] S. Chelly, M. Chelly, R. Zribi, R. Gdoura, H. Bouaziz-Ketata, and G. Neri, *ACS Omega*, 6 (2021) 23666−23675.

[5] W.T. Wahyuni, B.R. Putra, R. Heryanto, E. Rohaeti, D.H.Y. Yanto, A. Fauzi, *International Journal Electrochemical Science*, 16 (2021) 21022.

[6] R. Rezaeia, M.M. Foroughia, H. Beitollahib, and R. Alizadehc, *Russian Journal of Electrochemistry*, 54 (2018) 860–866.

[7] F.S.d. Cruz, F.d.S. Paula, D.L. Franco, W.T.P.d. Santos, L.F. Ferreira, *Journal of Electroanalytical Chemistry*, (2017).

[8] A.V. Shabalina, V.A. Svetlichnyi, K.A. Ryzhinskaya, and I.N. Lapin, *Analytical sciences*, 33 (2017) 1415-1419.

[9] G.E. Uwaya, O.E. Fayemi, *Journal of Cluster Science*, 33 (2021) 1035-1043.

[10] M.R. Ganjali, F.G. Nejad, H. Beitollahi, S. Jahani, M. Rezapour, B. Larijan, *International Journal Electrochemical Science*, 12 (2017) 3231 – 3240.

[11] H. Ernst, M. Knoll, *Analytica Chimica Acta*, 449 (2001) 129–134.

[12] K.B. Oldham, *Journal of Electroanalytical Chemistry*, 121 (1981) 34.

[13] A.M.M.P. Sakita, R.D. Noce, C.S. Fugivara, and A.V. Benedetti, *Journal of analytical Chemistry.*, (2017).

[14] E.A. Khudaish, J.A. Rather, *Journal of Electroanalytical Chemistry*, (2016).

[15] X. Wang, N. Yang, Q. Wan, X. Wang, *Sensors and Actuators B*, 128 (2007) 83–90.

[16] M.M. Ardakani, Z. Akrami, H. Kazemian, H.R. Zare, *Journal of Electroanalytical Chemistry*, 586 (2006) 31–38.

[17] R.S. Nicholson, *analytical Chemistry*, 37 (1965) 1351–1355.

[18] E. Laviron, *Journal of Electroanalytical Chemistry*, 101 (1979) 19-28

[19] S. Houam, A.M. Affoune, I. Atek, F. Kesri, R.S. Guermeche, M. L. Chelaghmia, M. Nacef, O. Khelifi , C.E. Banks, *Electrochimica Acta*, 449 (2023) 142200.

[20] H. Matsuda, Y. Ayabe, *Zeicschrift Elektrochemie*, 59 (1955) 494–503.

[21] J. Kwak, Bull. Korean. *Chemistry Society*, 15 (1994) 57–63.

[22] K. Qu, W. Dai, Y. Bai, Y. Chen, Z. Chen, M. Deng, *Journal of Electroanalytical Chemistry,* 878 (2020) 114702.

<u>Conclusions</u>

Conclusions

We believe that this work has made a significant contribution to the development of the theory of linear sweep voltammetry for electrochemical soluble redox couples. Newly developed equations have been established for determining the standard rate constant k^0.

The simulation was based on the diffusion mass transport and the Butler-Volmer kinetics using semi-analytical method. The developed algorithmic of LSV and theoretical equations were validated experimentally through electrochemical oxidation of ferrocyanide, dopamine (DA), uric acid (UA) and ascorbic acid (AA) on screen-printed graphite electrodes (SPGEs).

In the simulation study, a theoretical analysis of linear sweep voltammetry responses was presented. The effects of charge transfer coefficient (α) and dimensionless kinetic rate constant (Λ) on the shape and position of voltammograms were investigated. Through the coupling effects of both α and Λ on peaks characteristics including peak current, half peak width and peak potential, different kinetics diagrams were established.

Based on the qualitative and quantitative analysis of kinetics diagrams, limitation zones for reversible, quasi-reversible, and irreversible systems were obtained. The reversible zone is in $\Lambda \geq 10^3$, the quasi-reversible zone is in $10^{-3} < \Lambda < 10^3$, and the irreversible zone is in $\Lambda \leq 10^{-3}$. Then, a series of kinetic equations were developed, which enables an easy determination of the standard rate constant for *quasi*-reversible soluble/soluble systems.

The electrochemical oxidation of ferrocyanide $Fe(CN)_6^{4-}$ on screen-printed graphite electrodes was studied to verified the obtained theoretical results. The different kinetic properties of the oxidation ferrocyanide were determined using different approaches. The charge transfer coefficient α was obtained by Tafel plots and found to be 0.259 as well as the diffusion coefficient was calculated using a semi-integral voltammetry, and was 6.45×10^{-6} cm^2 s^{-1}. Using the developed equations, the standard kinetic rate constant was determined to be 6,7129 $\times 10^{-4}$ cm s^{-1}, revealing that

the electrochemical of oxidation of ferrocyanide $Fe(CN)_6^{4-}$ on SPGEs is quasi-reversible process.

In the application of electrochemical sensors, a voltammetric study for the electrochemical detection of three biomolecules of interest, namely dopamine, uric acid, and ascorbic acid, on screen-printed graphite electrodes was presented. The sensor show good results in the determination of DA, UA and AA with linear concentration range of 1 to 500 μM, 1 to 200 μM and 5 to 500 μM, respectively. The detection limit was found to be 0.89 μM for DA, 3.22 μM for UA, 9.19 μM for AA.

The kinetic and mass transport parameters of the detection of dopamine, uric acid and ascorbic acid on SPGEs were obtained using approaches presented in this thesis. For dopamine, the charge transfer coefficient α was equal to 0.2 and the diffusion coefficient was obtained to be 4.85×10^{-6} cm^2 s^{-1}. The value of the standard rate kinetic constant k^0 was calculated and was equal to 1.15334×10^{-3} cm s^{-1}. For uric acid, the charge transfer coefficient α was equal to 0.24 and the diffusion coefficient was to be 2.6×10^{-6} cm^2 s^{-1}. The k^0 was determined to be 3.85063×10^{-4} cm s^{-1}. For AA, the charge transfer coefficient α was equal to 0.27 and the diffusion coefficient was to be 1.195×10^{-6} cm^2 s^{-1}. The k^0 was determined to be 1.713292×10^{-4} cm s^{-1}. Besides these results, the electro-oxidation behaviours of dopamine, uric acid and ascorbic acid are kinetically quasi-reversible processes.

The results obtained made it possible to establish diagnostic criteria allowing the calculation of the kinetic parameters of quasi-reversible soluble-soluble systems. Experimental studies were carried out to validate the theoretical results obtained. The analysis of the simulation results confirmed that the calculated values of the standard speed constant k^0 make it possible to establish theoretical curves very close to the corresponding experimental curves. This constitutes a good validation of the theoretical equations obtained for the standard rate constant k^0.

Considering the findings of this study, we propose an extension of our approach to analyse cyclic voltammetry responses more comprehensively. Moreover, we suggest investigating the impact of the combined anodic and cathodic transfer coefficients on refining the theoretical equations developed.